NASA Technical Memorandum 80055

Effect of Nose Bluntness and Afterbody Shape on Aerodynamic Characteristics of a Monoplanar Missile Concept With Bodies of Circular and Elliptical Cross Sections at a Mach Number of 2.50

Ervald B. Graves and Roger H. Fournier

JUNE 1979

NASA

NASA Technical Memorandum 80055

Effect of Nose Bluntness and Afterbody Shape on Aerodynamic Characteristics of a Monoplanar Missile Concept With Bodies of Circular and Elliptical Cross Sections at a Mach Number of 2.50

Ernald B. Graves and Roger H. Fournier
Langley Research Center
Hampton, Virginia

SUMMARY

A wind-tunnel investigation has been conducted to determine the effect of nose bluntness and afterbody shape on the aerodynamic characteristics of a family of circular and modified elliptical missile configurations. These configurations were of monoplanar wing design with constant wing span. Tail surfaces were mounted flush at the body base with a dihedral angle of $\pm 30^\circ$. The tests were performed at a Mach number of 2.50 and at angles of attack from about -4° to 32°.

The results indicate that increasing nose bluntness increases zero-lift drag and decreases both the maximum lift-drag ratio and the level of directional stability. The center of pressure generally moves forward with increasing nose size; however, small nose radii on the modified elliptical configurations move the center of pressure rearward.

Results also indicate that the circular-bodied configurations exhibit the greatest longitudinal stability and the least directional stability. Concepts with the variable geometry afterbody contour display the most directional stability and the greatest zero-lift drag.

INTRODUCTION

The National Aeronautics and Space Administration supports continuing research in missile related aerodynamics. Reference 1 suggests that innovative concepts such as a missile which combines an elliptical body having low-geometric profile and high maneuverability need to be explored. The U.S. Air Force, as part of its Maneuvering Air-to-Air Missile Program, is supporting investigation of some specific elliptical-bodied configurations for possible monoplanar missile applications (refs. 2 and 3).

Recently, a wind-tunnel study was undertaken to compare the aerodynamic characteristics of a pointed-nose monoplanar missile concept having an elliptical body with one of circular body cross section (ref. 4). The results of this study showed some aerodynamic advantages for the elliptically configured concept. Missile subsystem technologies, however, may require some geometric deviations from these missile designs. The objective of this study is to determine the effect of nose bluntness and afterbody shape on the aerodynamic characteristics of a monoplanar missile concept having bodies of circular and elliptical cross sections. The study configurations consisted of both body alone and wing-body-tail concepts.

SYMBOLS

All aerodynamic data are presented about the body system of axes, and the longitudinal aerodynamic data are also presented about the stability system of

axes. All moments are referred to a point on the model center line at 60.00 percent of the body length measured from the nose.

A reference area (based on maximum body cross-sectional area), 0.008107 m^2

C_A axial-force coefficient, $\dfrac{\text{Axial force}}{qA}$

C_D drag coefficient, $\dfrac{\text{Drag}}{qA}$

$C_{D,o}$ drag coefficient at zero lift

C_L lift coefficient, $\dfrac{\text{Lift}}{qA}$

C_l rolling-moment coefficient, $\dfrac{\text{Rolling moment}}{qAd}$

C_{l_β} effective dihedral parameter, $\left(\dfrac{\Delta C_l}{\Delta \beta}\right)_{\beta=0^\circ,3^\circ}$, per degree

C_m pitching-moment coefficient, $\dfrac{\text{Pitching moment}}{qAd}$

C_{m_α} longitudinal stability parameter, $\dfrac{\partial C_m}{\partial \alpha}$, through $\alpha = 0^\circ$, per degree

C_N normal-force coefficient, $\dfrac{\text{Normal force}}{qA}$

C_{N_α} normal-force curve slope, $\dfrac{\partial C_N}{\partial \alpha}$, through $\alpha = 0^\circ$, per degree

C_n yawing-moment coefficient, $\dfrac{\text{Yawing moment}}{qAd}$

C_{n_β} directional-stability parameter, $\left(\dfrac{\Delta C_n}{\Delta \beta}\right)_{\beta=0^\circ,3^\circ}$, per degree

C_Y side-force coefficient, $\dfrac{\text{Side force}}{qA}$

C_{Y_β} side-force parameter, $\left(\dfrac{\Delta C_Y}{\Delta\beta}\right)_{\beta=0^\circ,3^\circ}$, per degree

d equivalent circular body reference diameter (maximum diameter), 0.1016 m

l body length, 0.7112 m

L/D lift-drag ratio, $\dfrac{C_L}{C_D}$

$(L/D)_{max}$ maximum lift-drag ratio

M Mach number

q free-stream dynamic pressure, kPa

r/d ratio of equivalent local circular body radius to equivalent circular body reference diameter

R_n/d ratio of nose radius to equivalent circular body reference diameter

x/l ratio of local body station to body reference length (measured from body nose along the body longitudinal axis)

x_{cp} center-of-pressure location, $\left(\dfrac{C_{m_\alpha}}{C_{N_\alpha}}\right)\left(\dfrac{d}{l}\right)$, percent body length from nose

α angle of attack, deg

β angle of sideslip, deg

Model component designations:

B body

T tail

W wing

3

TEST FACILITY

Tests were conducted in the high Mach number test section of the Langley Unitary Plan wind tunnel. This facility is a variable-pressure, continuous-flow wind tunnel with an asymmetric sliding-block nozzle ahead of each test section that permits continuous variation in Mach number. The test section is approximately 2.1 m long and 1.2 m square.

MODELS

Drawings of the monoplanar missile concepts are shown in figure 1. The longitudinal area development of bodies with pointed noses (figs. 1(c), 1(f), and 1(i)) is identical to the development of the Adams minimum-wave-drag bodies (ref. 5). Each of these concepts has a fineness ratio of 7. All other concepts have minimum wave drag bodies (Adams) which have been truncated to accommodate one of two hemispherical nose caps and still maintain a fineness ratio of 7 based on the maximum equivalent circular body diameter.

The concepts in figures 1(d) and 1(e) have bodies with cross-sectional area distributions identical to the circular bodies in figures 1(a) and 1(b), respectively. These modified bodies (figs. 1(d) and 1(e)) vary in geometry from a circular cross section at the nose-forebody juncture to a 3:1 ellipse at the maximum body cross-sectional area station (68 percent body length) and back to a circle at the body base; i.e., body eccentricity varies as the local cross-sectional area. The concept in figure 1(i) has a constant 3:1 elliptical body cross-sectional shape with cross-sectional area distribution identical to the circular body in figure 1(c). Table I provides details of the body cross-sectional shape variations.

Since the configuration geometry changes are systematic, the following list of study configuration concepts is useful:

Figure	Body	Nose shape	Forebody cross-sectional shape	Afterbody cross-sectional shape	Base shape
1(a)	I	Large hemisphere	Circular	Circular	Circular
1(b)	II	Small hemisphere	Circular	Circular	Circular
1(c)	III	Pointed	Circular	Circular	Circular
1(d)	IV	Large hemisphere	Variable	Variable	Circular
1(e)	V	Small hemisphere	Variable	Variable	Circular
1(f)	VI	Pointed	Elliptical	Variable	Circular
1(g)	VII	Large hemisphere	Variable	Elliptical	Elliptical
1(h)	VIII	Small hemisphere	Variable	Elliptical	Elliptical
1(i)	IX	Pointed	Elliptical	Elliptical	Elliptical

The concepts have constant wing span using the basic wing planform shape shown in figure 1(j). Thus, the exposed wing planform area for specific configurations varies according to the body projected planform area for those concepts. The concepts use identical tail surfaces (fig. 1(k)) which are mounted flush at the base with ±30° dihedral. The projected tail span varies slightly with afterbody cross-sectional eccentricity, since a suitable mounting position which permits large tail surface deflections varies with cross-sectional shape. Some general geometric characteristics of the models are listed in table II.

Sketches comparing the planform for circular forebodies, for modified forebodies, and for all afterbodies are shown in figures 1(l), 1(m), and 1(n), respectively. A photograph displaying the model components is shown in figure 2.

TEST CONDITIONS, MEASUREMENTS, AND CORRECTIONS

Force and moment tests were performed at the following nominal conditions:

Mach number 2.50
Stagnation temperature . . . . 339 K
Stagnation pressure . . . . 81.36 kPa
Reynolds number . . . . 6.56×10^6 per m

In order to insure a turbulent boundary layer, transition grit consisting of ASTM size 35 sand particles was affixed to the nose, wing, and tail surfaces of the models. Transition particles were spaced a nominal 0.14 cm apart, 3.05 cm aft of the nose and 1.02 cm aft (streamwise) of the leading edges of both wing and tail surfaces. This procedure is based on unpublished data from experiments performed in the Langley Unitary Plan wind tunnel and reference 6.

All aerodynamic forces and moments were measured by means of an internally mounted electrical strain-gage balance, which in turn was rigidly fastened to a sting-tunnel support system. Static pressures were measured in the model chamber and at the model base.

Angles of attack have been adjusted for tunnel airflow misalinement and model sting-balance deflection due to aerodynamic loads. Axial-force and drag data have been adjusted to free-stream static pressure acting at the model base.

Flow visualization tests were conducted using the vapor screen technique (ref. 7) with a camera mounted in the test section downstream of the model. Schlieren photographs were also obtained.

PRESENTATION OF DATA

The data are plotted in comparative form so that the effect of various configuration changes can readily be seen. The following list of abbreviated figure legends is presented as an aid in locating specific data:

5

RESULTS AND DISCUSSION

Discussion of the aerodynamic characteristics for the various missile concepts is limited to remarks concerning the general effects of nose bluntness and afterbody shape. A detailed discussion concerning the aerodynamic differences associated with the pointed nose configurations at subsonic through supersonic speeds is presented in reference 4.

The summary data presented in figure 34 clearly show that increasing the nose bluntness correspondingly increases zero-lift drag, and decreases both the maximum lift-drag ratio and the level of directional stability (values of C_{n_β} become less positive). The center of pressure (c.p.) moves forward with increasing nose size for the circular body concepts. This trend is expected as a result of the associated increase in forebody planform area forward of the moment reference point (fig. 1(l)). For concepts with modified elliptical bodies, however, the data indicate that small nose radii can provide a rearward shift in c.p. location.

The shift in c.p. location for the modified elliptical bodies can be explained, as was done in reference 8, by noting that increasing nose bluntness is associated with both an increase in local planform area (fig. 1(m)) and a delay in vortex development (fig. 33). The pointed-nose concept is dominated by early vortex development which provides a forward-acting induced lift. (See fig. 16 or 26.) This induced lift acts farther aft on the large blunt-nosed concepts as a result of the delay in vortex development, but compensation is provided by the increase in forward planform area so that C_m is relatively unchanged. The small blunt-nosed concepts with an aft-acting vortex lift component, however, have insufficient forward planform area to compensate. The result is a more negative C_m and a c.p. located farther aft for these configurations with small blunt noses.

The effect of afterbody shape on some of the aerodynamic parameters of the missile concept is worth noting. The circular concepts exhibit the most longitudinal aerodynamic stab'lity (most rearward c.p. location) but the least directional stability. Concepts with the variable-geometry afterbody section display the most directional stability, but they also demonstrate the most zero-lift drag. The elliptical-afterbody concepts have the more moderate parameter variations. They generally provide less zero-lift drag with slightly more $(L/D)_{max}$. Although the concepts for the elliptical afterbody do not possess the most directional stability, they are directionally stable at the moment reference location to an angle of attack of about 20° (fig. 31). (Note that ref. 4 did not provide lateral-directional data for the missile concept with pointed nose and elliptical afterbody at $M = 2.50$. However, data that were available at higher and lower Mach numbers and data trends from the body-alone tests suggest an engineering estimate of the level of directional stability for this concept at $M = 2.50$ and $\alpha = 0^{\circ}$ as indicated by the dashed line in fig. 34(a).)

CONCLUSIONS

A wind-tunnel investigation has been conducted at Mach 2.50 to determine the effect of nose bluntness and afterbody shape on the aerodynamic characteristics of a monoplanar missile concept with bodies of circular and elliptical cross sections. The test results have provided the following conclusions:

1. Increasing nose bluntness increases zero-lift drag and decreases the maximum lift-drag ratio.

2. Increasing nose bluntness decreases the level of directional stability and generally moves the center-of-pressure location forward. However, for the modified elliptical concepts, small nose radii can provide a rearward shift in center-of-pressure location.

3. Small changes in the planform area distribution associated with the modified elliptical configurations can strongly influence longitudinal stability.

4. Modifying a constant-eccentricity elliptical cross-sectional afterbody to become circular at the base results in a slight increase in both directional stability and zero-lift drag.

Langley Research Center
National Aeronautics and Space Administration
Hampton, VA 23665
May 7, 1979

8

REFERENCES

1. Sawyer, Wallace C.; Jackson, Charlie M., Jr.; and Blair, A. B., Jr.: Aerodynamic Technologies for the Next Generation of Missiles. Paper presented at the AIAA/ADPA Tactical Missile Conference (Gaithersburg, Maryland), Apr. 27-28, 1977.

2. Smith, Dale K.: Aerodynamic Characteristics of Three Maneuvering Air-to-Air Missile Models at Mach Numbers From 0.5 to 1.6. AEDC-TR-77-25, AFATL-TR-77-3, U.S. Air Force, June 1977. (Available from DDC as AD B018 815L.)

3. Sawyer, Wallace C.; and Sangiorgio, Giuliana: Stability and Control Characteristics of a Monoplanar Elliptic Missile Model at Mach Numbers From 1.60 to 2.86. NASA TP-1352, 1978.

4. Graves, Ernald B.: Aerodynamic Characteristics of a Monoplanar Missile Concept With Bodies of Circular and Elliptical Cross Sections. NASA TM-74079, 1977.

5. Adams, Mac C.: Determination of Shapes of Boattail Bodies of Revolution for Minimum Wave Drag. NACA TN 2550, 1951.

6. Braslow, Albert L.; and Knox, Eugene C.: Simplified Method for Determination of Critical Height of Distributed Roughness Particles for Boundary-Layer Transition at Mach Numbers From 0 to 5. NACA TN 4363, 1958.

7. McGregor, I.: Part IV - Development of the Vapour Screen Method of Flow Visualization in a 3 ft × 3 ft Supersonic Tunnel. Flow Visualization in Wind Tunnels Using Indicators, R. L. Maltby, Compiler, AGARDograph 70, Apr. 1962, pp. 111-164.

8. Graves, Ernald B.; and Robins, A. Warner: Supersonic Aerodynamic Trade Data for a Low-Profile Monoplanar Missile Concept. AIAA Paper 79-0222, Jan. 1979.

TABLE I.- BODY COORDINATES

(a) Large hemispherical nose with $R_n/d = 0.2894$

x/l	r/d	Eccentricity of body –		
		I	IV	VII
0	0	1.0000	1.0000	1.0000
.0414	.2894		1.0000	1.0000
.1023	.3230		1.3174	1.3174
.1664	.3563		1.6353	1.6353
.2305	.3868		1.9236	1.9236
.2946	.4140		2.1832	2.1832
.3587	.4383		2.4137	2.4137
.4228	.4593		2.6138	2.6138
.4873	.4770		2.7806	2.7806
.5510	.4905		2.9091	2.9091
.5895	.4963		2.9642	2.9642
.6151	.4990		2.9899	2.9899
.6800	.5000		3.0000	3.0000
.7000	.4989		2.9736	
.7292	.4936		2.8502	
.7500	.4903		2.7722	
.7833	.4803		2.5360	
.8000	.4767		2.4526	
.8314	.4622		2.1354	
.8500	.4603		2.0653	
.8716	.4498		1.8198	
.9000	.4428		1.6536	
.9250	.4343		1.4546	
.9500	.4266		1.2720	
.9750	.4201		1.1202	
1.0000	.4164		3.0000	

TABLE I.- Continued

(b) Small hemispherical nose with $R_n/d = 0.1516$

x/l	r/d	Eccentricity of body -		
		II	V	VIII
0	0	1.0000	1.0000	1.0000
.0216	.1516		1.0000	1.0000
.0258	.1543		1.0165	1.0165
.0799	.2060		1.3144	1.3144
.1340	.2520		1.5777	1.5777
.1881	.2933		1.8147	1.8147
.2423	.3308		2.0293	2.0293
.2964	.3648		2.2238	2.2238
.3505	.3953		2.3994	2.3994
.4046	.4225		2.5562	2.5562
.4587	.4468		2.6940	2.6940
.5669	.4835		2.9057	2.9057
.6210	.4953		2.9724	2.9724
.6481	.4988		2.9925	2.9925
.6800	.5000		3.0000	3.0000
.7000	.4989		2.9736	
.7292	.4936		2.8502	
.7500	.4903		2.7722	
.7833	.4803		2.5360	
.8000	.4767		2.4526	
.8314	.4622		2.1354	
.8500	.4603		2.0653	
.8716	.4498		1.8198	
.9000	.4428		1.6536	
.9250	.4343		1.4546	
.9500	.4266		1.2720	
.9750	.4201		1.1202	
1.0000	.4164		1.0000	

TABLE I.- Concluded

(c) Pointed nose with $R_n/d = 0$

x/l	r/d	Eccentricity of body -		
		III	VI	IX
0	0	1.0000	3.0000	3.0000
.0100	.0285			
.0200	.0478			
.0250	.0565			
.0500	.0944			
.0750	.1271			
.1000	.1567			
.1250	.1840			
.1500	.2095			
.2000	.2560			
.2500	.2979			
.3000	.3357			
.3500	.3699			
.4000	.4007			
.4500	.4280			
.5000	.4519			
.5750	.4803			
.6000	.4875			
.6250	.4934			
.6500	.4977			
.6800	.5000			
.7000	.4989		2.9736	
.7292	.4936		2.8502	
.7500	.4903		2.7722	
.7833	.4803		2.5360	
.8000	.4767		2.4526	
.8314	.4632		2.1354	
.8500	.4603		2.0653	
.8716	.4498		1.8198	
.9000	.4428		1.6536	
.9250	.4343		1.4546	
.9500	.4266		1.2720	
.9750	.4201		1.1202	
1.0000	.4164		1.0000	

TABLE II.- MODEL GEOMETRIC CHARACTERISTICS

Body:
  Length, m 0.7112
  Fineness ratio 7.00
  Maximum cross-section area, m^2 . . . . 0.008107
  Base area, m^2 . . . . 0.00562

Wing:
  L.E. sweep, deg 75.0
  T.E. sweep, deg 60.0
  Span, m 0.229
  Dihedral angle, deg 0

Tail:
  Inboard L.E. sweep, deg 45.0
  Outboard L.E. sweep, deg 14.0
  T.E. sweep, deg 0
  Outboard taper ratio 0.75
  Inboard taper ratio 0.44
  Dihedral angle, deg . . . . ±30.0
  Surface area, m^2 . . . . 0.0048

Maximum body
diameter, 0.1016 m

Moment reference location

	Planform area, m^2
B	0.062
BT	.063
BWT	.097
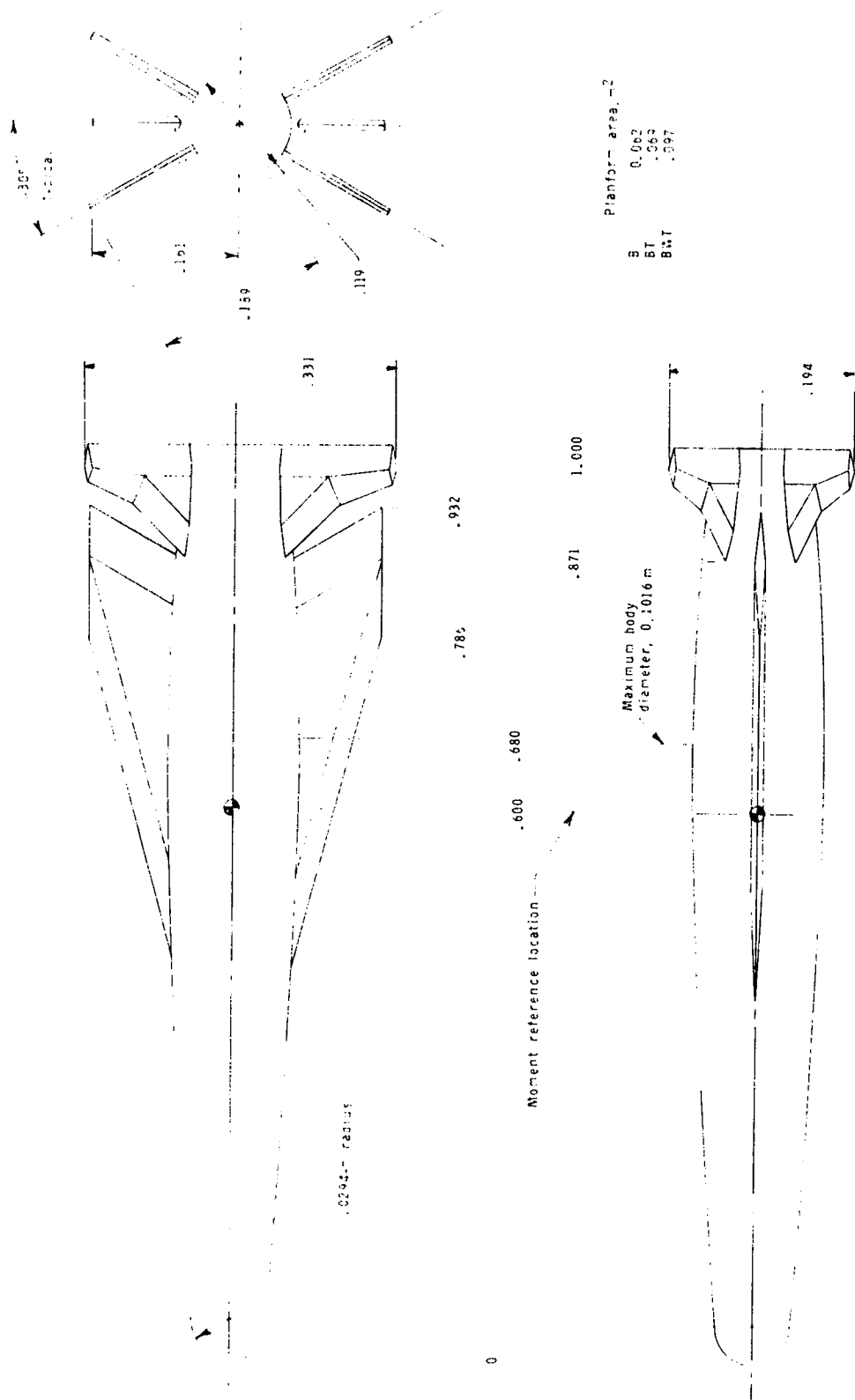
(a) Circular configuration concept with large hemispherical nose. Body I
(Reference length = 0.7112 m).

Figure 1.- Details of model configurations. Linear dimensions are given in
fractions of reference length.
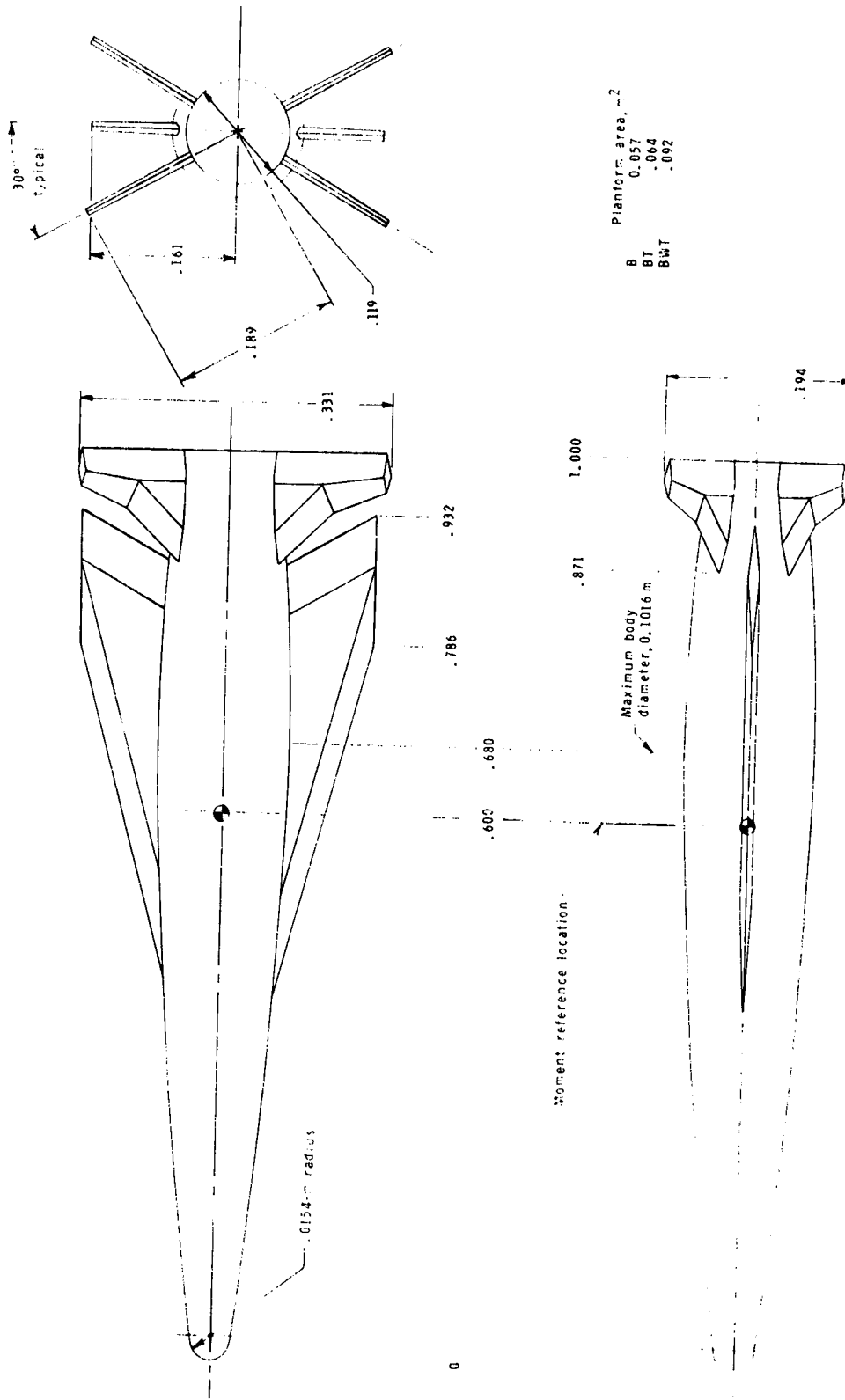
(b) Circular configuration concept with small hemispherical nose. Body II
(Reference length = 0.7112 m).
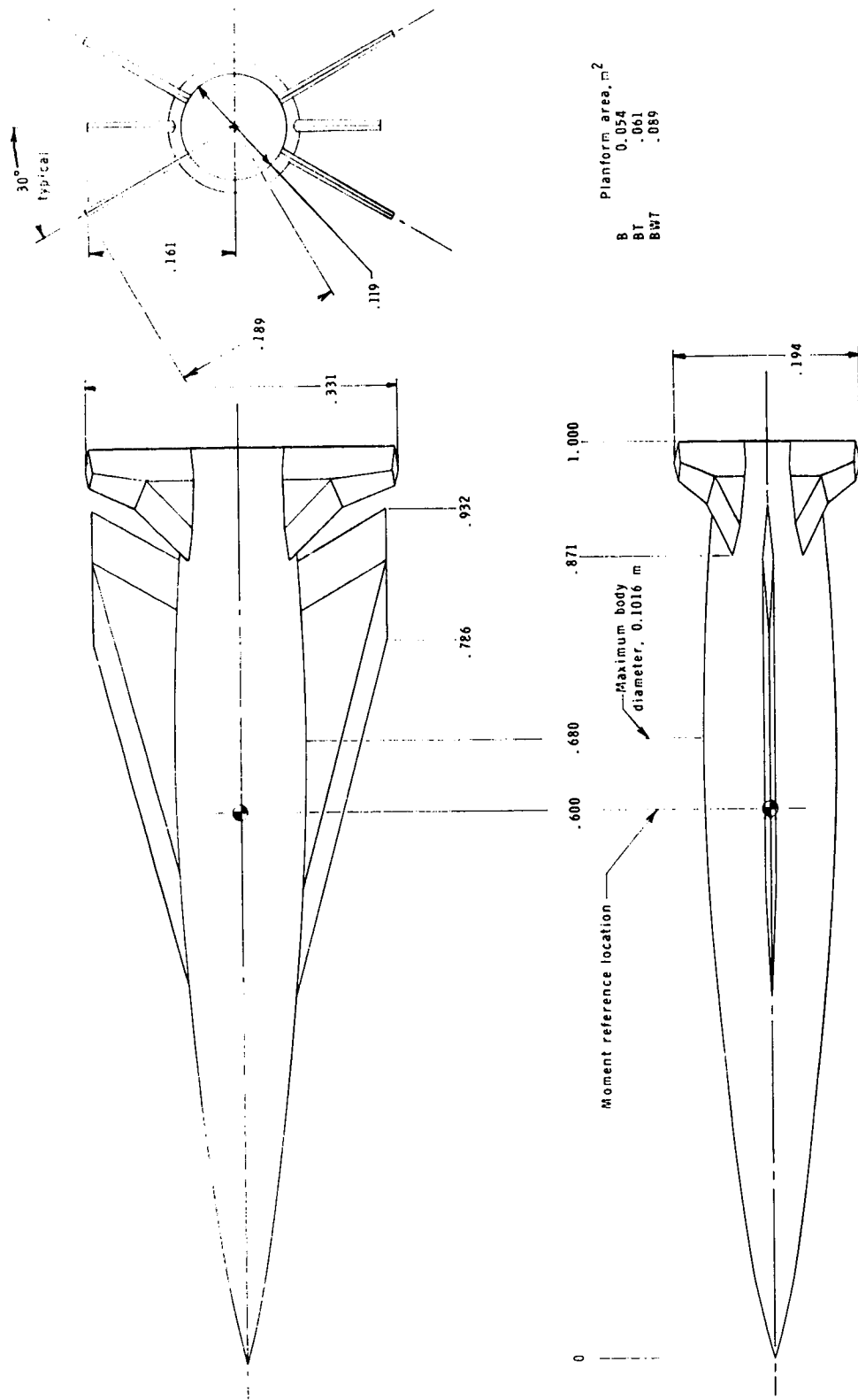
Figure 1.- Continued.

(c) Circular configuration concept with pointed nose. Body III (Reference length = 0.7112 m).

Figure 1.- Continued.

16
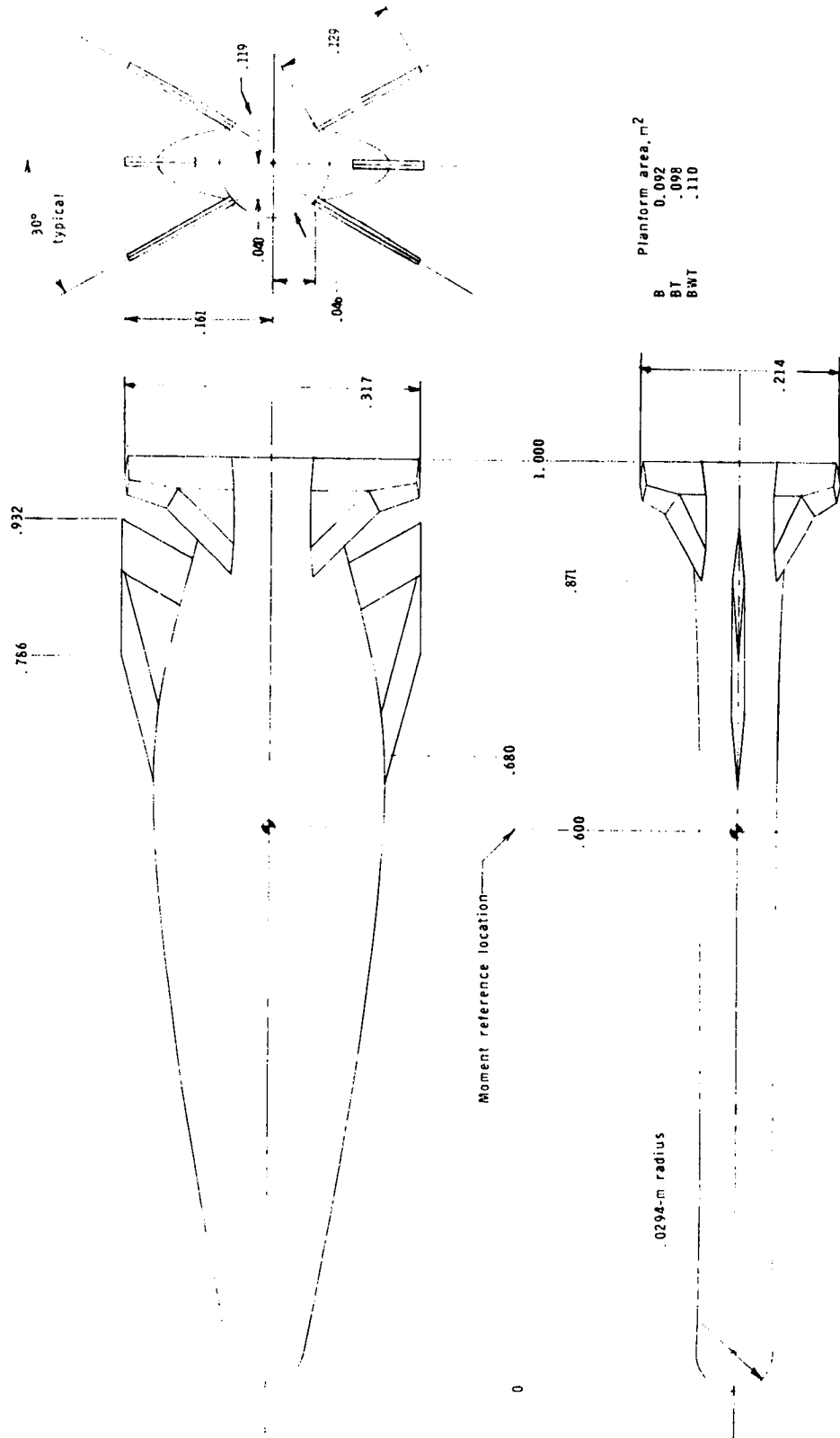
(d) Modified configuration concept with large hemispherical nose and circular base. Body IV (Reference length = 0.7112 m).

Figure 1.- Continued.

Planform area, m²

B	0.085
BT	.091
BWT	.103
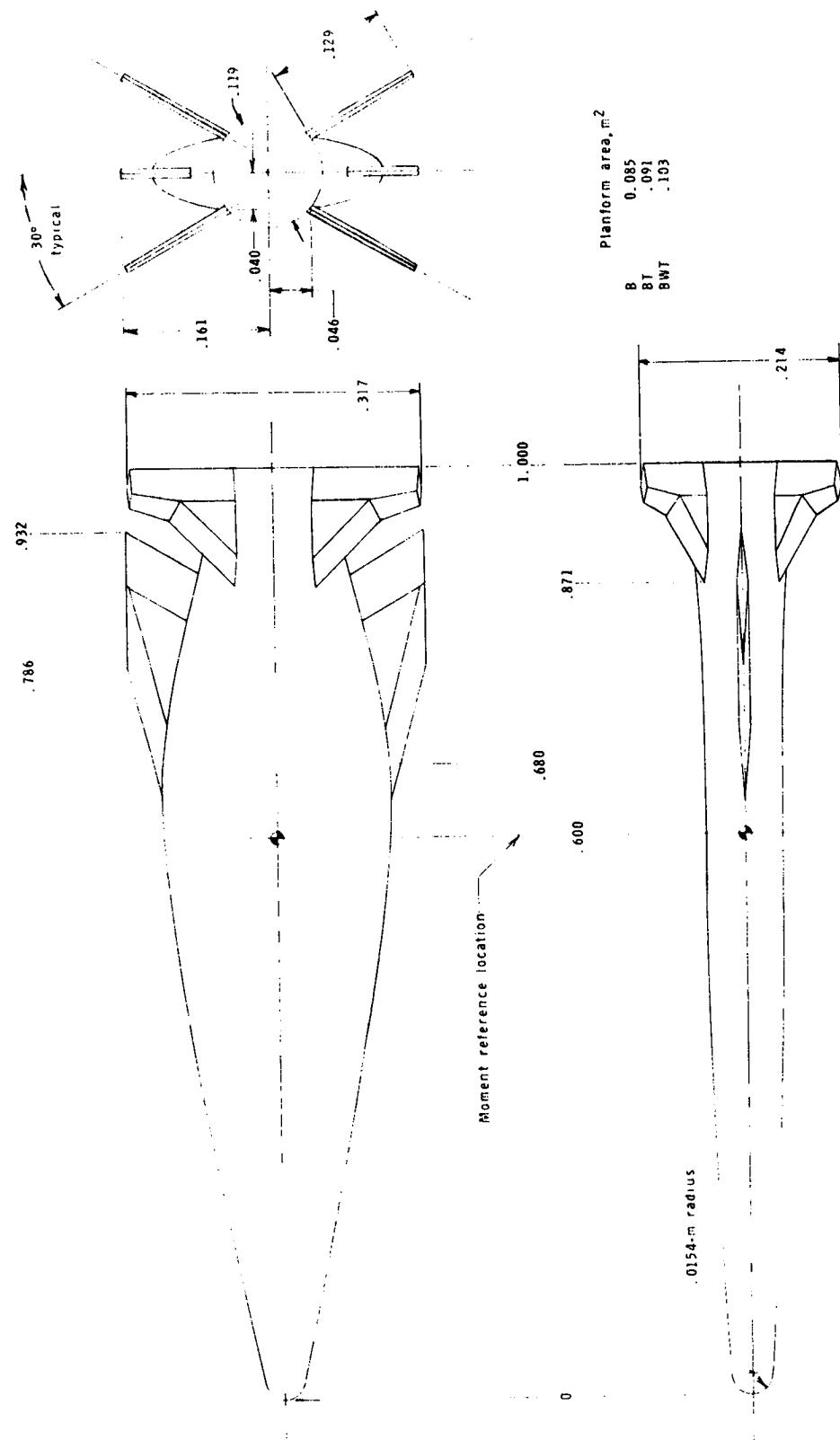
(e) Modified configuration concept with small hemispherical nose and circular base. Body V (Reference length = 0.7112 m).
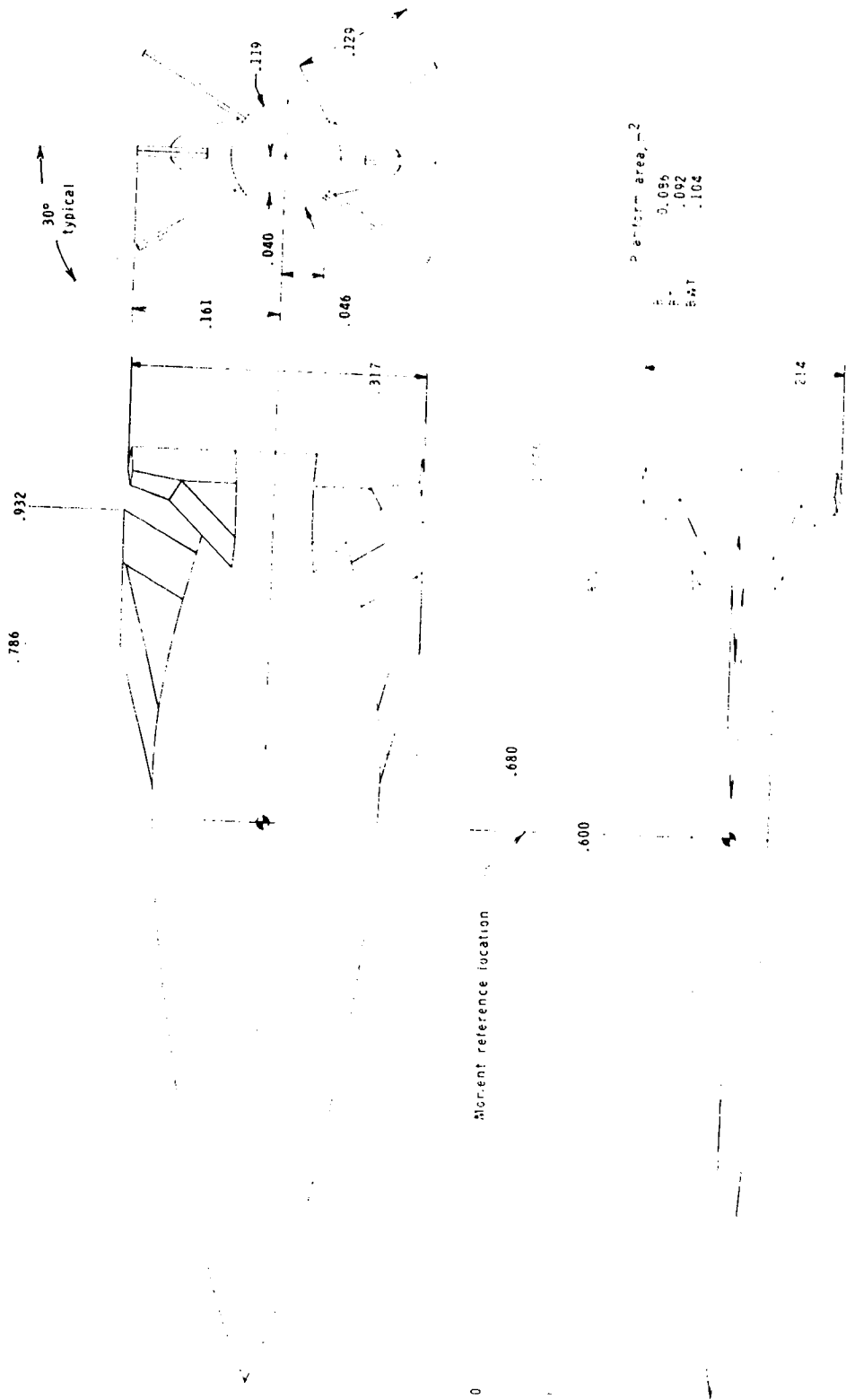
Figure 1.- Continued.

(f) Modified configuration concept with pointed nose and circular base. Body VI
(Reference length = 0.7112 m).
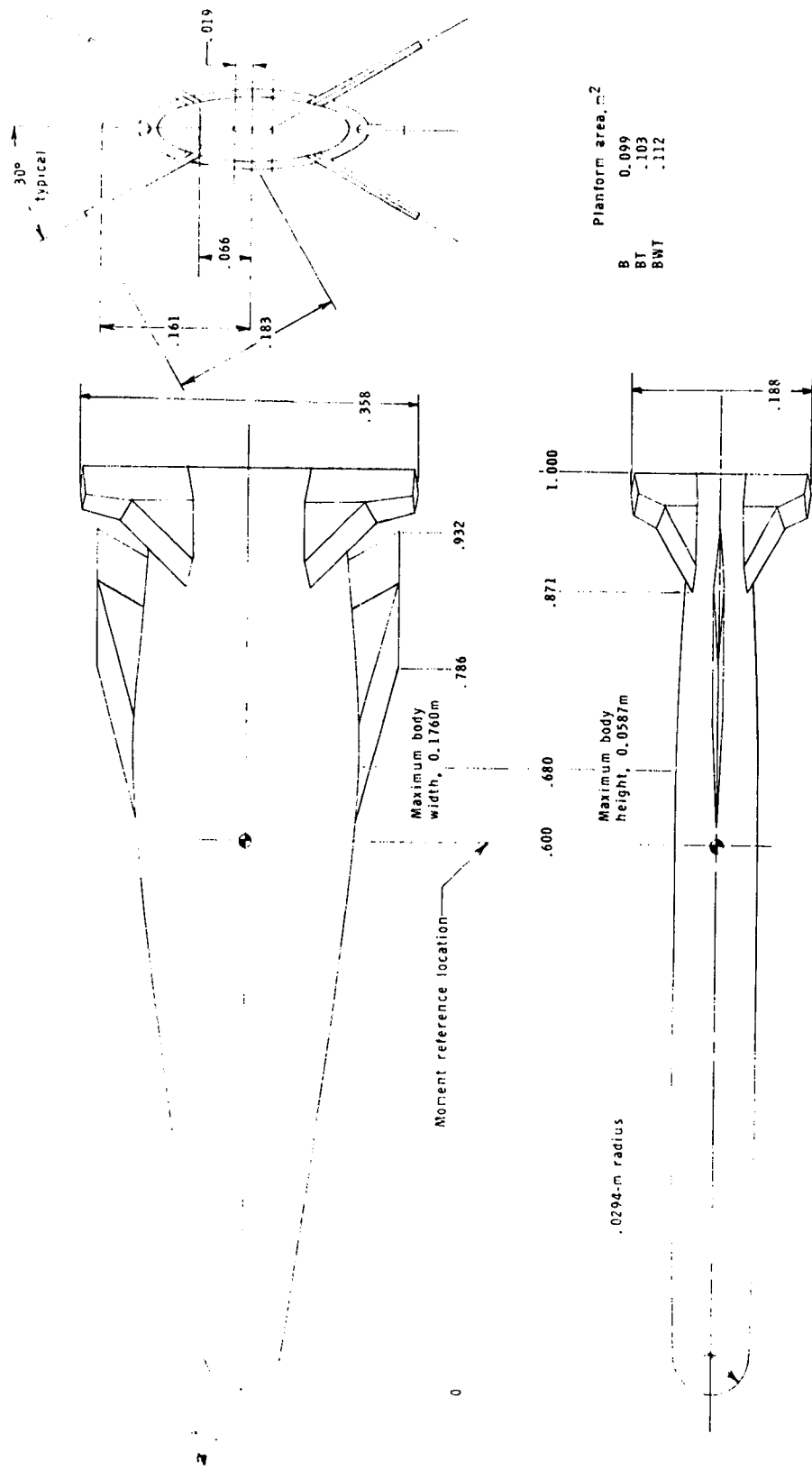
Figure 1.- Continued.

(g) Modified configuration concept with large hemispherical nose and elliptical base. Body VII (Reference length = 0.7112 m).
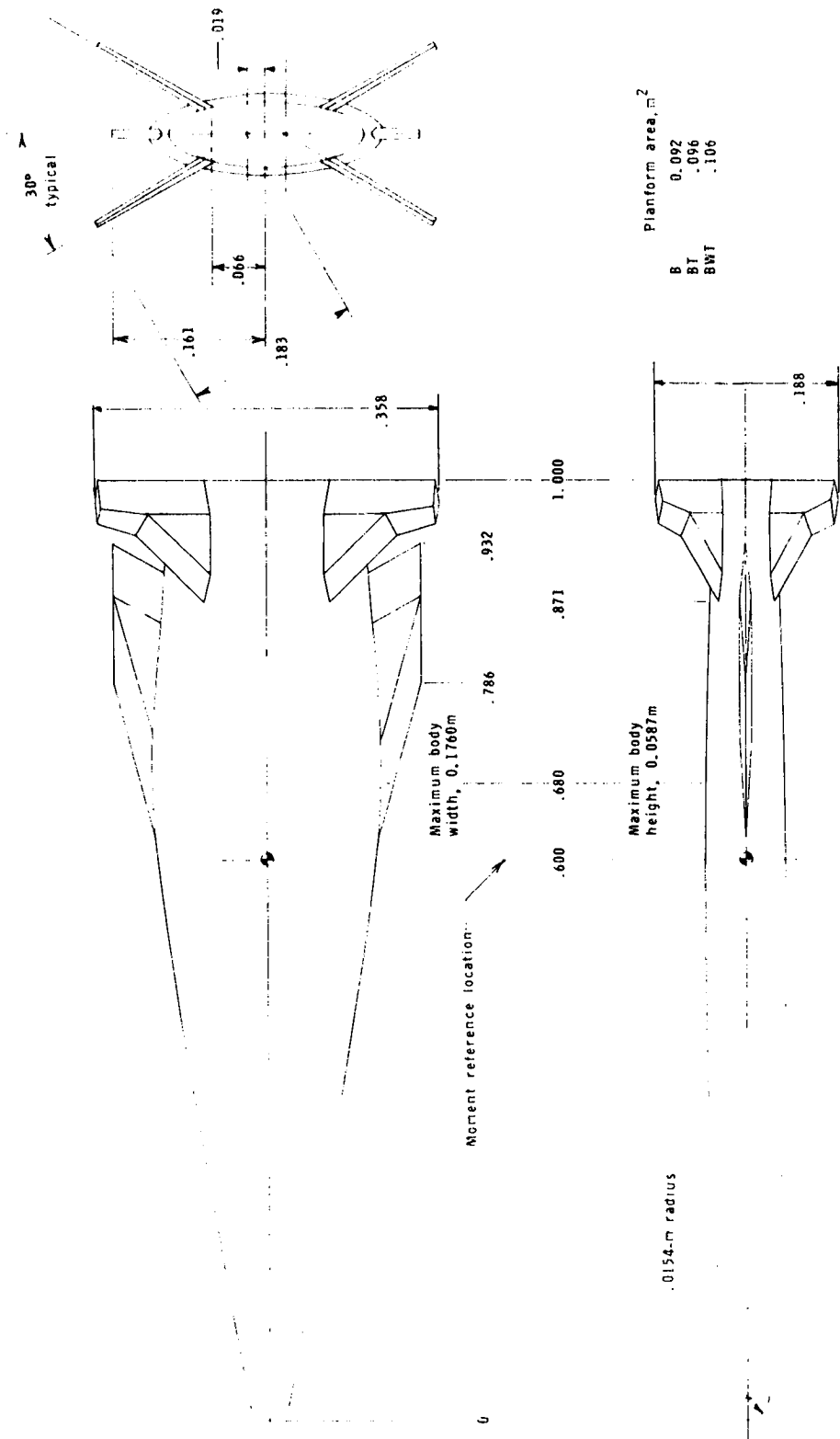
Figure 1.- Continued.

(h) Modified configuration concept with small hemispherical base and elliptical base. Body VIII (Reference length = 0.7112 m).
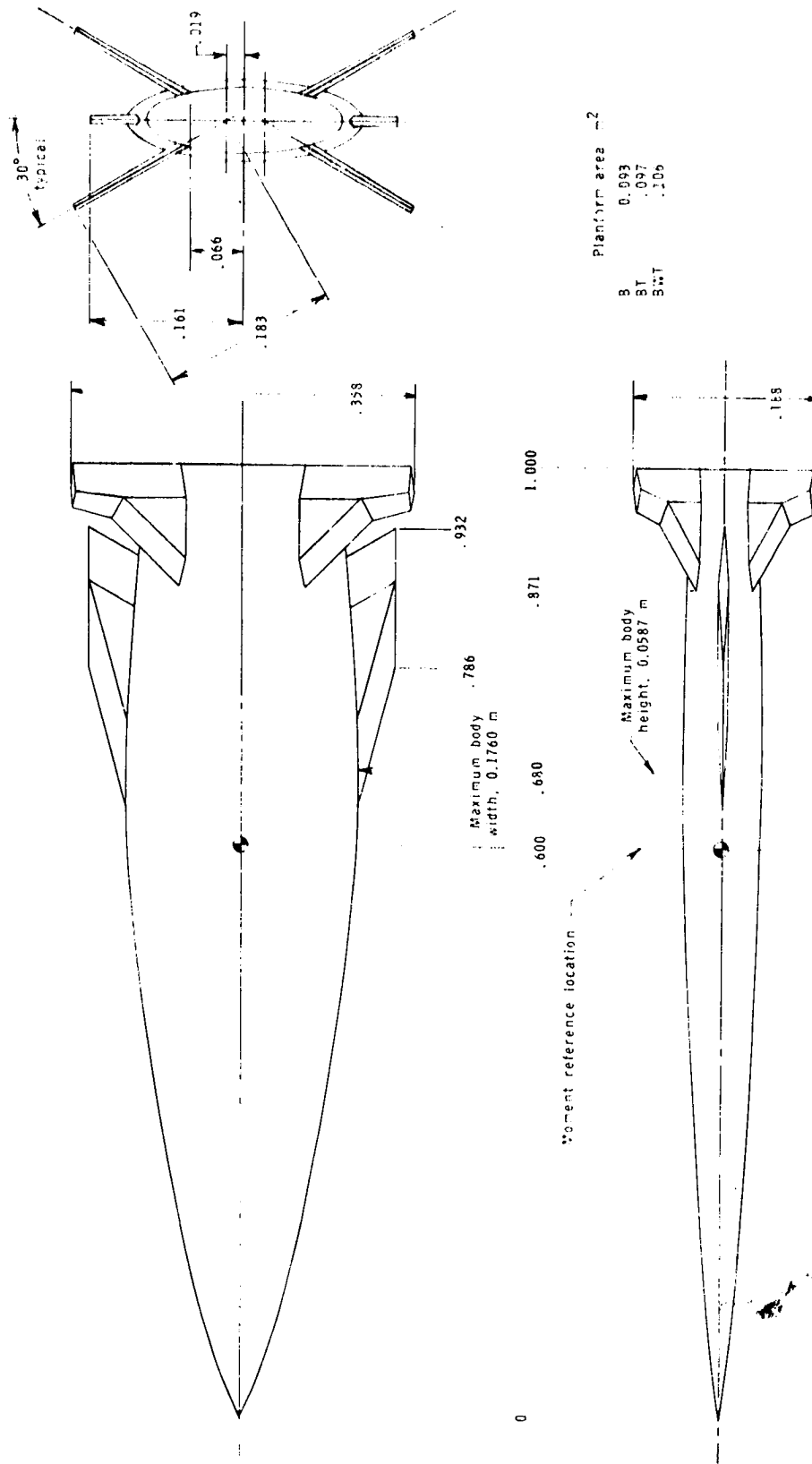
Figure 1.– Continued.

(i) Elliptical configuration concept with pointed nose. Body IX
(Reference length = 0.7112 m).
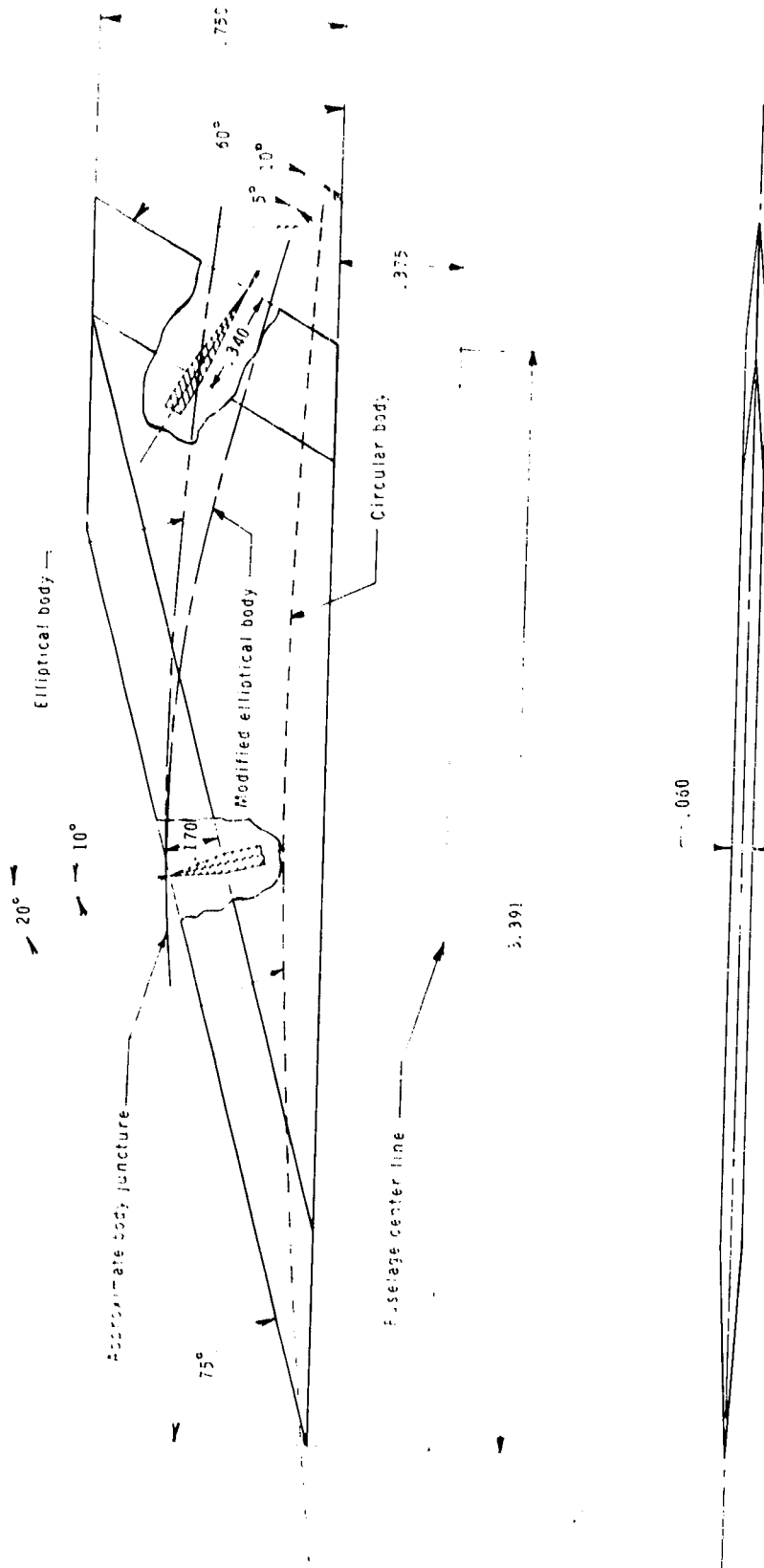
Figure 1.- Continued.

(j) Wing. (Reference length = 0.1016 m.)

Figure 1.- Continued.

Planform area = .0045 m²

.045

.063

.900

.300

.600

.500

.500

14.0°

20°

-10°

45°

.170

.245

.900

.063

7°

14°
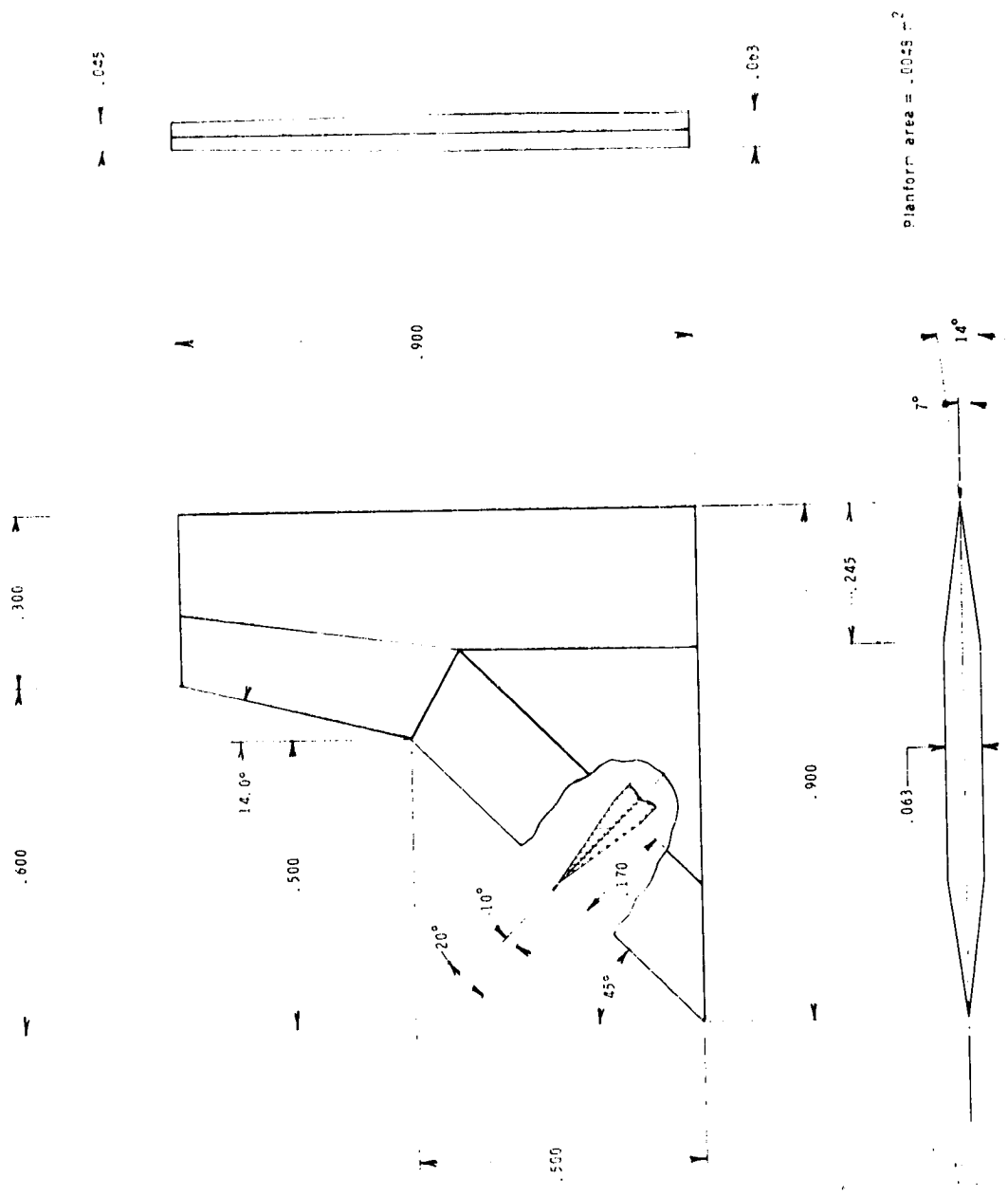
(k) Tail.   (Reference length = 0.1016 m.)
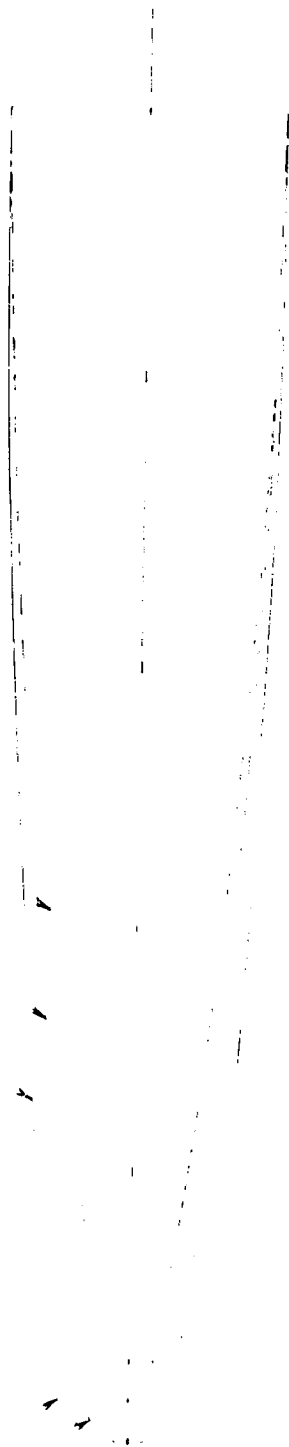
Figure 1.- Continued.

(1) Forebody geometry of circular models. (Reference length = 0.7112 m.)

Figure 1.- Continued.

Large hemispherical nose

Small hemispherical nose

Pointed nose

.0294-m radius

.0154-m radius
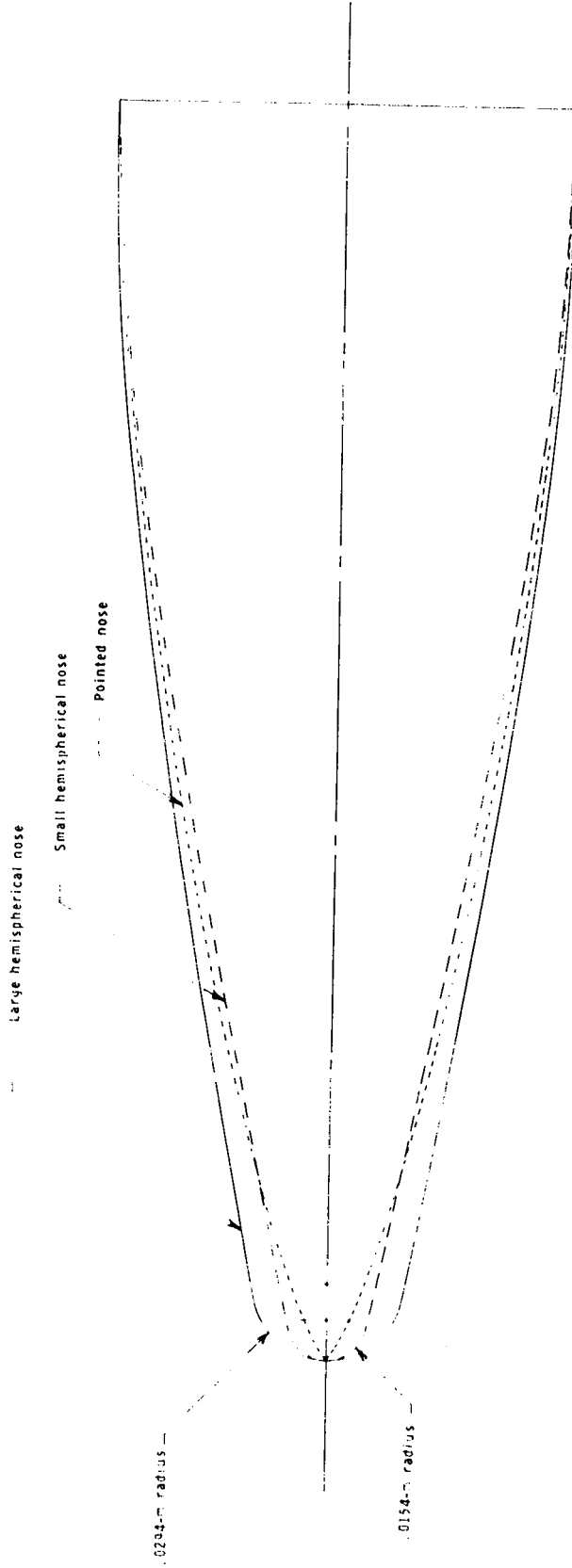
(m) Forebody geometry of modified models. (Reference length = 0.7112 m.)

Figure 1.- Continued.

26

.680   1.000

Circular afterbody

Variable afterbody

Planform view

Elliptical afterbody

Circular afterbody

Elliptical afterbody

Variable afterbody

Side view
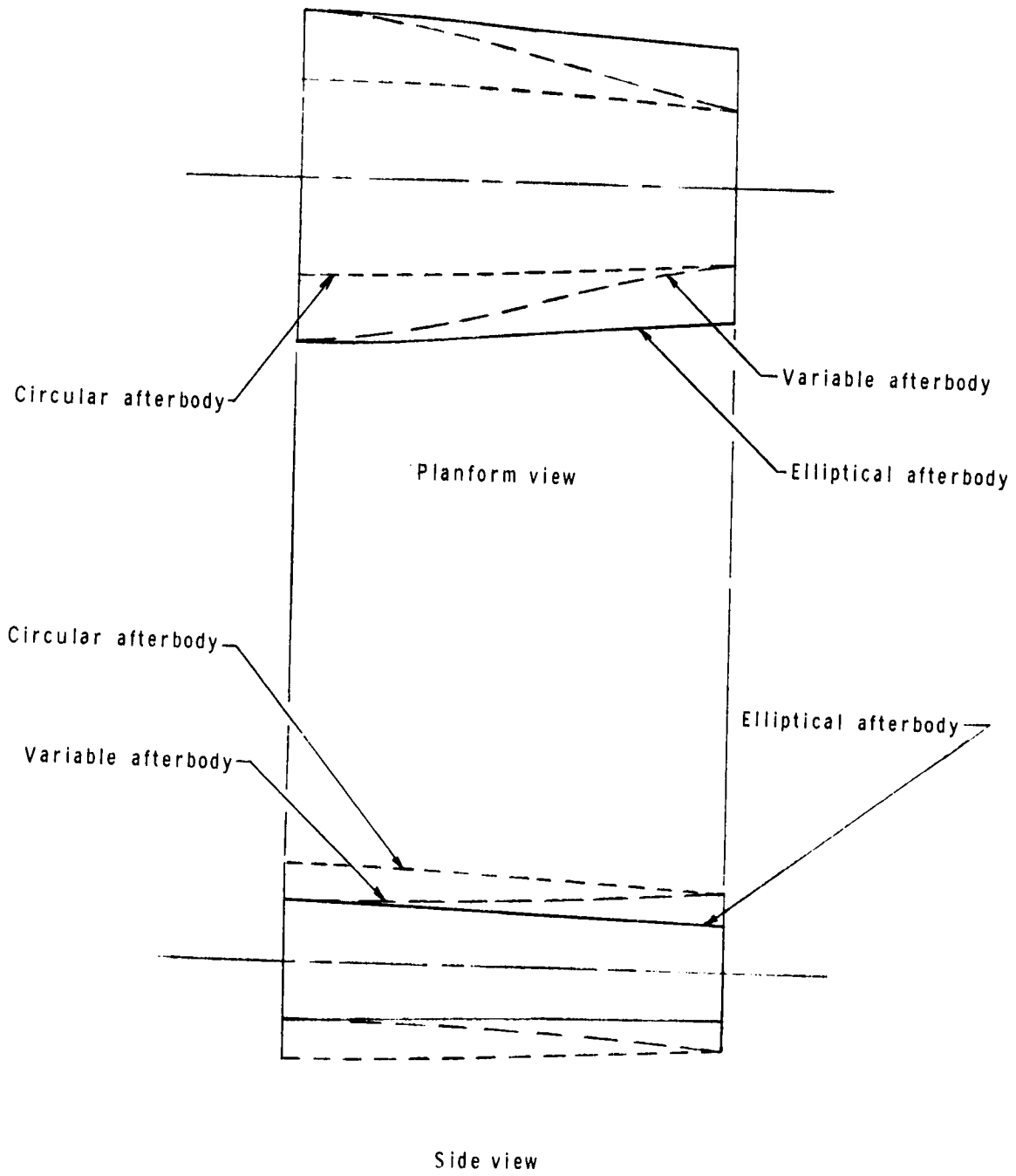
(n) Afterbodies of models.   (Reference length = 0.7112 m.)

Figure 1.- Concluded.

Figure 2.- Photograph of model components.

L-77-8400
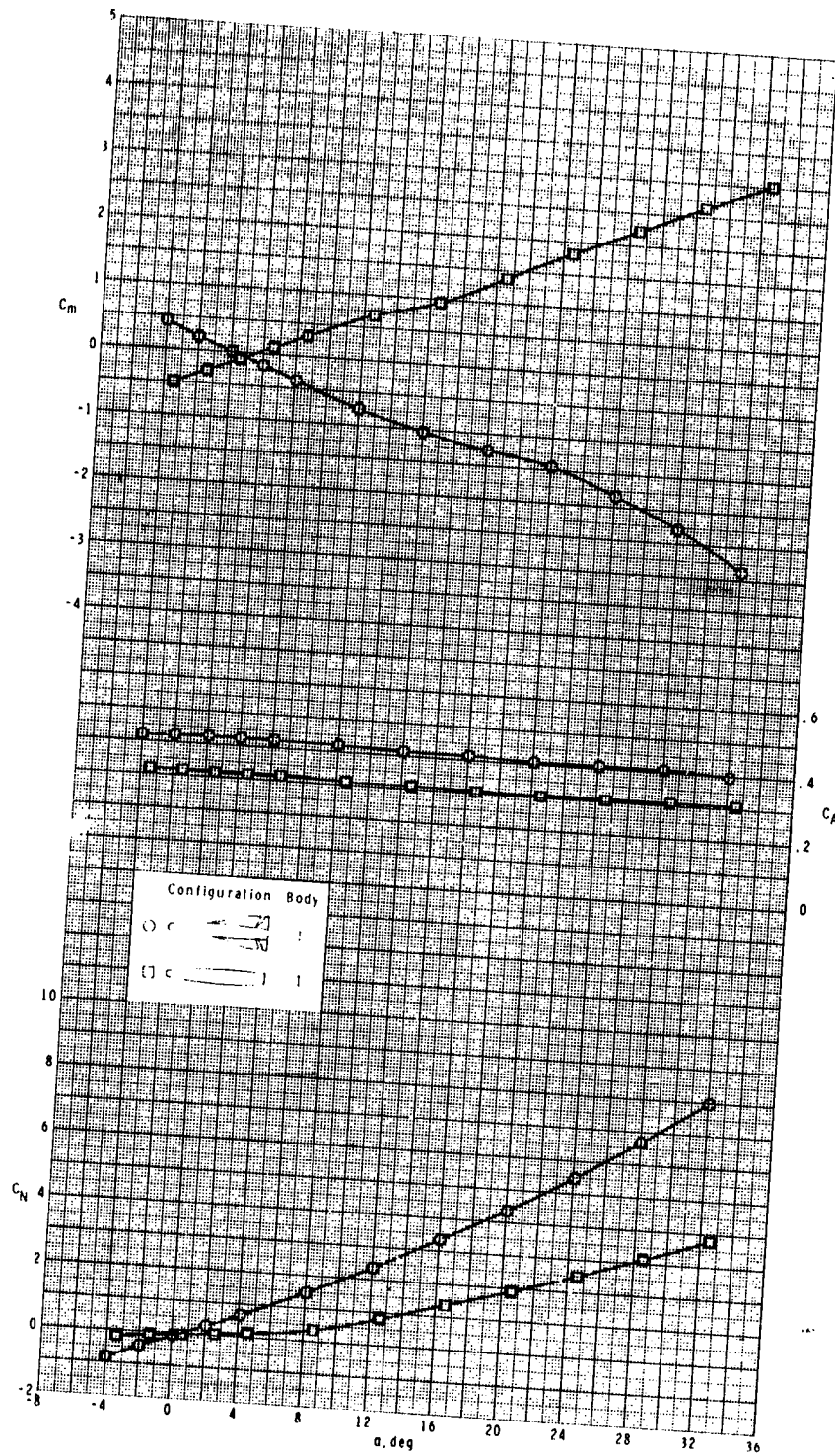
Figure 3.- Effect of wing and tail components on longitudinal aerodynamic characteristics of circular missile concept having large hemispherical nose.
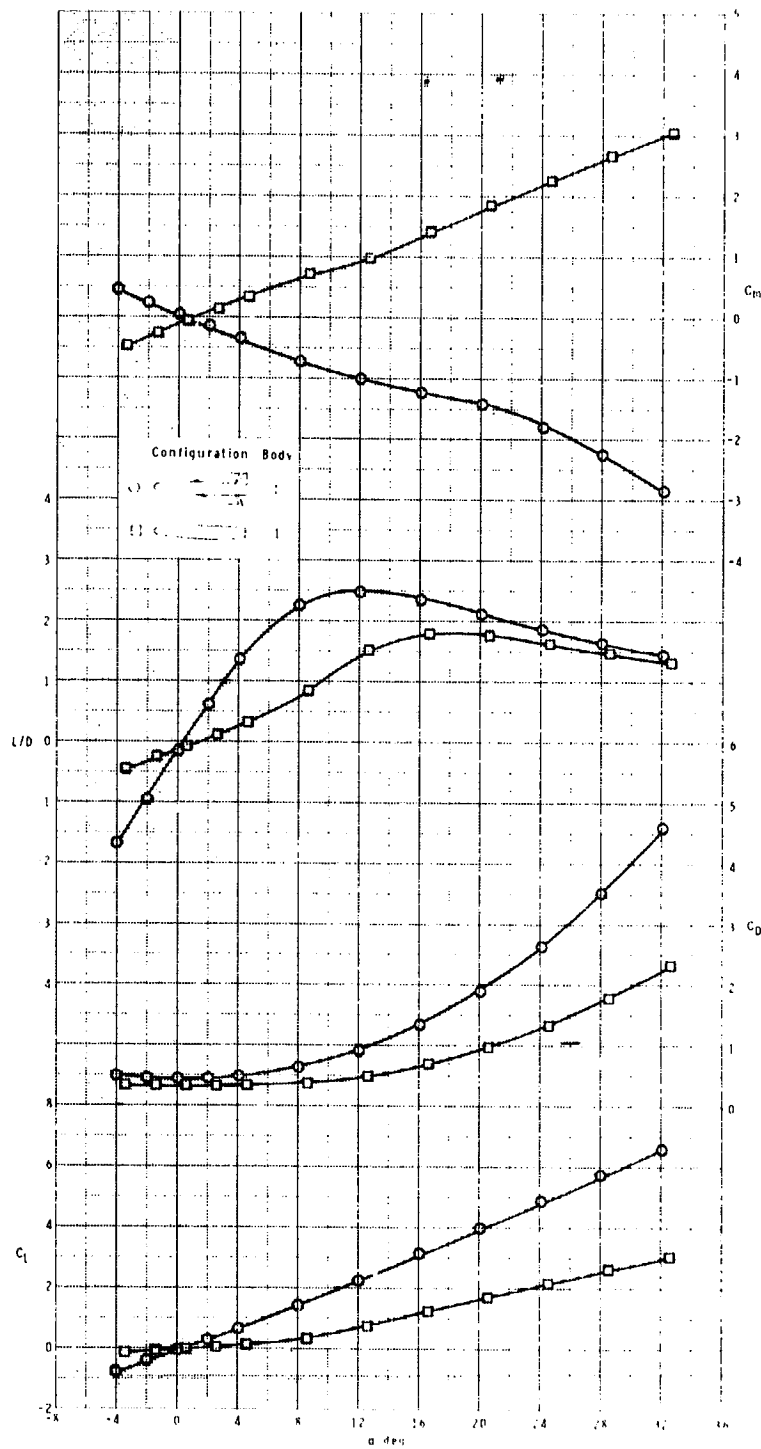
Figure 3.- Concluded.
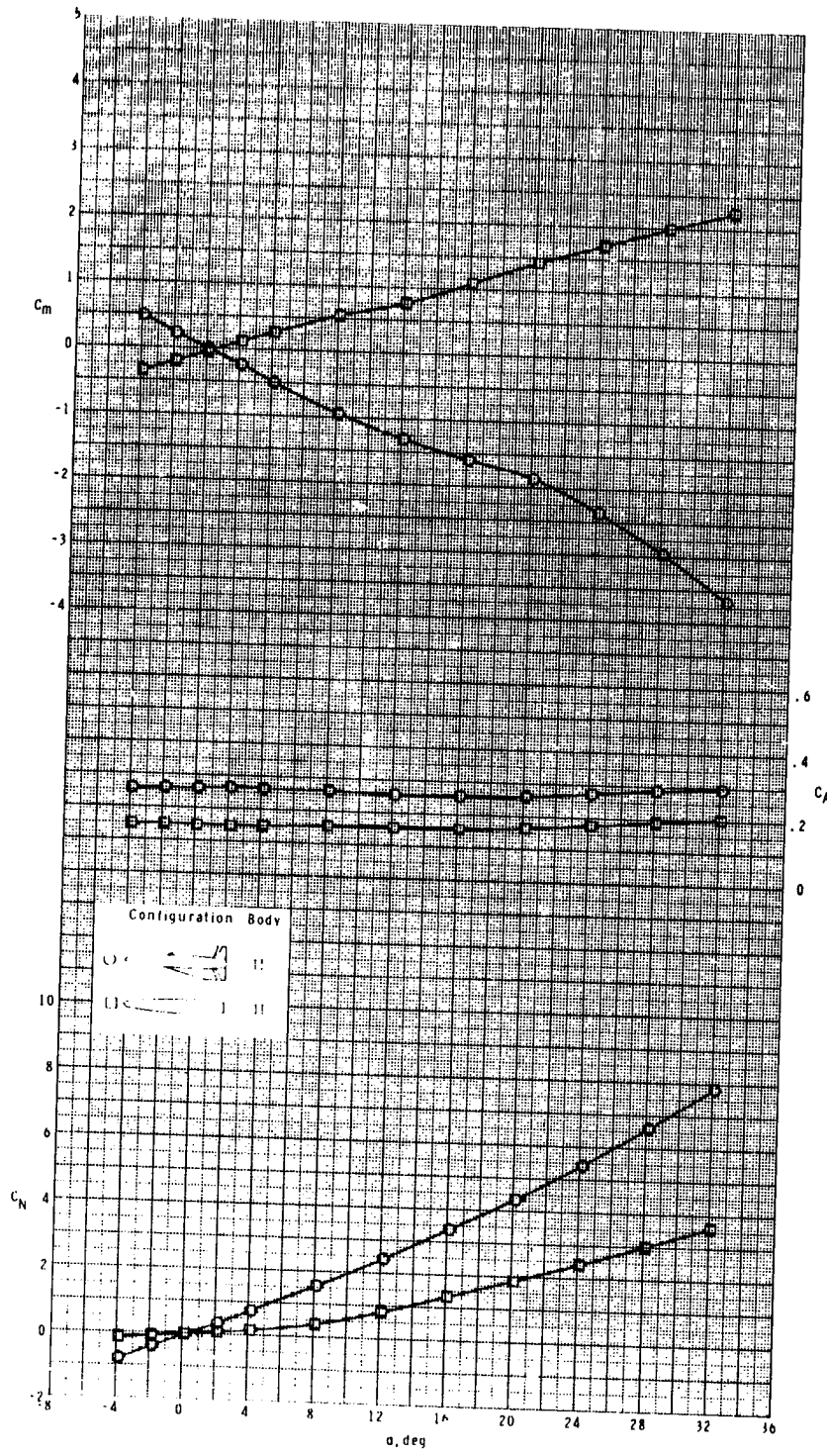
Figure 4.- Effect of wing and tail components on longitudinal aerodynamic characteristics of circular missile concept having small hemispherical nose.
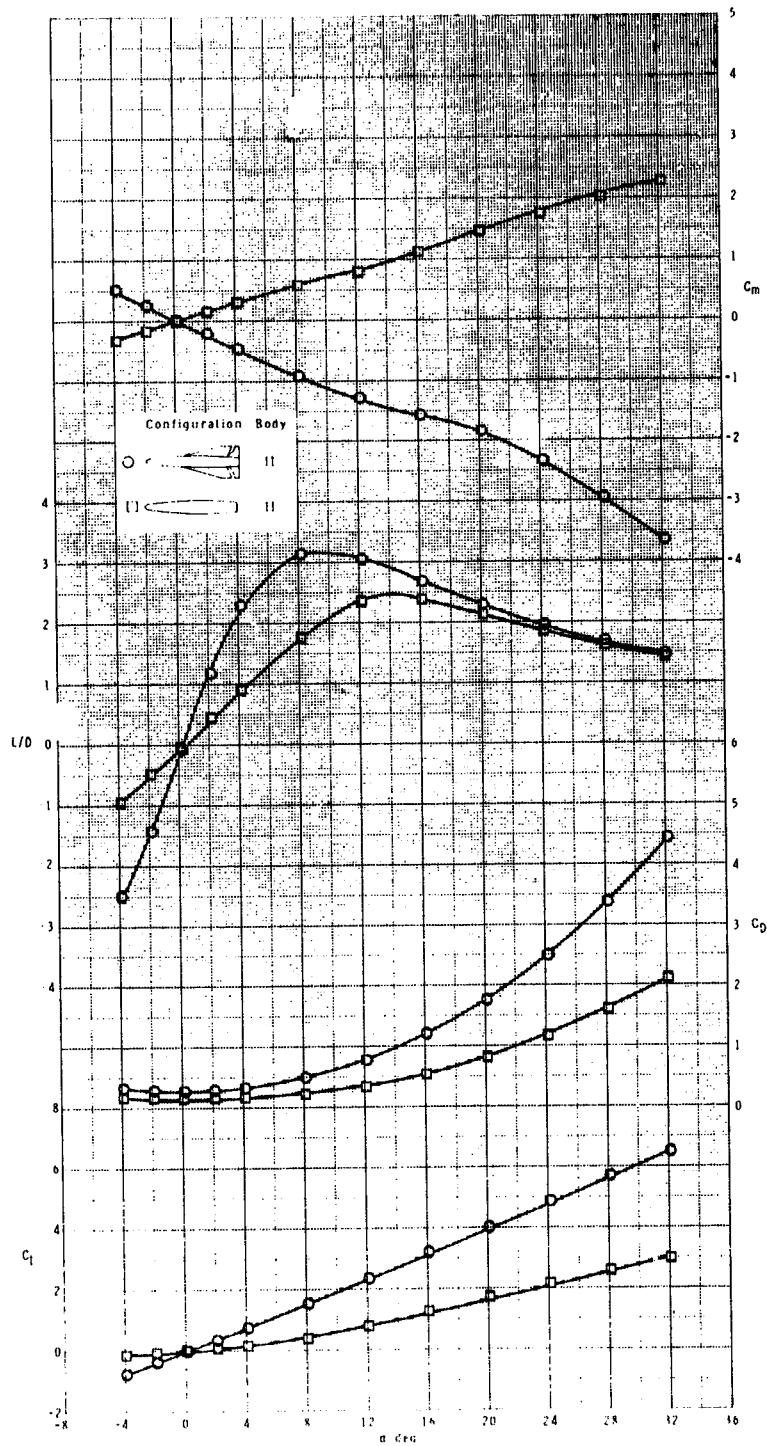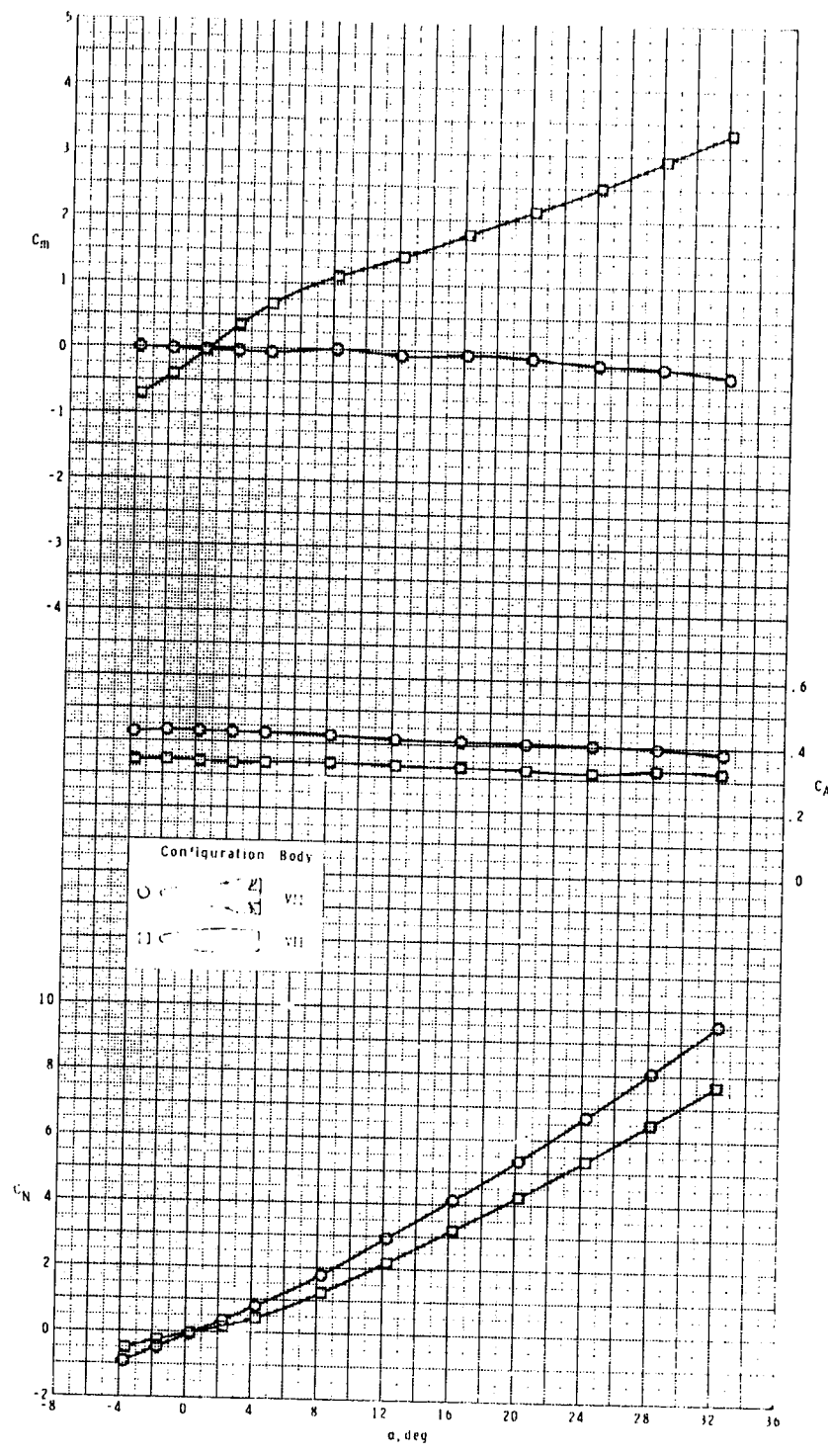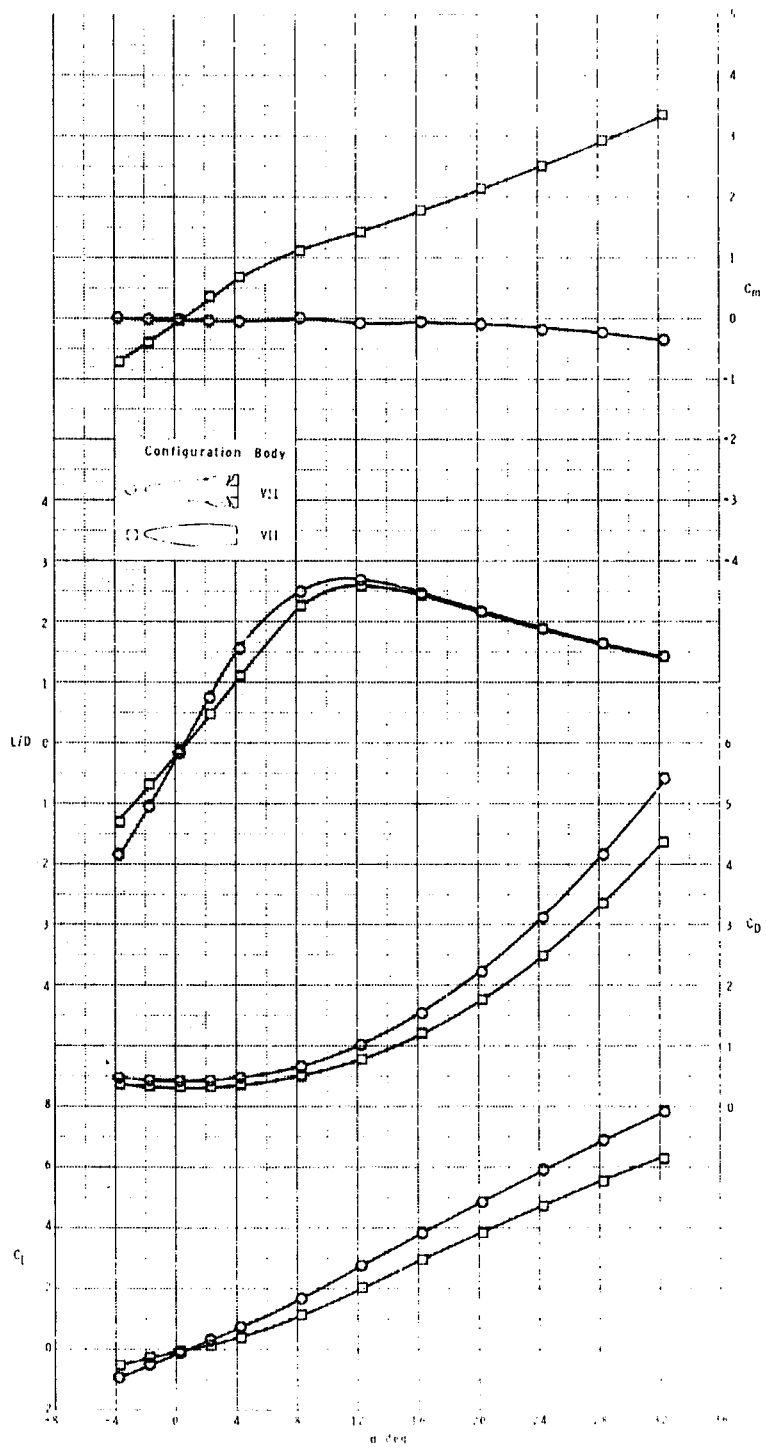
Figure 4.- Concluded.

32
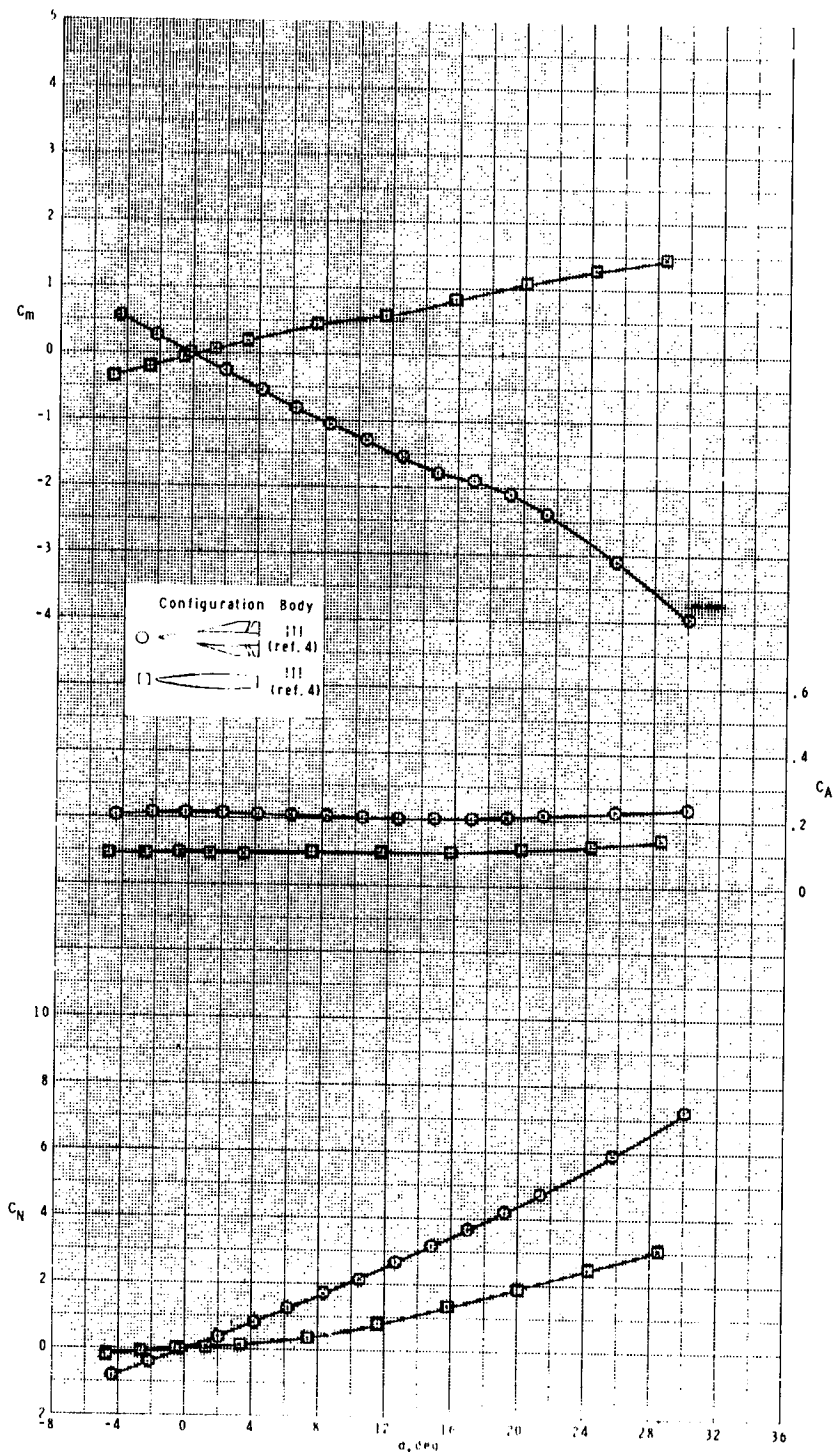
Figure 5.- Effect of wing and tail components on longitudinal aerodynamic
characteristics of circular missile concept having pointed nose.
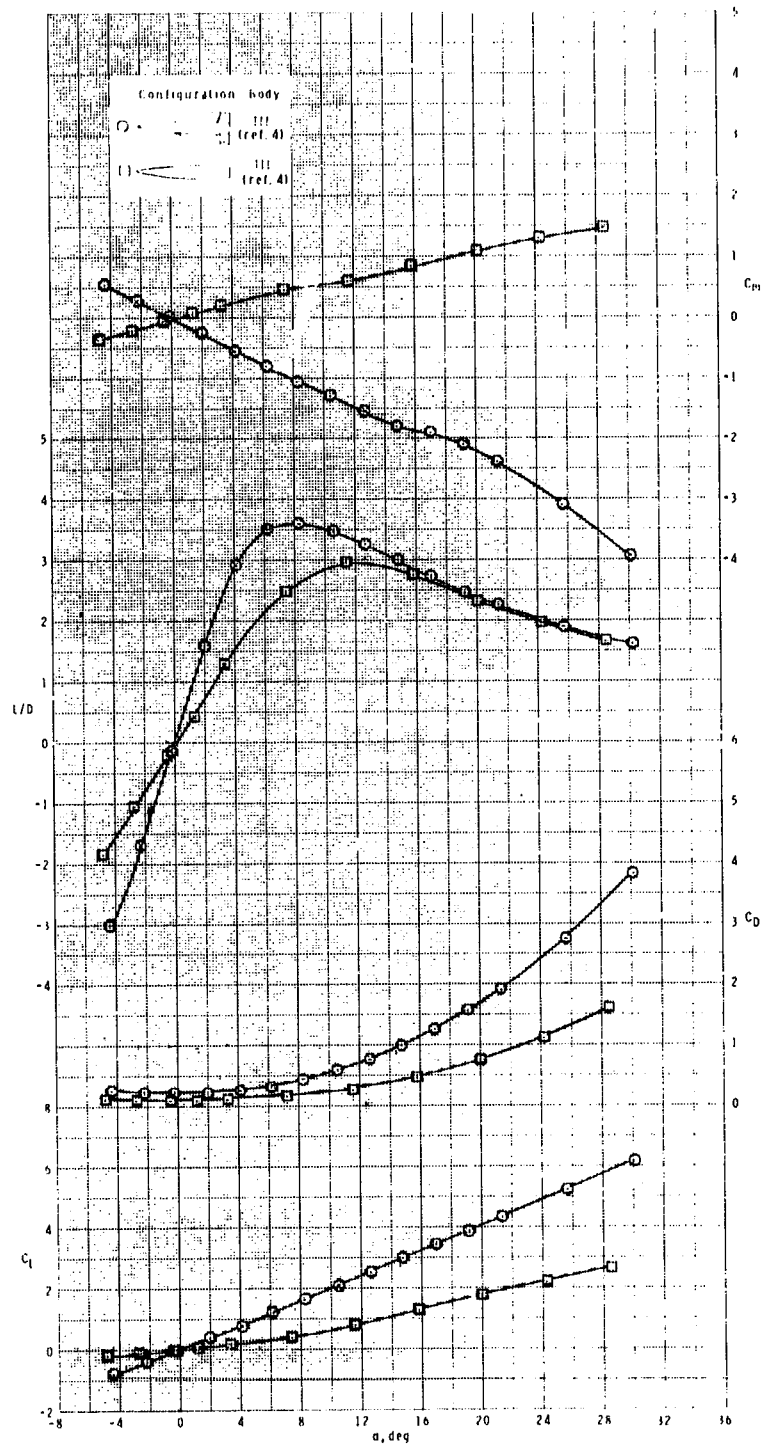
Figure 5.- Concluded.
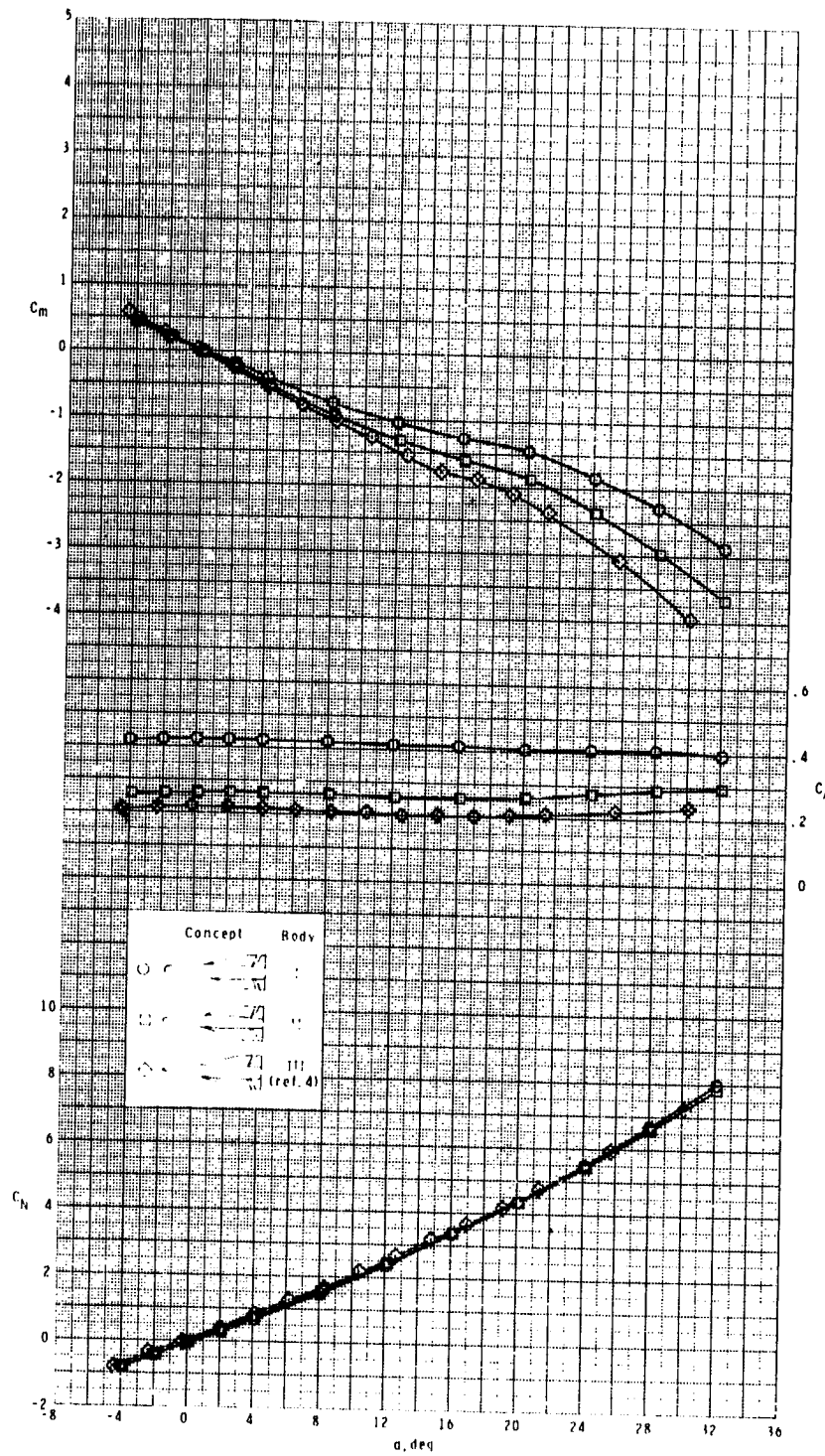
Figure 6.- Effect of nose size on longitudinal aerodynamic characteristics of missile concept having circular cross-sectional body.
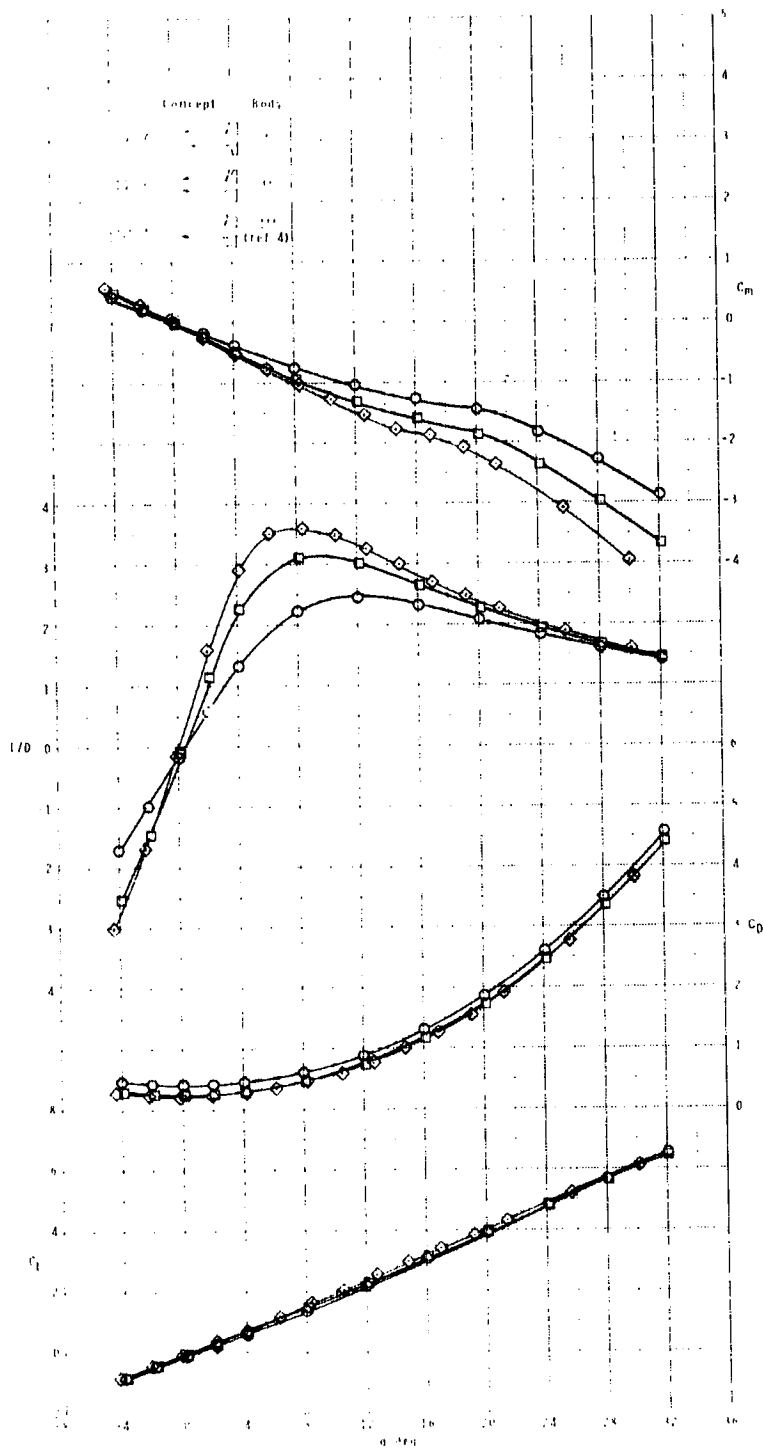
Figure 6.- Concluded.
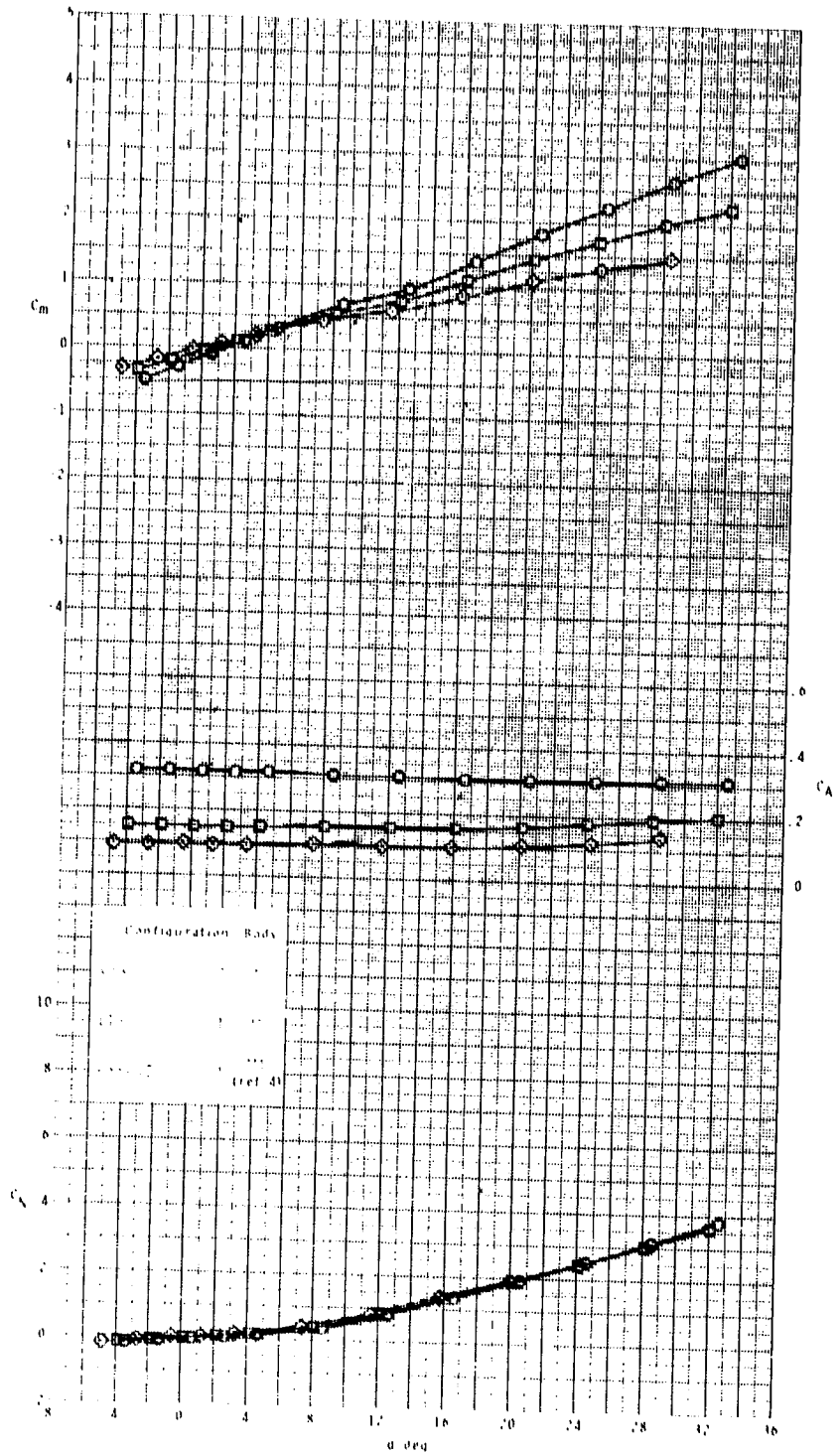
Figure 7.- Effect of nose size on longitudinal aerodynamic characteristics
of circular body.
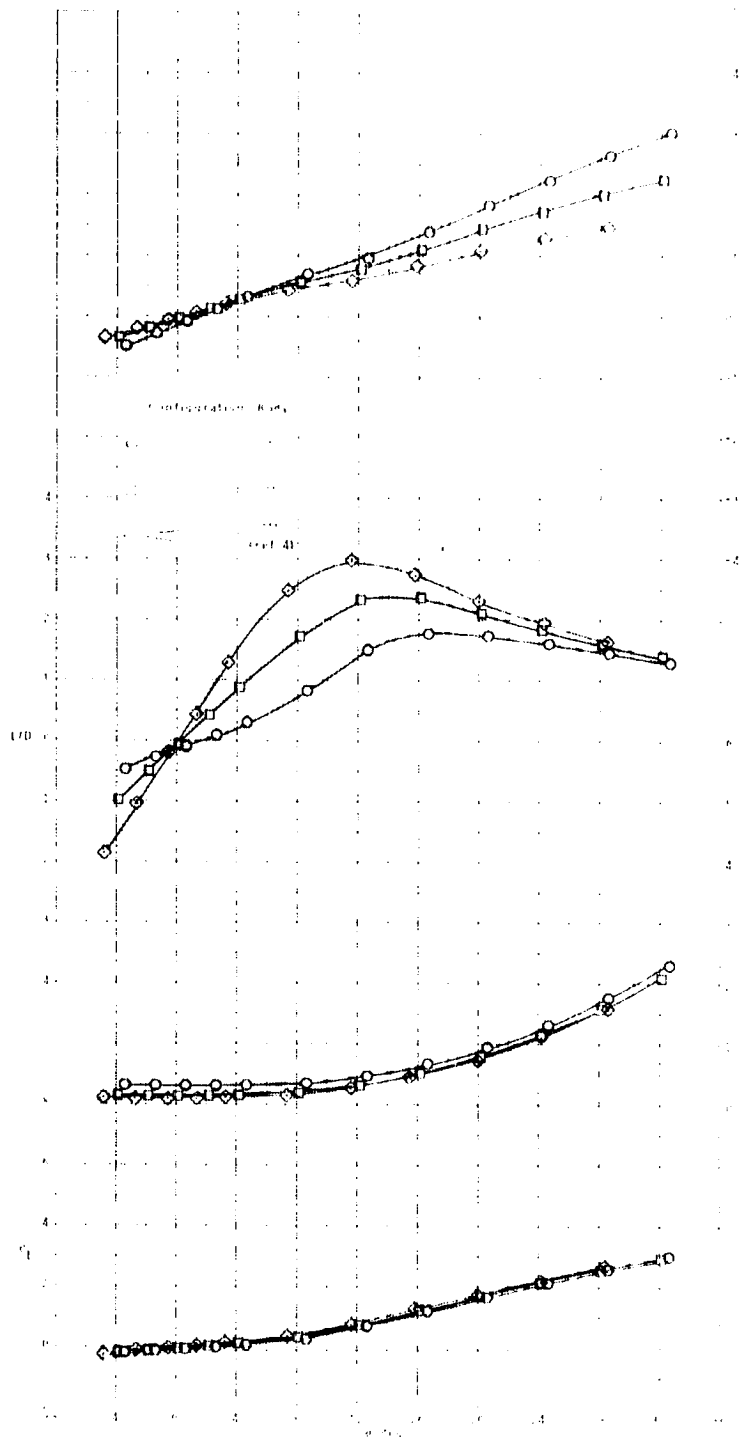
Figure 7.- Concluded.
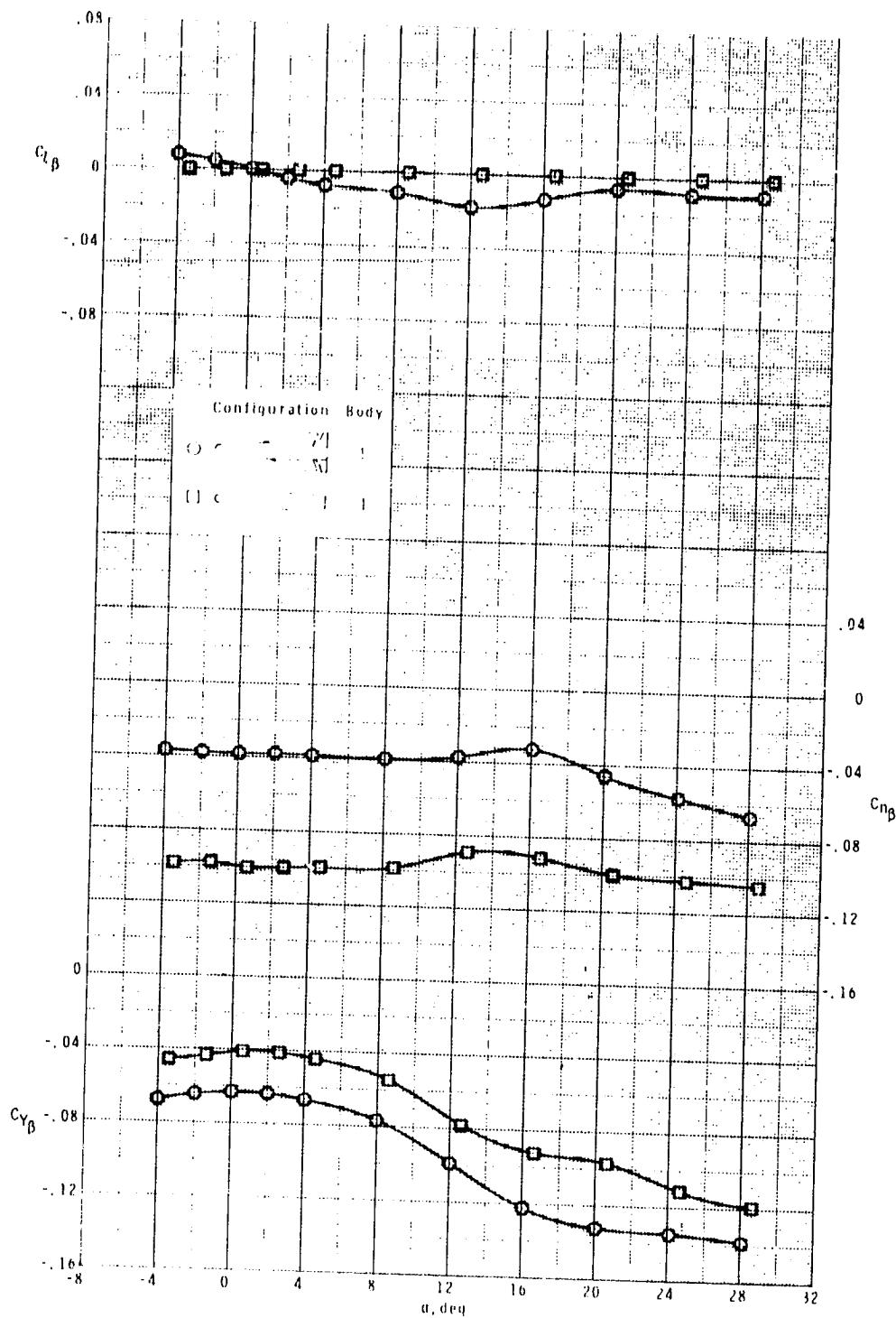
Figure 8.- Effect of wing and tail components on lateral-directional stability parameters of circular missile concept having large hemispherical nose.
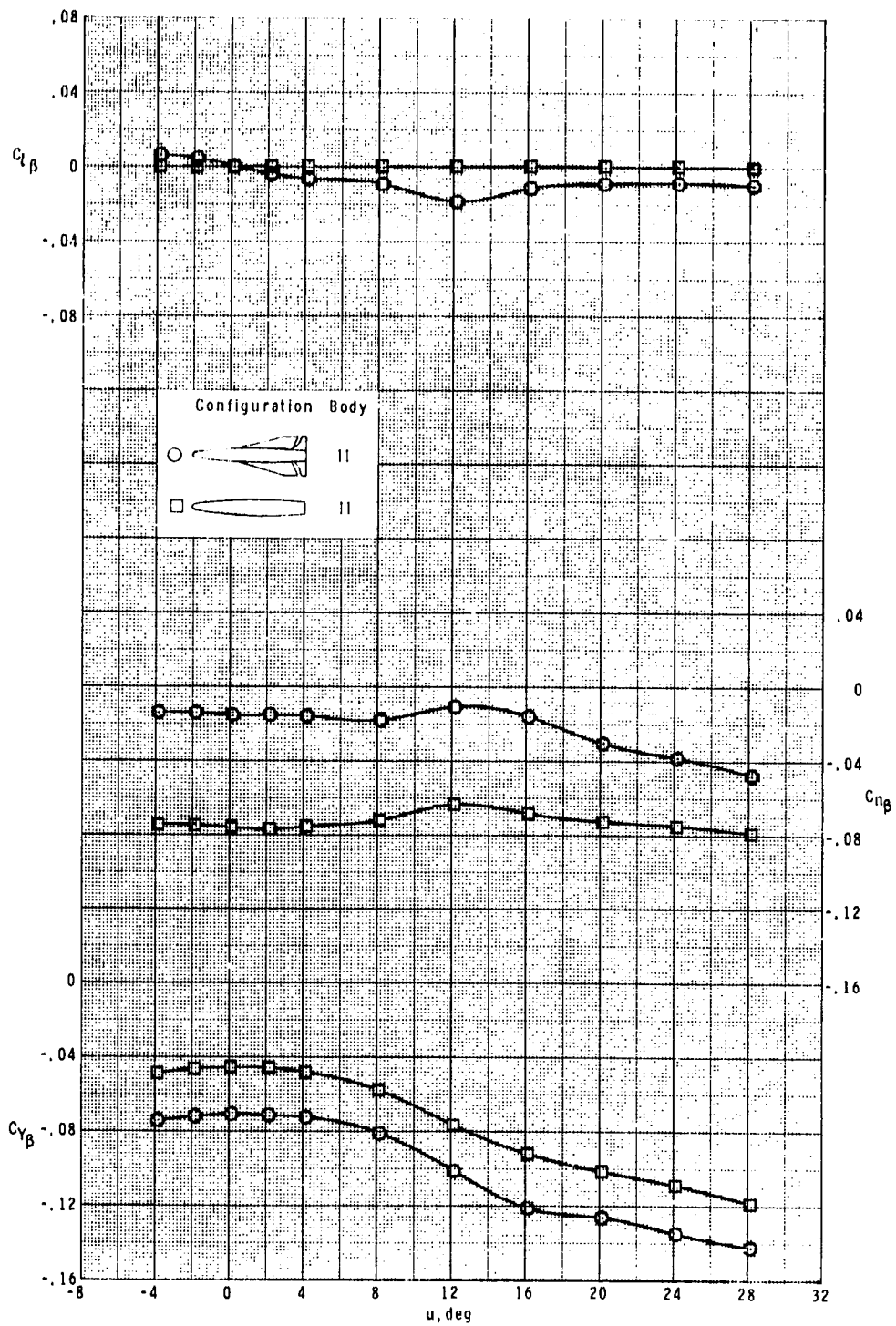
Figure 9.- Effect of wing and tail components on lateral-directional stability parameters of circular missile concept having small hemispherical nose.
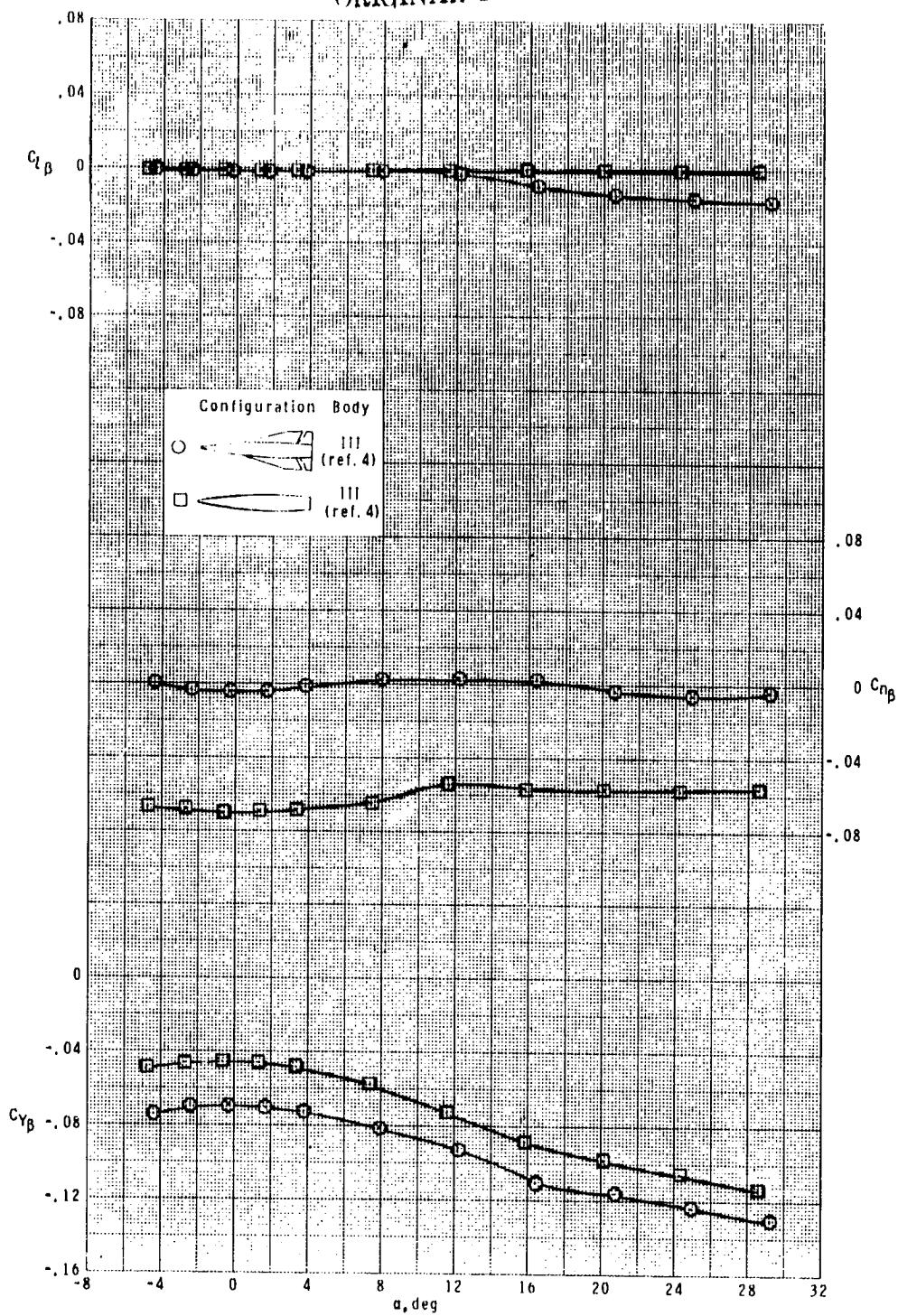
Figure 10.- Effect of wing and tail components on lateral-directional stability
parameters of circular missile concept having pointed nose.
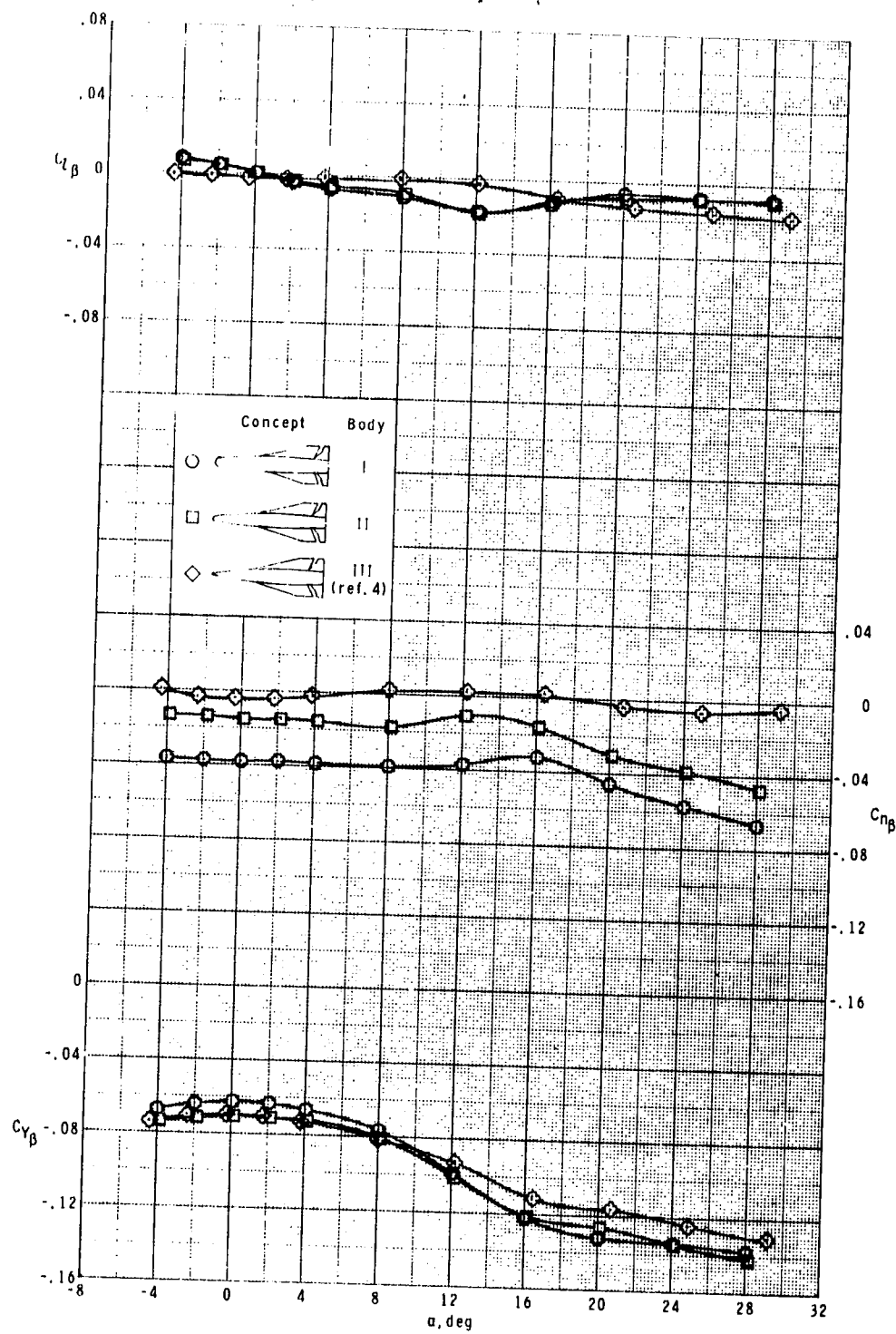
Figure 11.- Effect of nose size on lateral-directional stability parameters
of missile concept having circular cross-sectional body.

42
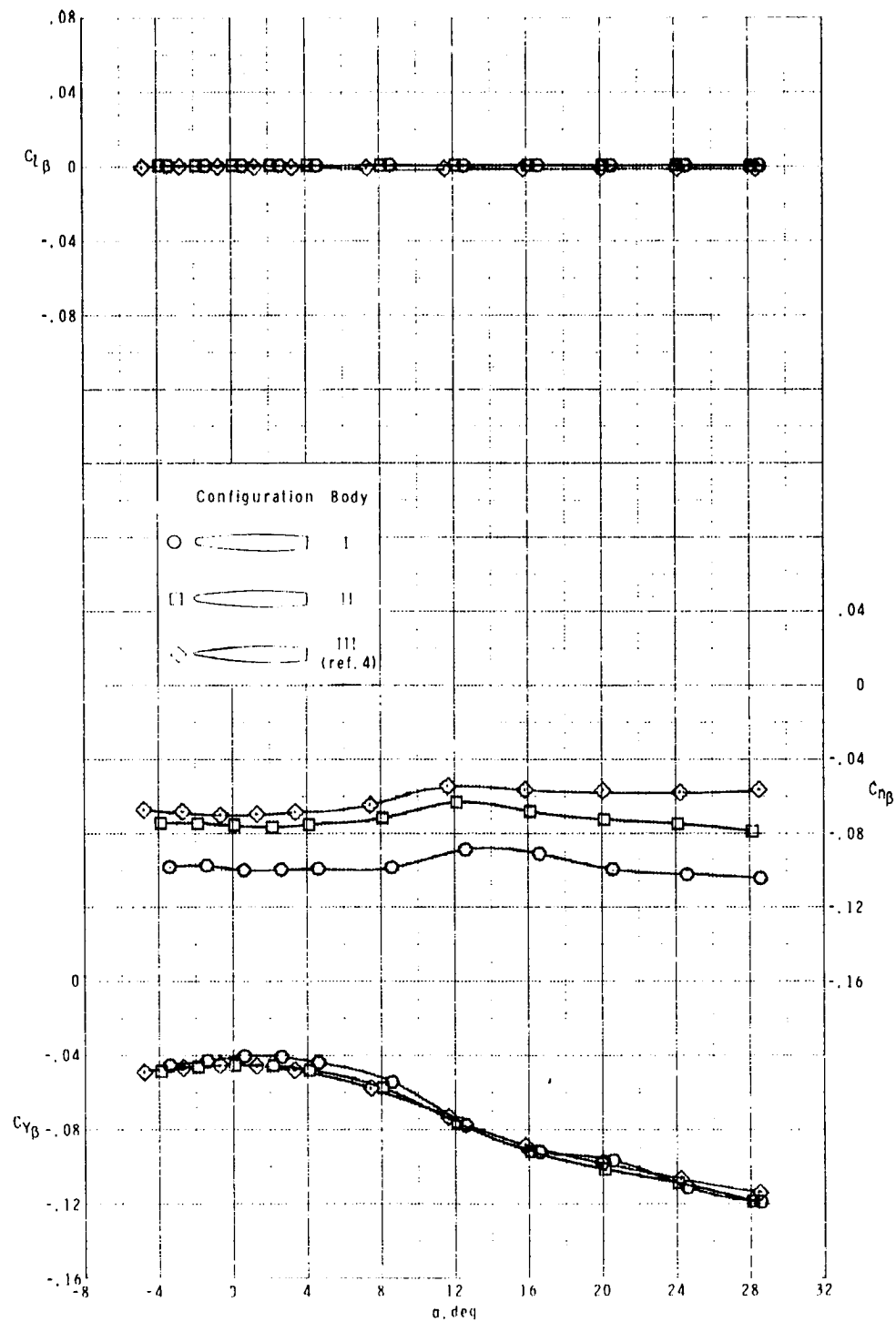
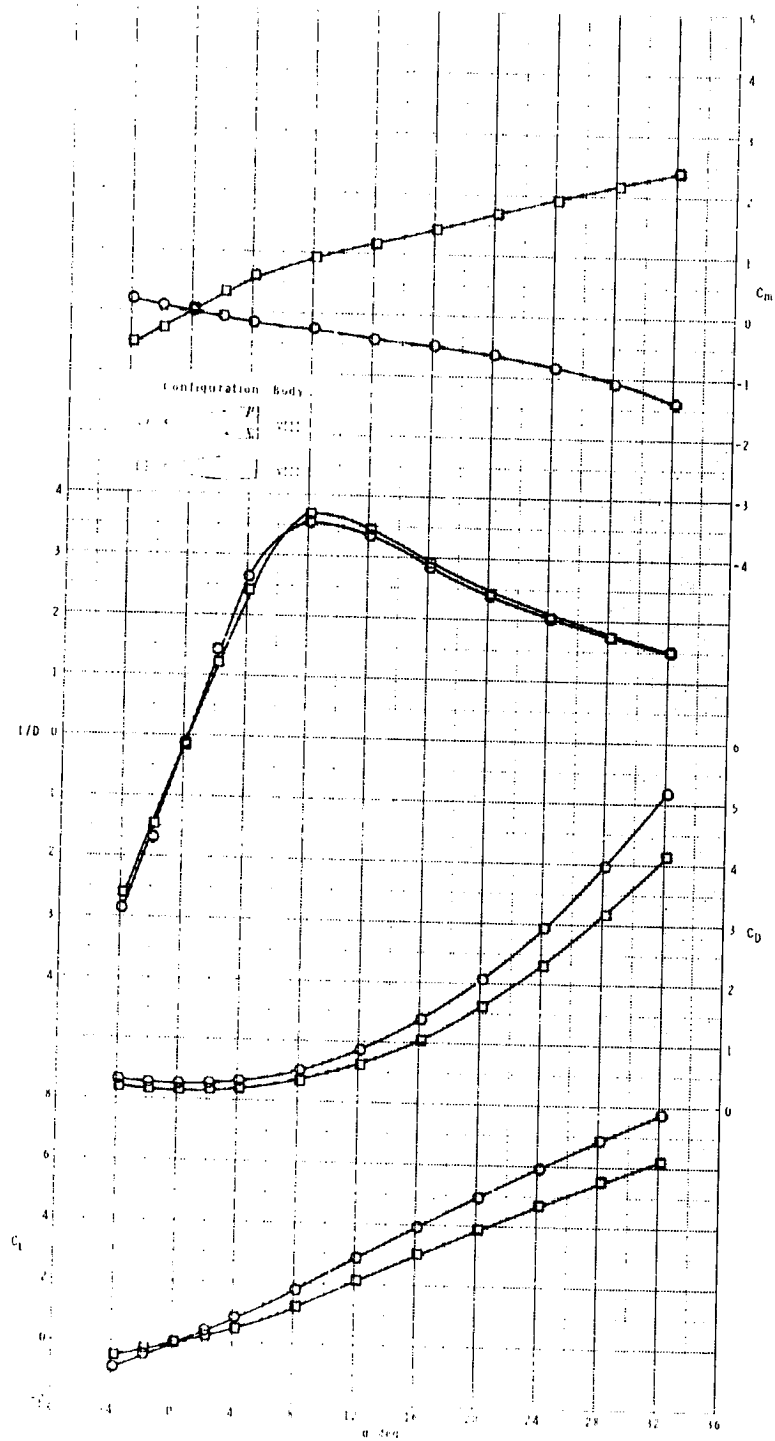Figure 12.- Effect of nose size on lateral-directional stability parameters on circular body.
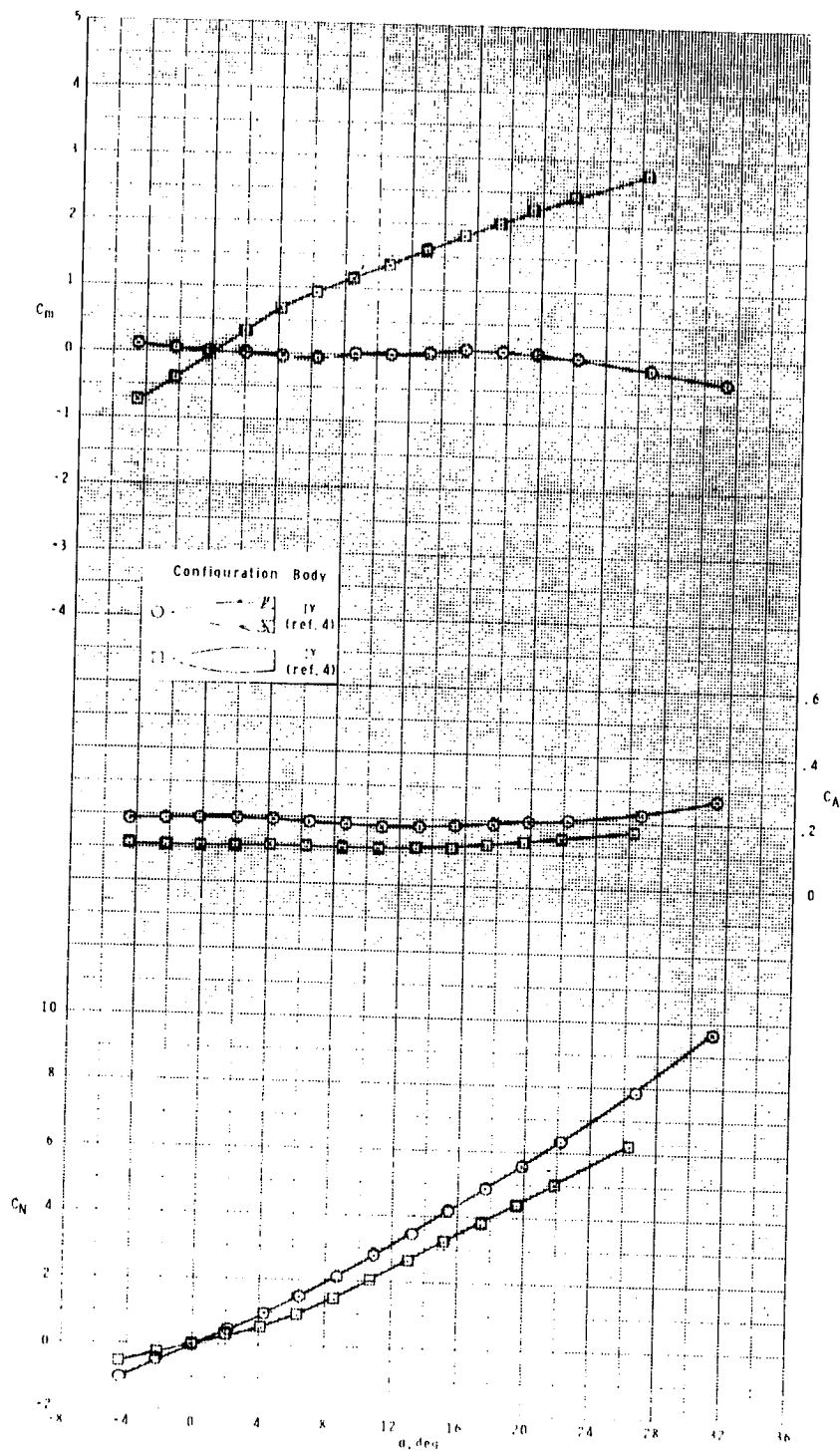
43
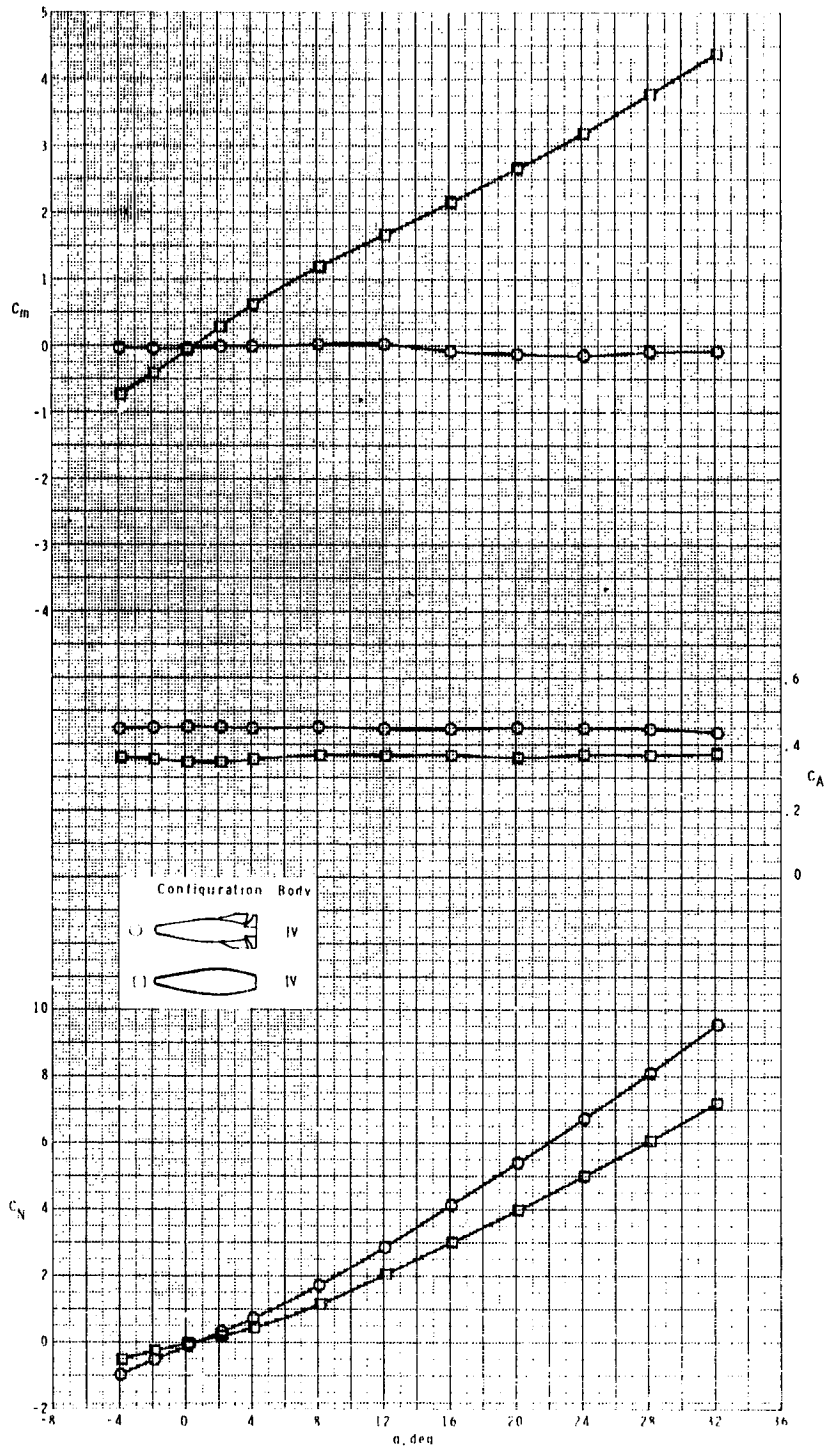
Figure 13.- Effect of wing and tail components on longitudinal aerodynamic characteristics of missile concept having variable cross-sectional eccentricity of forebody and afterbody with circular base and large hemispherical nose.

44
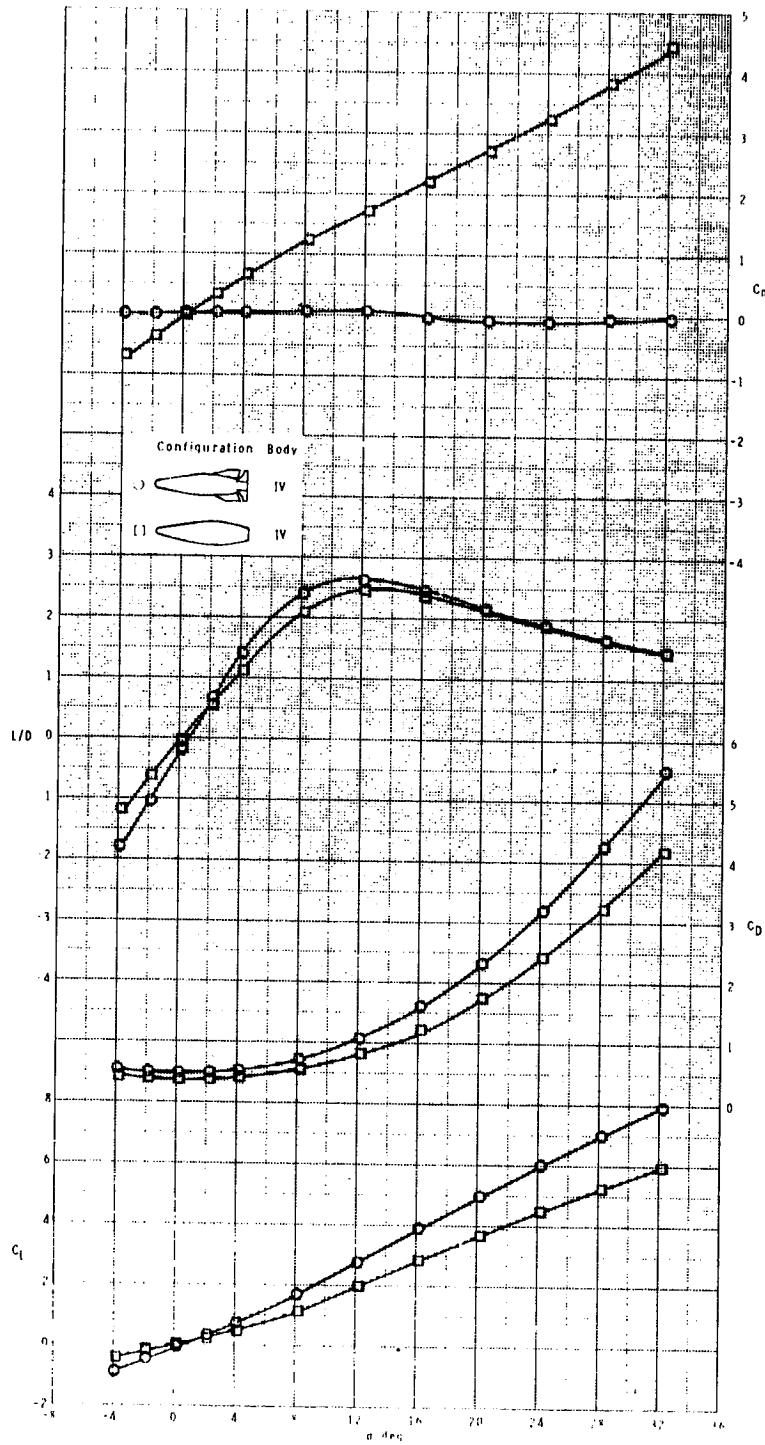
Figure 13.- Concluded.

45
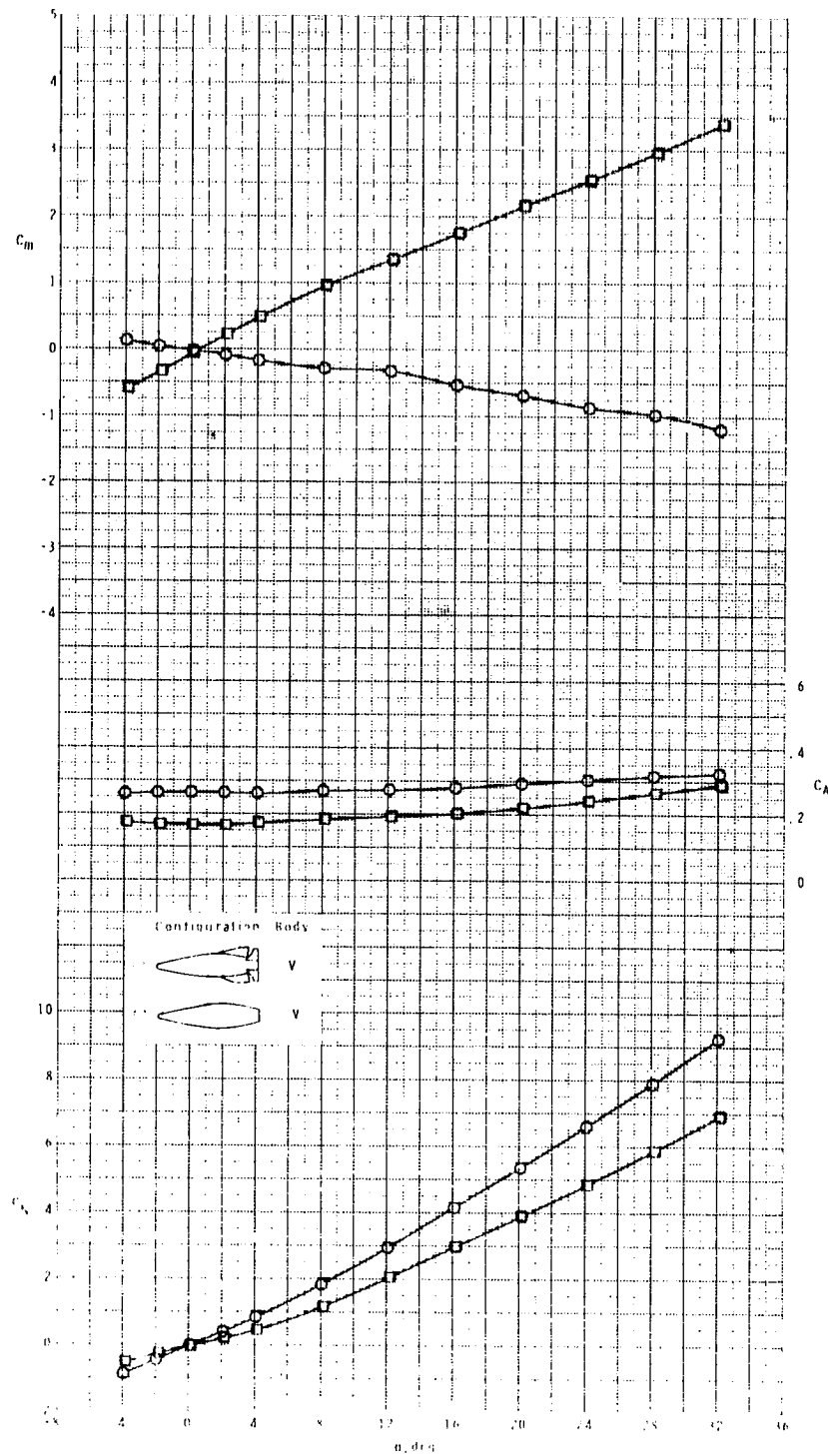
Figure 14.- Effect of wing and tail components on longitudinal aerodynamic characteristics of missile concept having variable cross-sectional eccentricity of forebody and afterbody with circular base and small hemispherical nose.

46
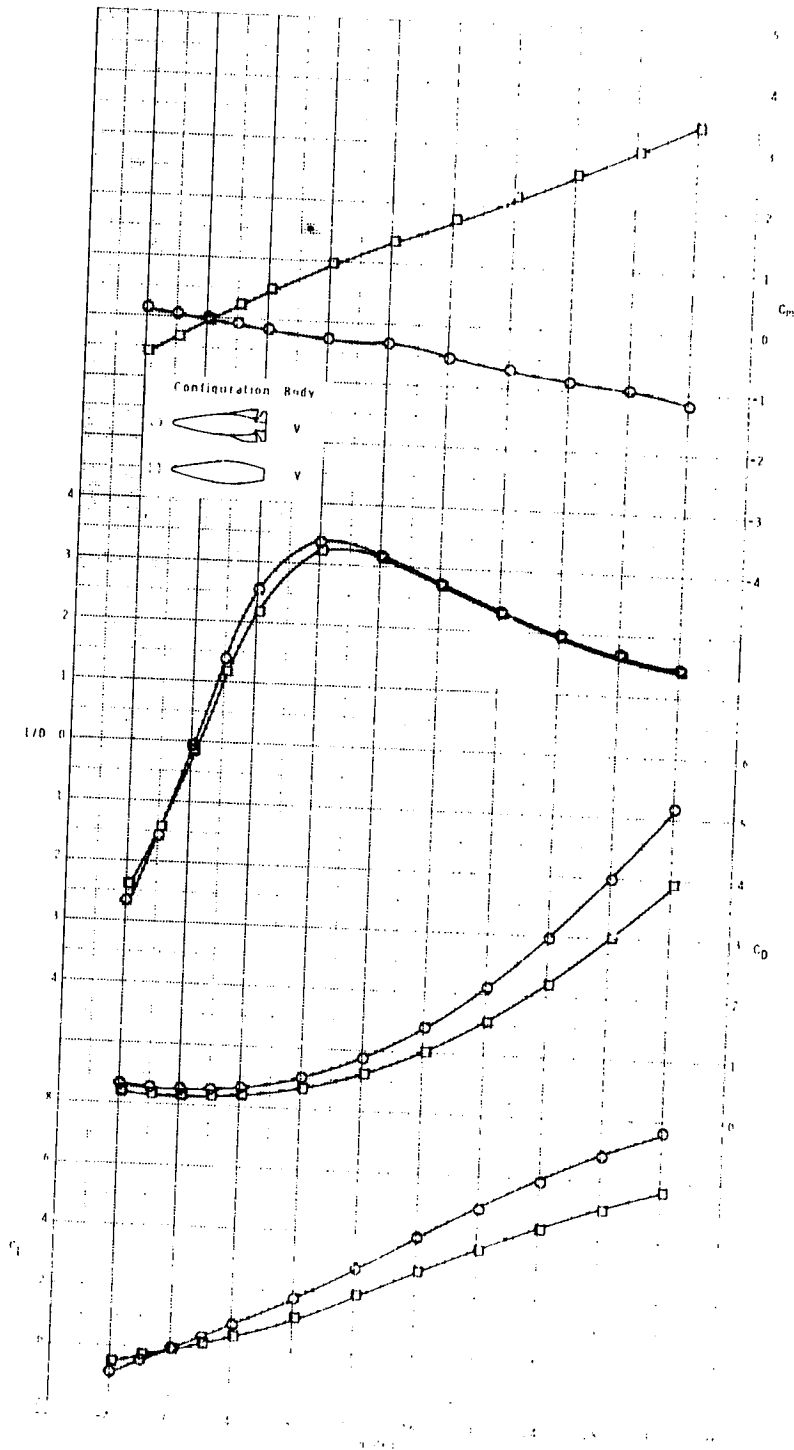
Figure 14.- Concluded.
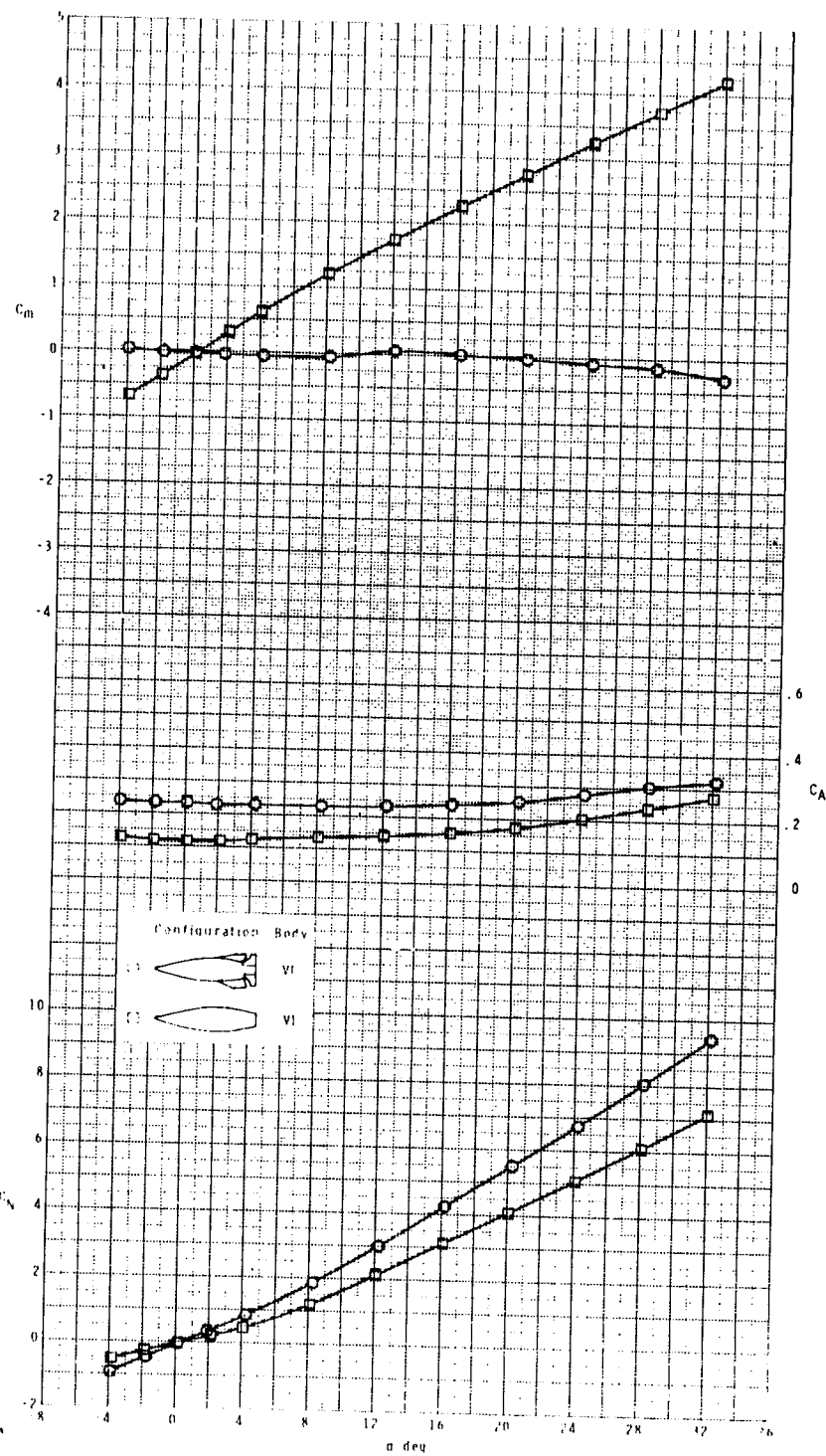
Figure 15.- Effect of wing and tail components on longitudinal aerodynamic characteristics of missile concept having constant cross-sectional eccentricity of forebody and variable cross-sectional eccentricity of afterbody with circular base and pointed nose.
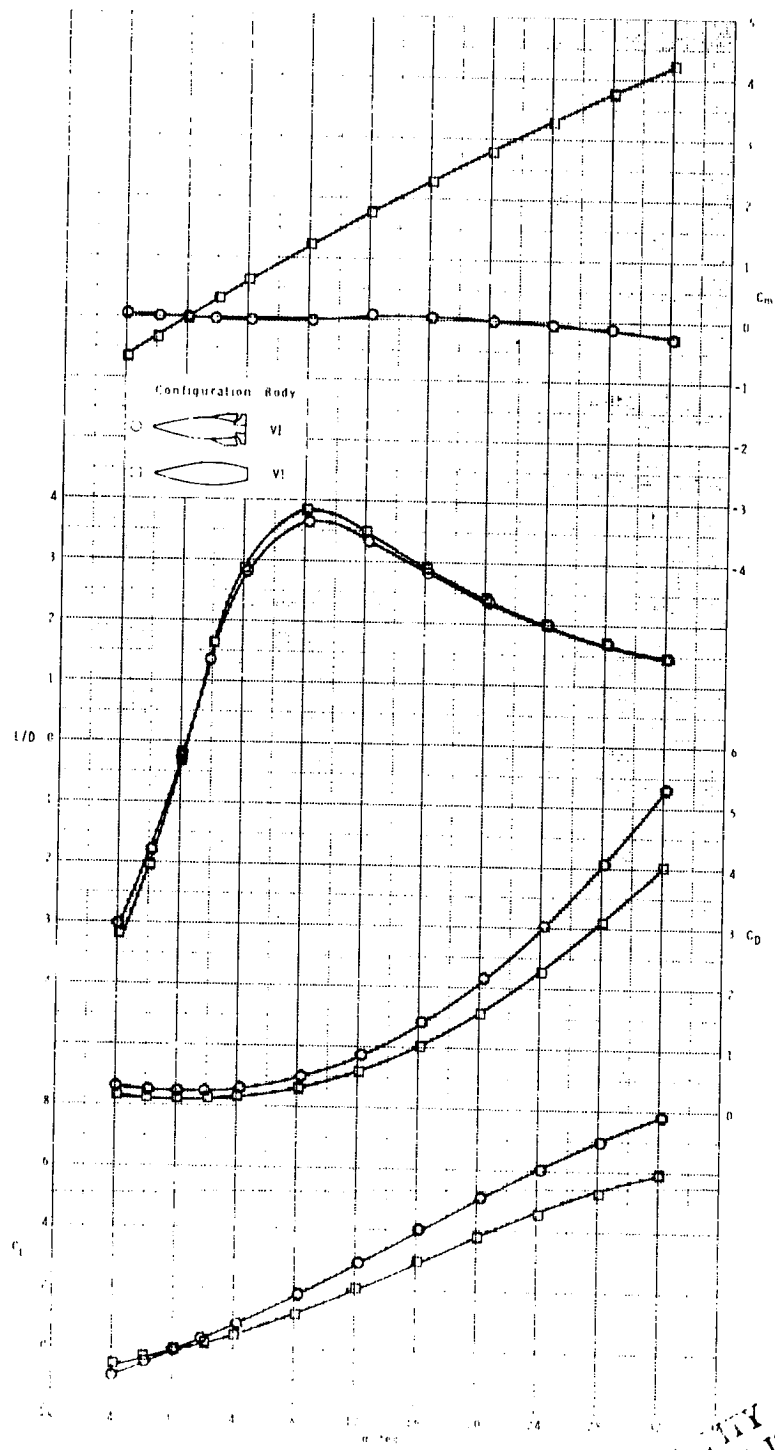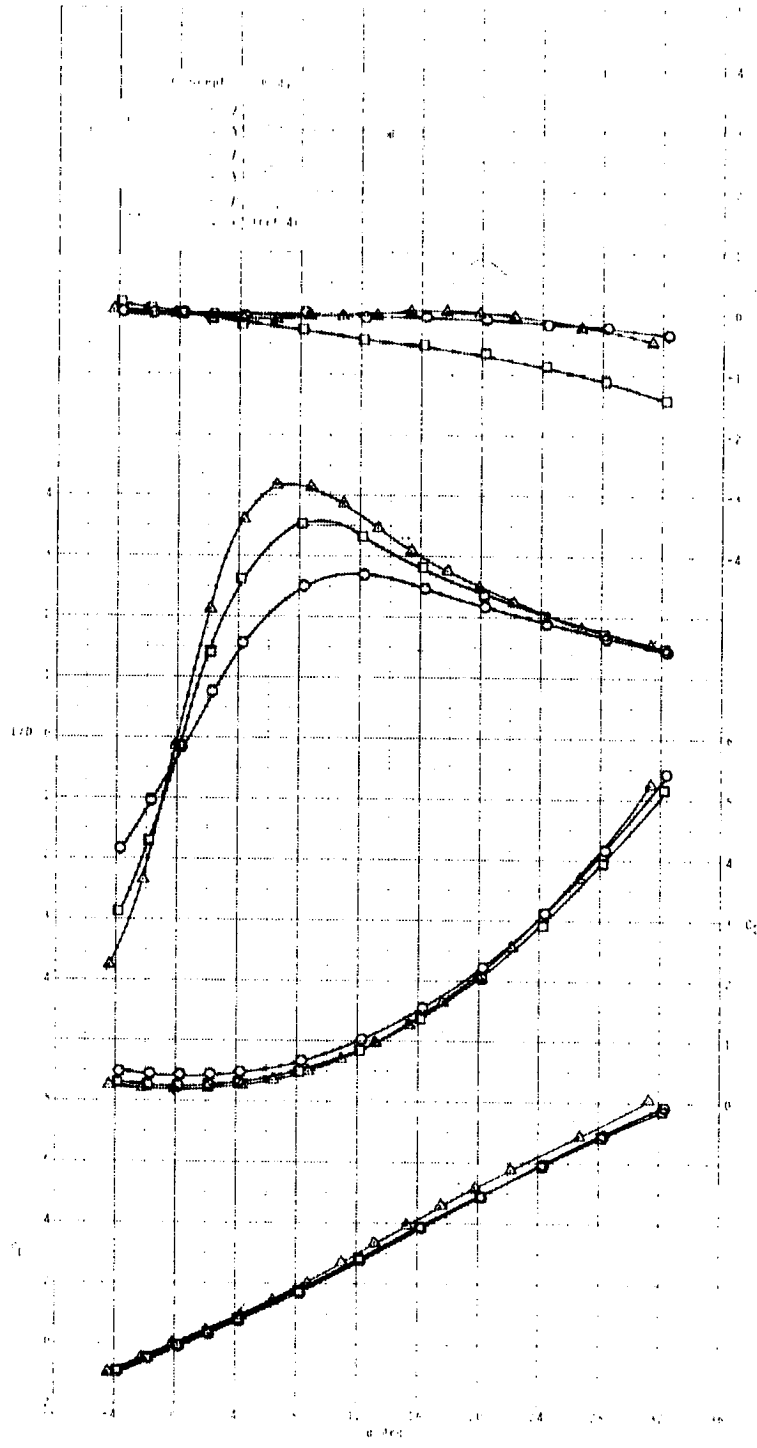
Figure 15.- Concluded.
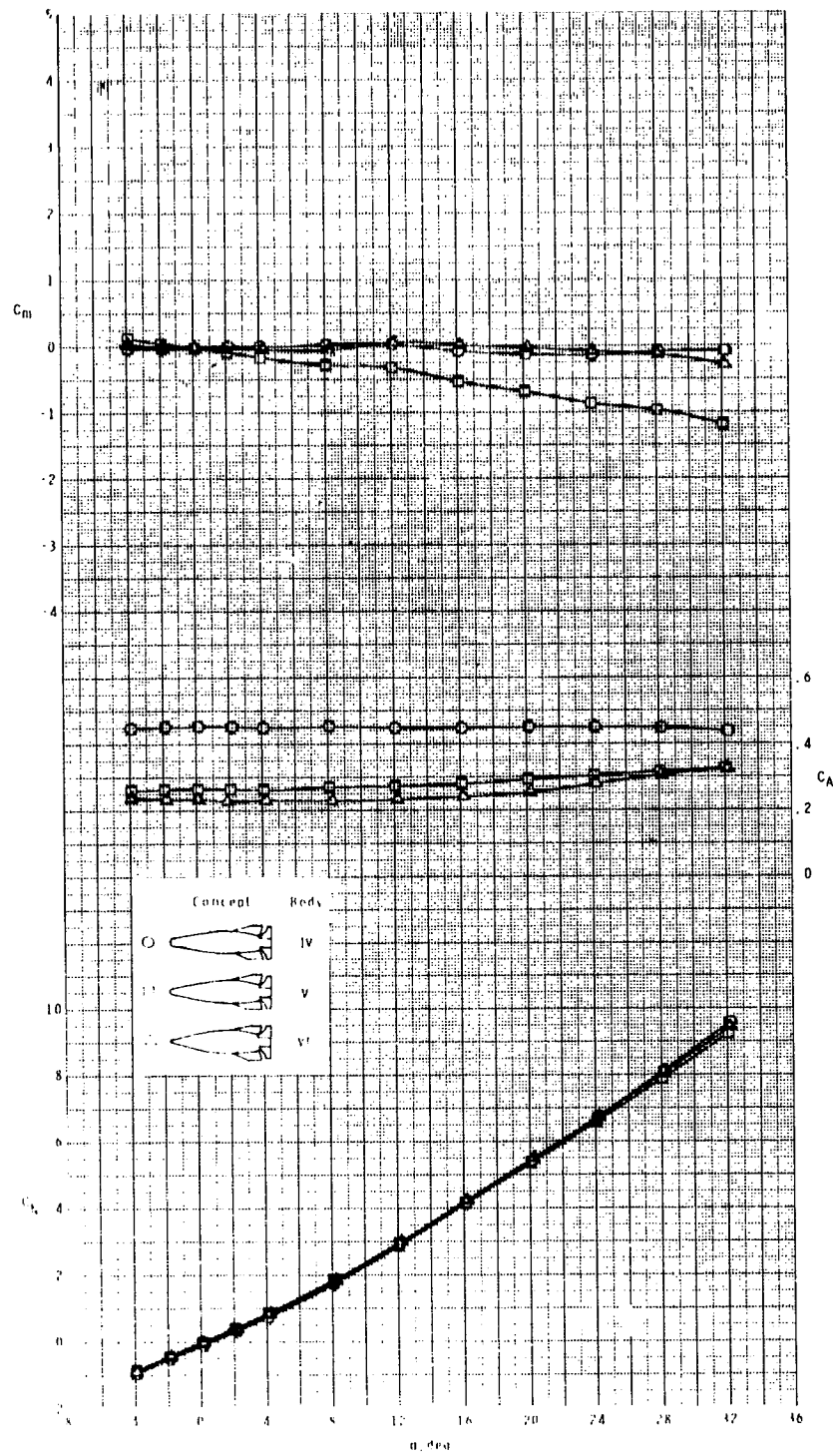
Figure 16.- Effect of some nose-forebody shapes on longitudinal aerodynamic characteristics of missile concept having variable cross-sectional eccentricity of afterbody with circular base.
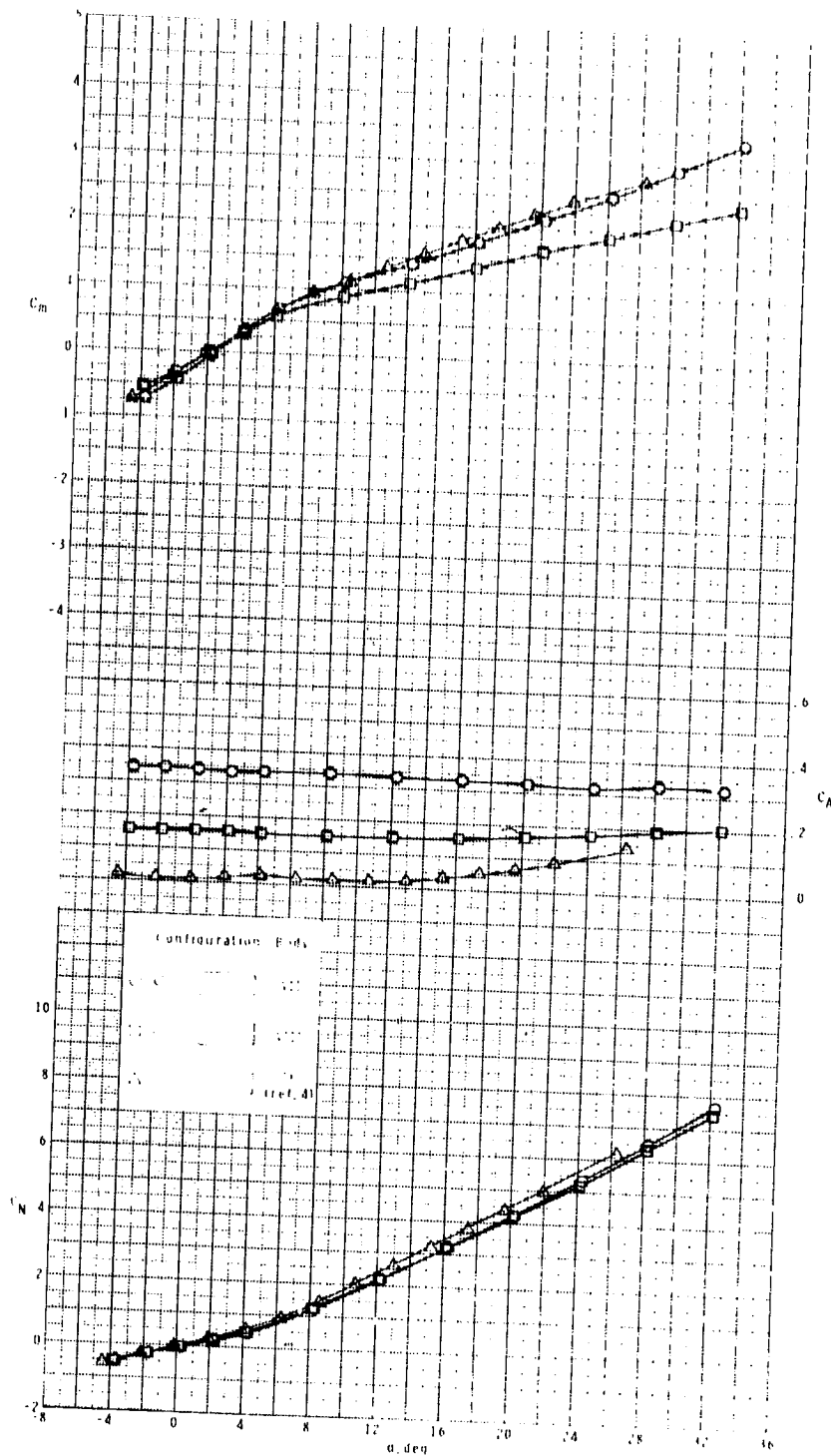
50
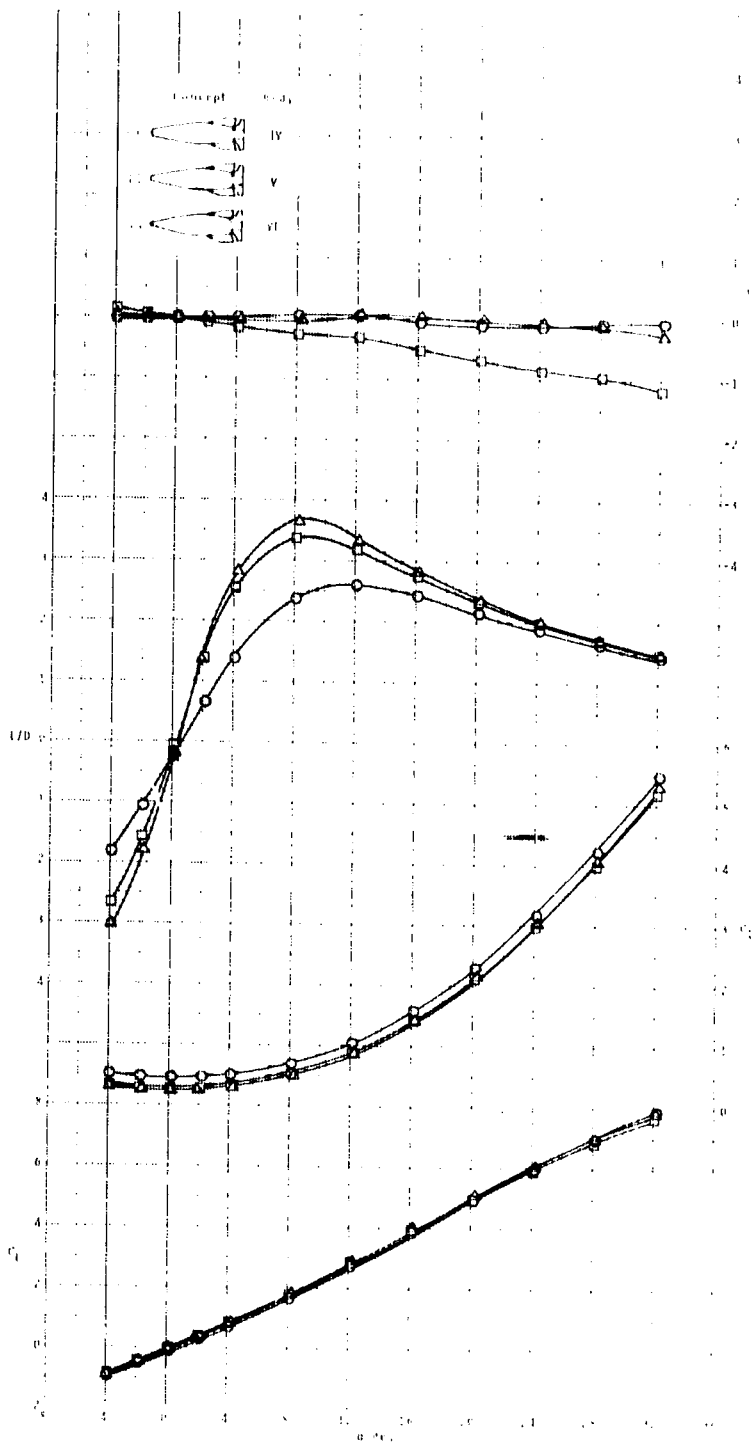
Figure 16.- Concluded.
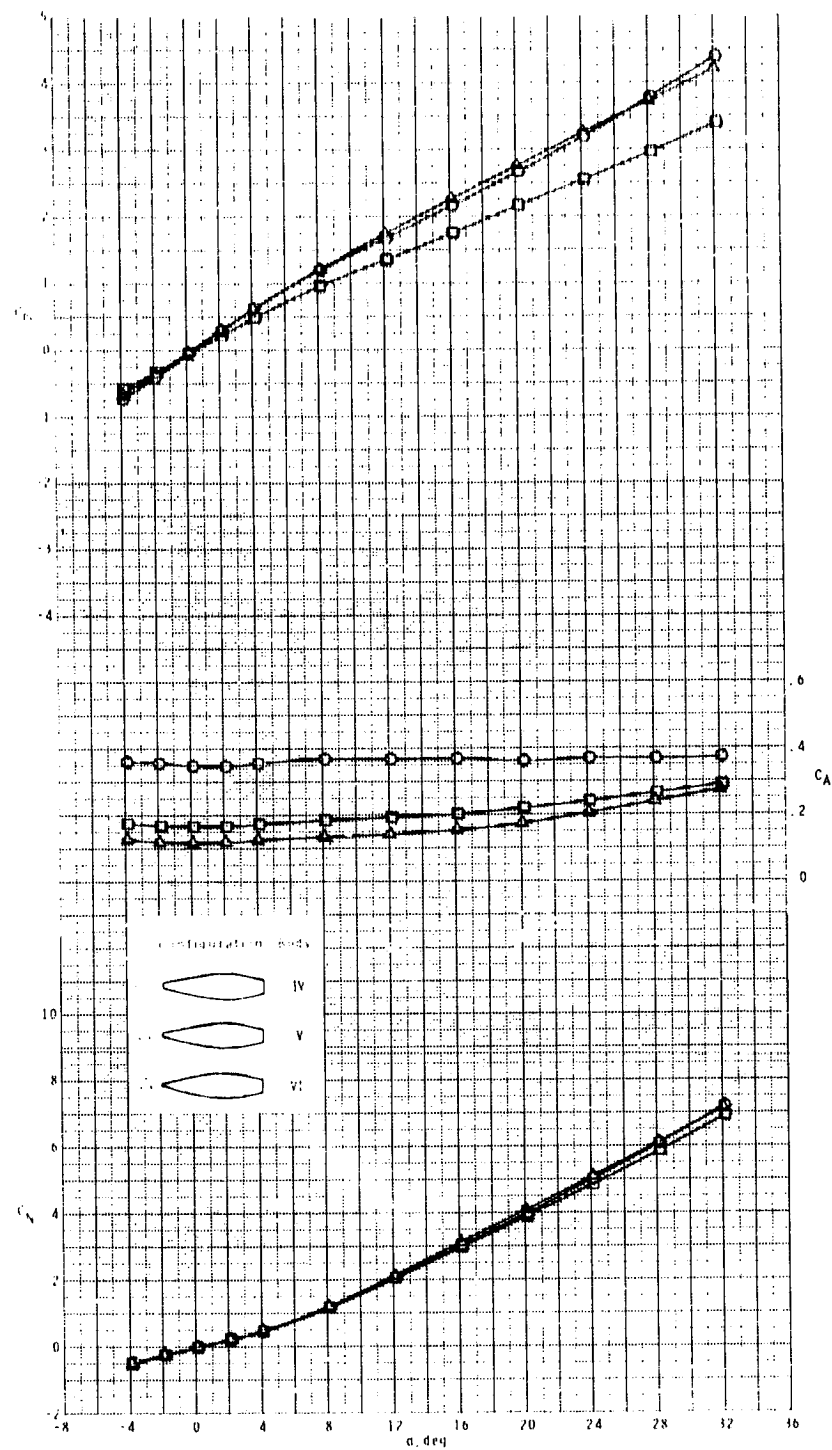
Figure 17.- Effect of some nose-forebody shapes on longitudinal aerodynamic characteristics of body having variable cross-sectional eccentricity of afterbody with circular base.
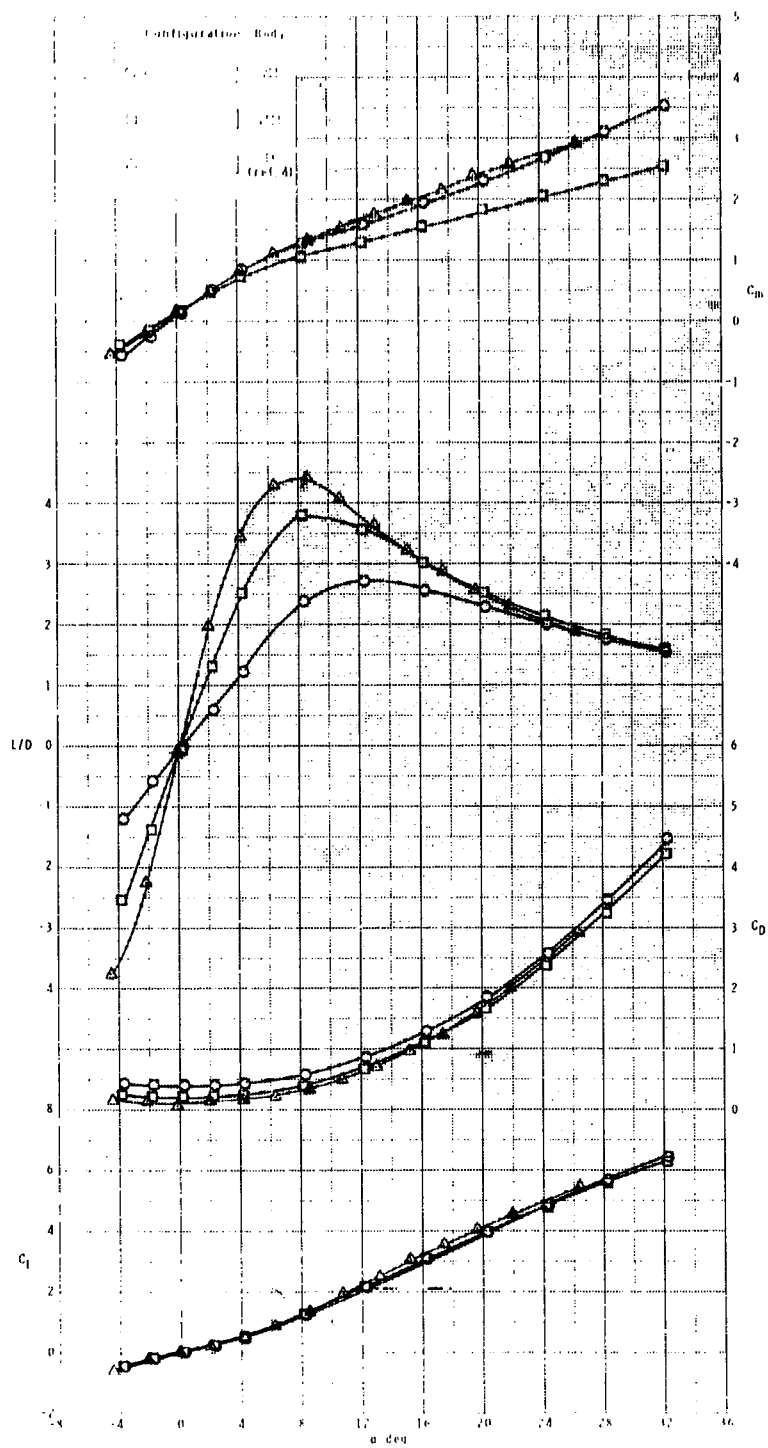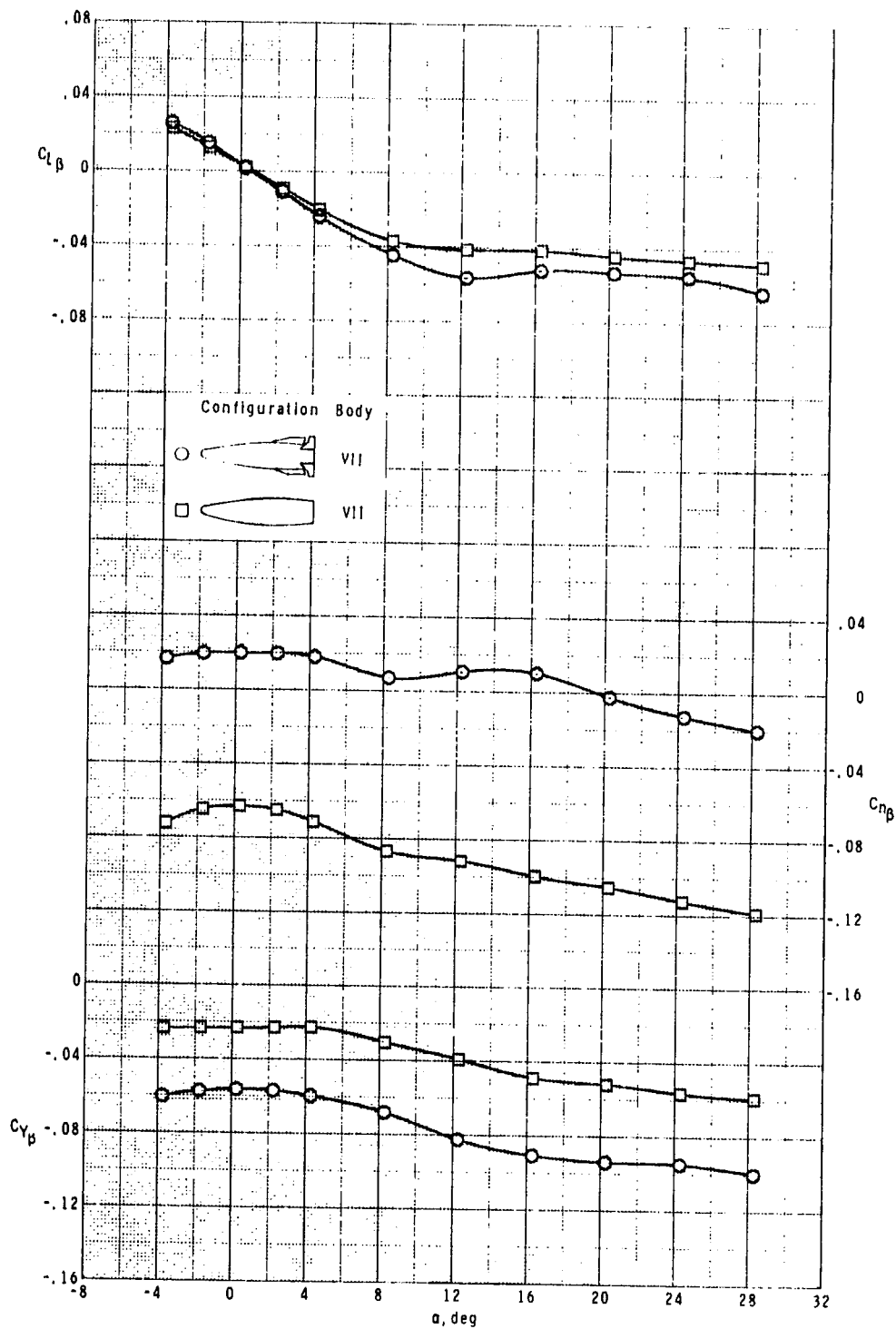
52
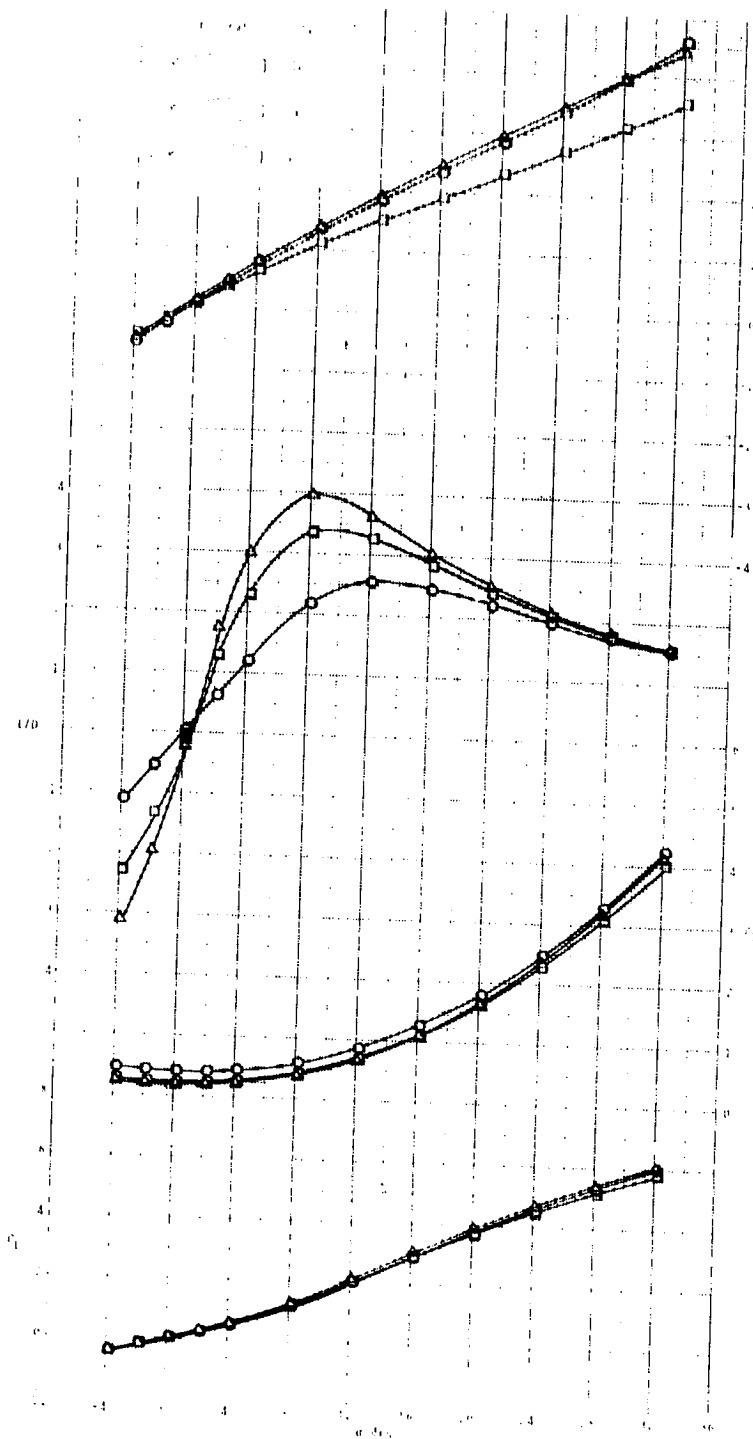
Figure 17.- Concluded.
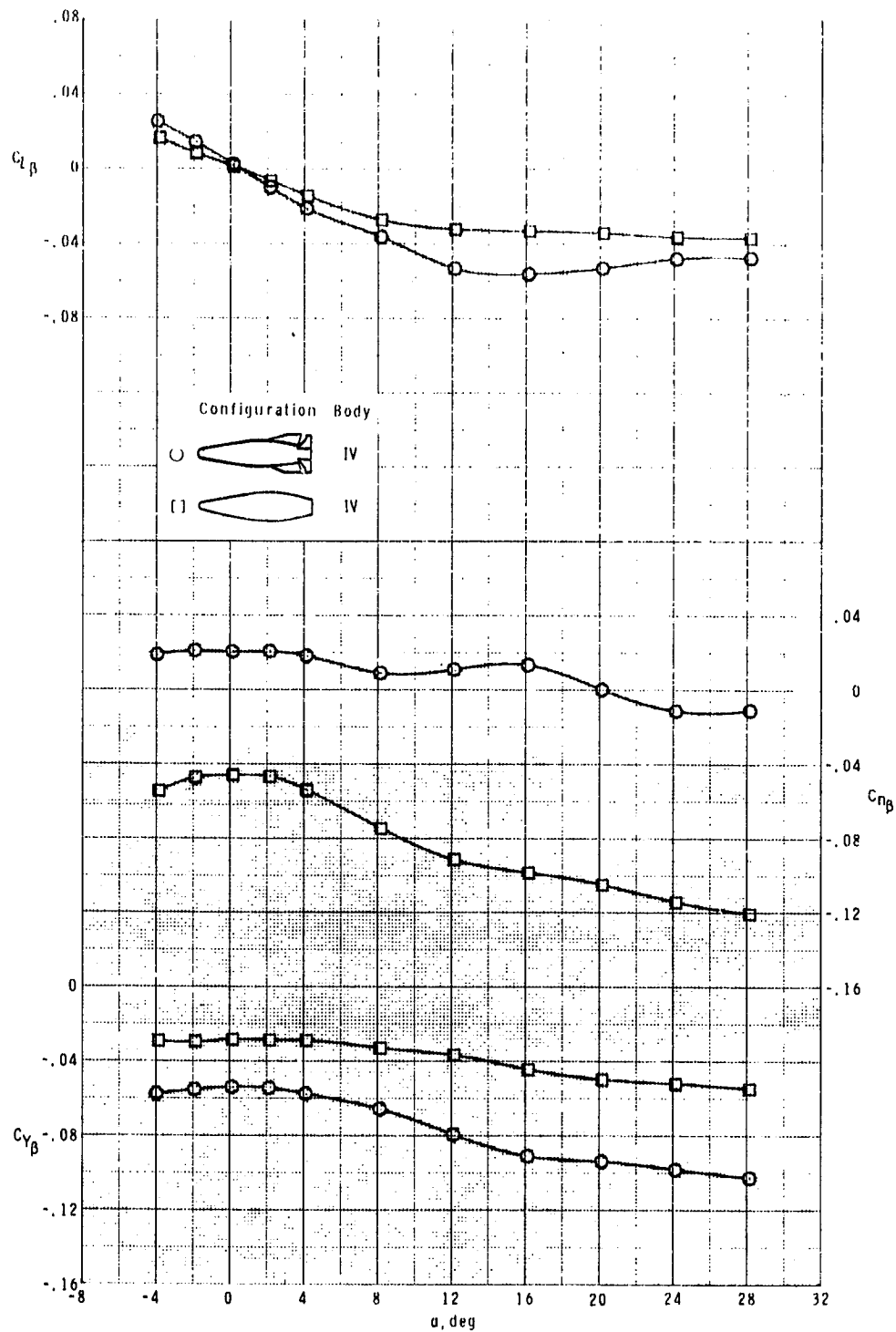
Figure 18.- Effect of wing and tail components on lateral-directional stability parameters of missile concept having variable cross-sectional eccentricity of forebody and afterbody with circular base and large hemispherical nose.
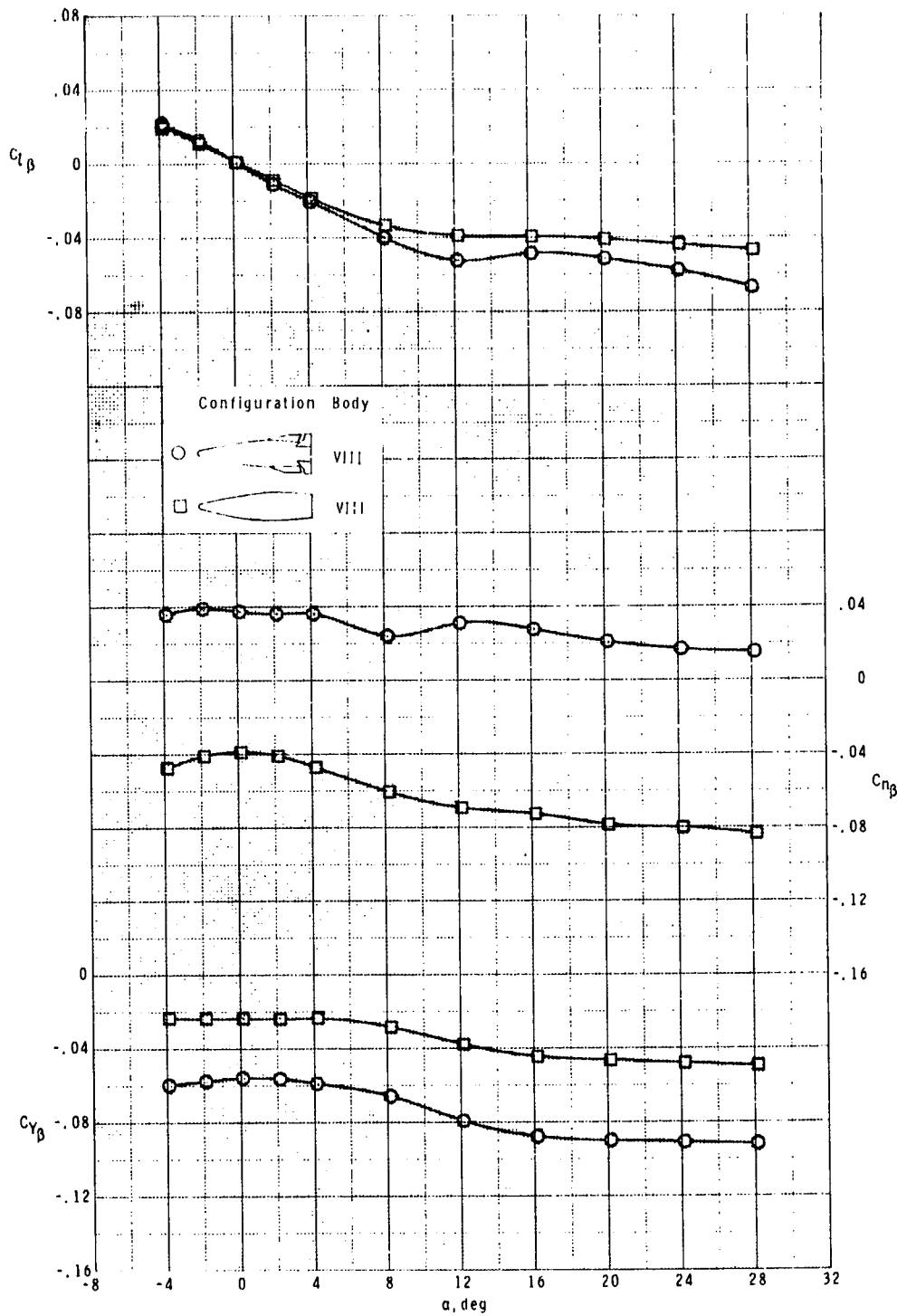
54
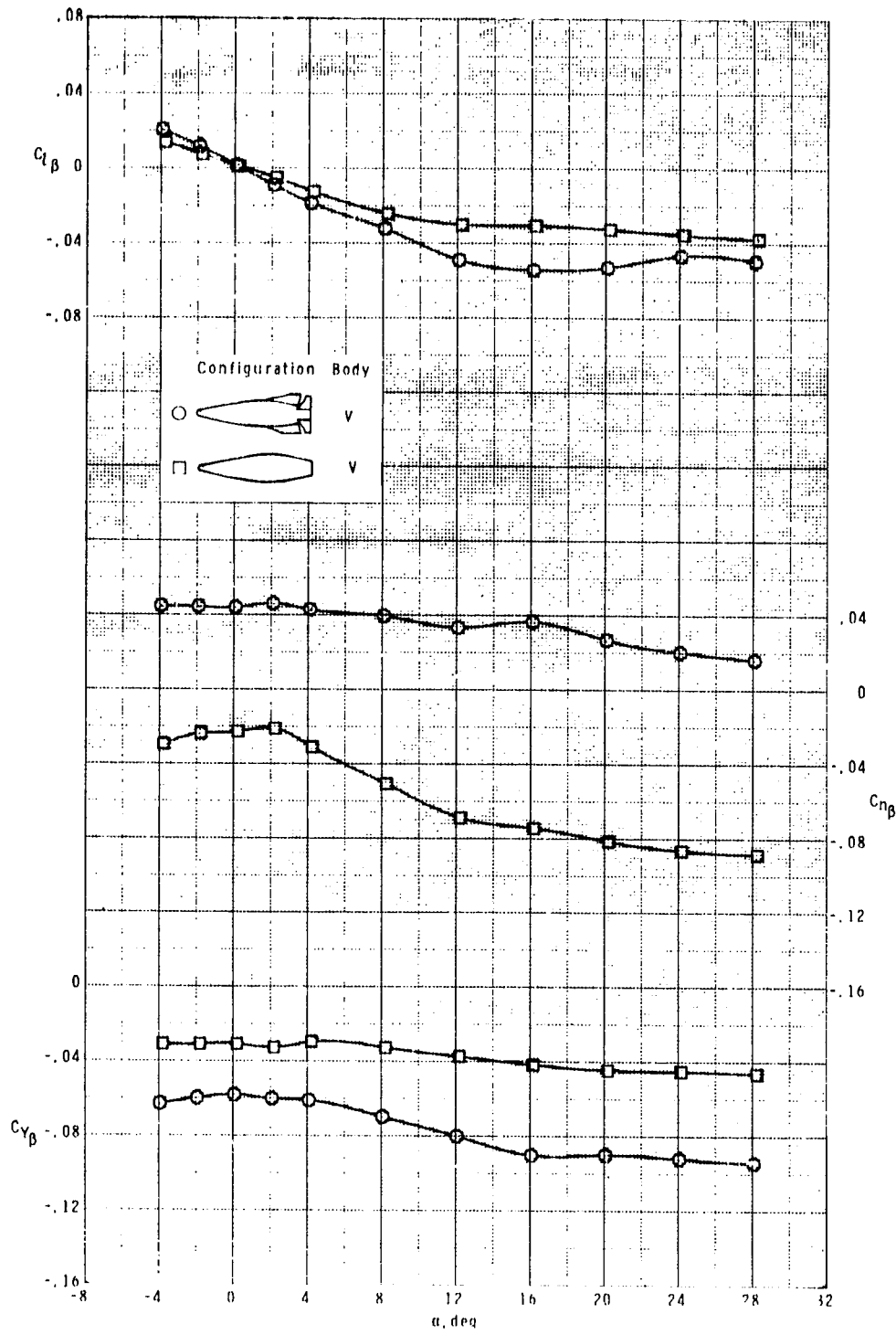
Figure 19.- Effect of wing and tail components on lateral-directional stability parameters of missile concept having variable cross-sectional eccentricity of forebody and afterbody with circular base and small hemispherical nose.
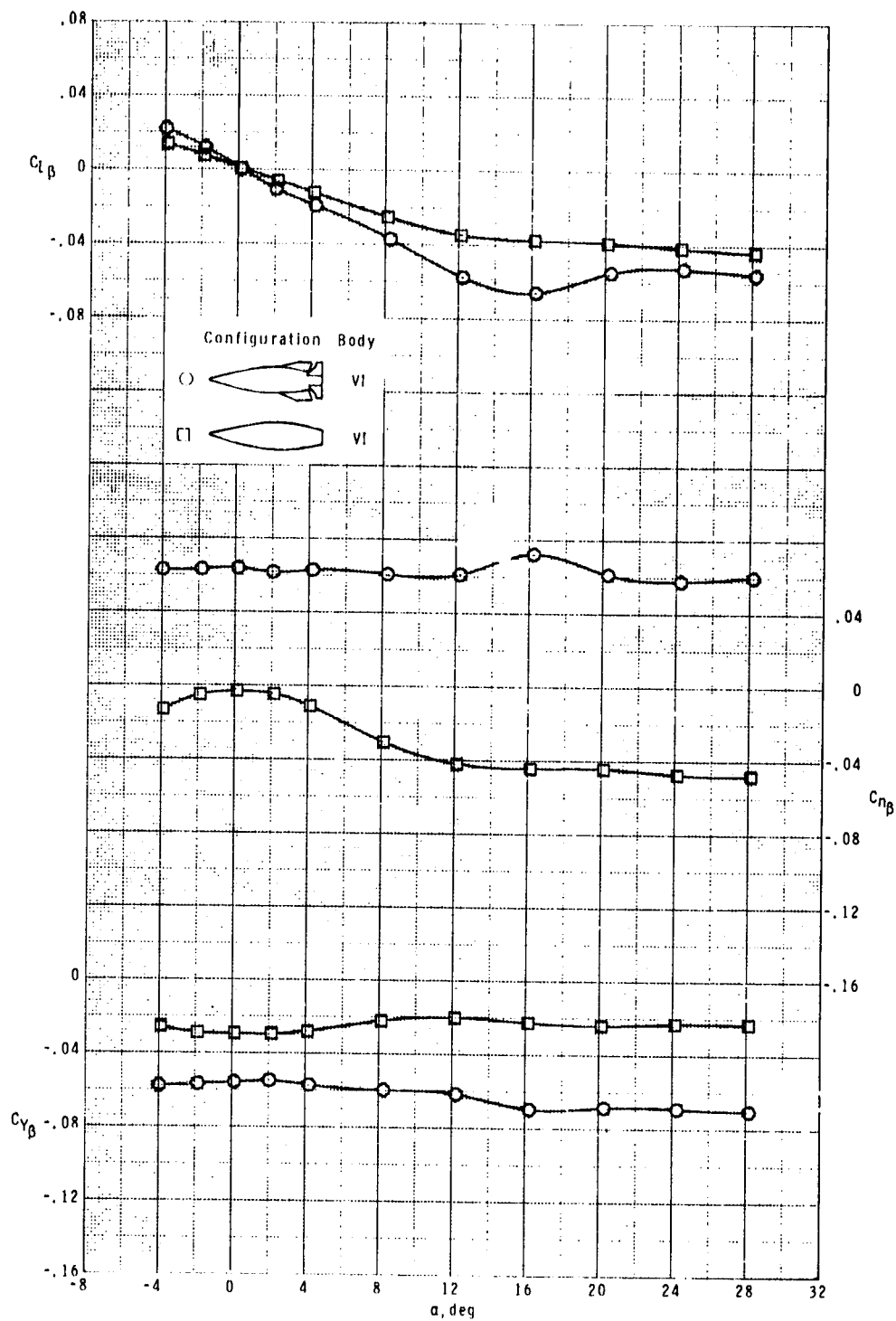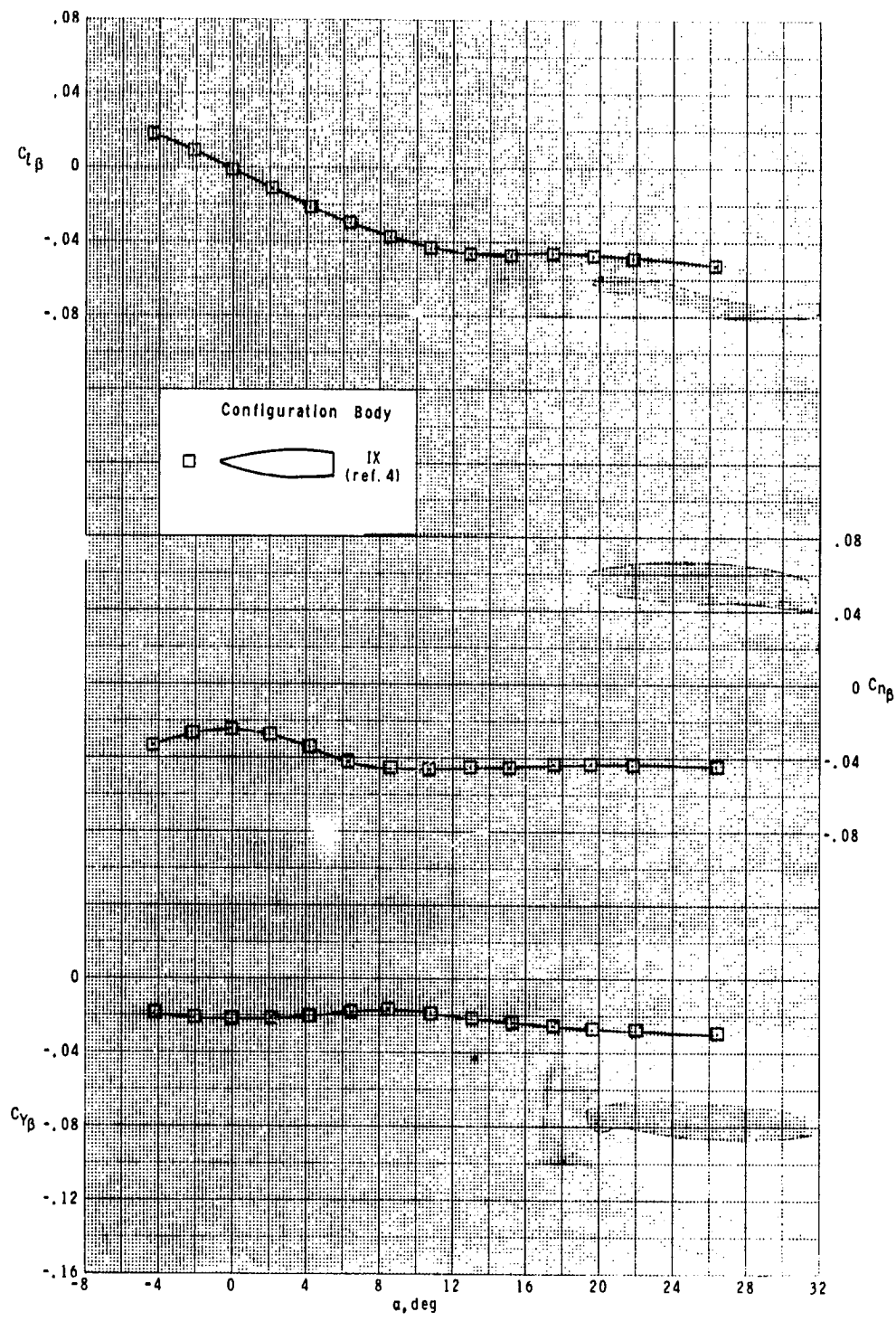
Figure 20.- Effect of wing and tail components on lateral-directional stability parameters of missile concept having constant cross-sectional eccentricity of forebody and variable cross-sectional eccentricity of afterbody with circular base and pointed nose.
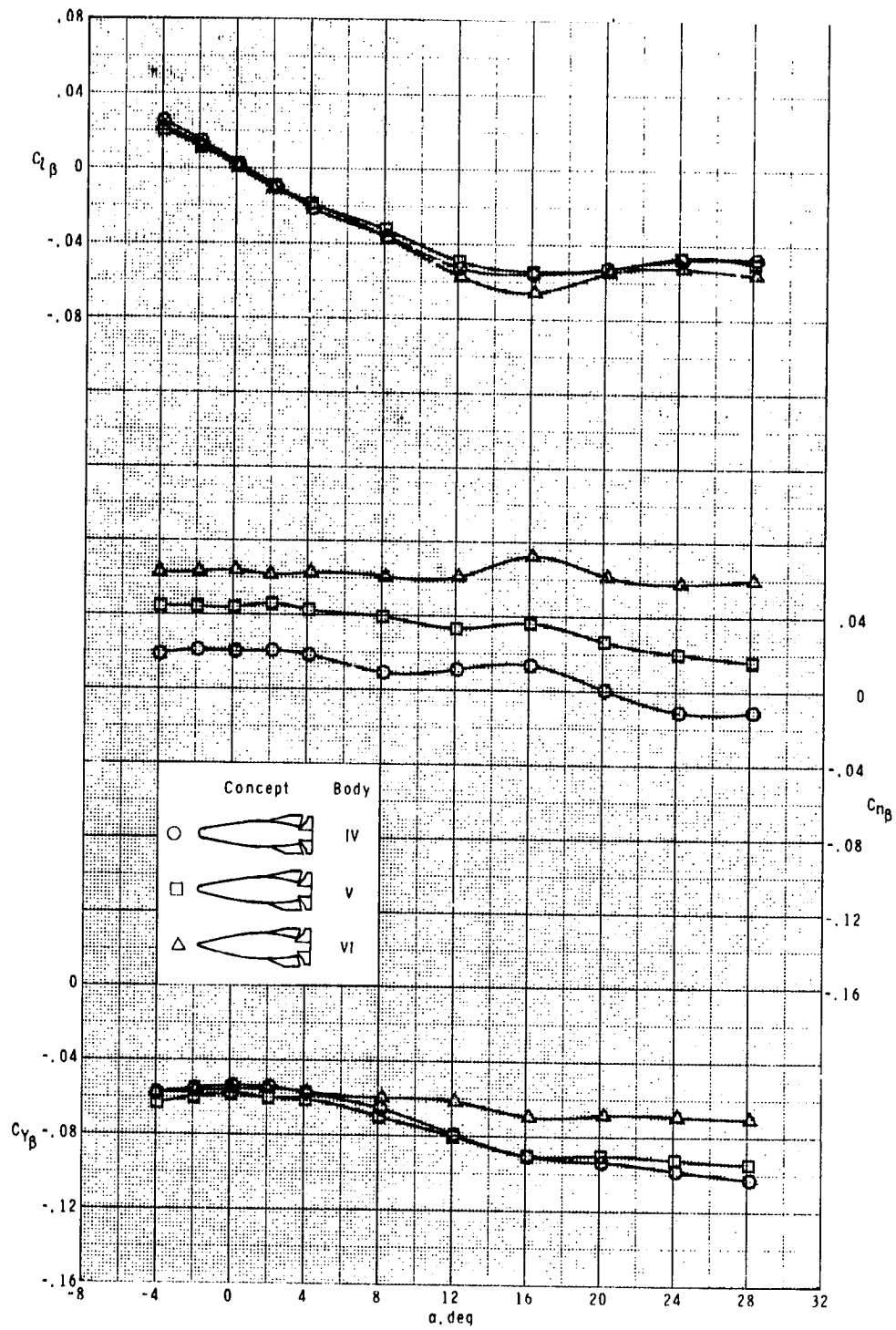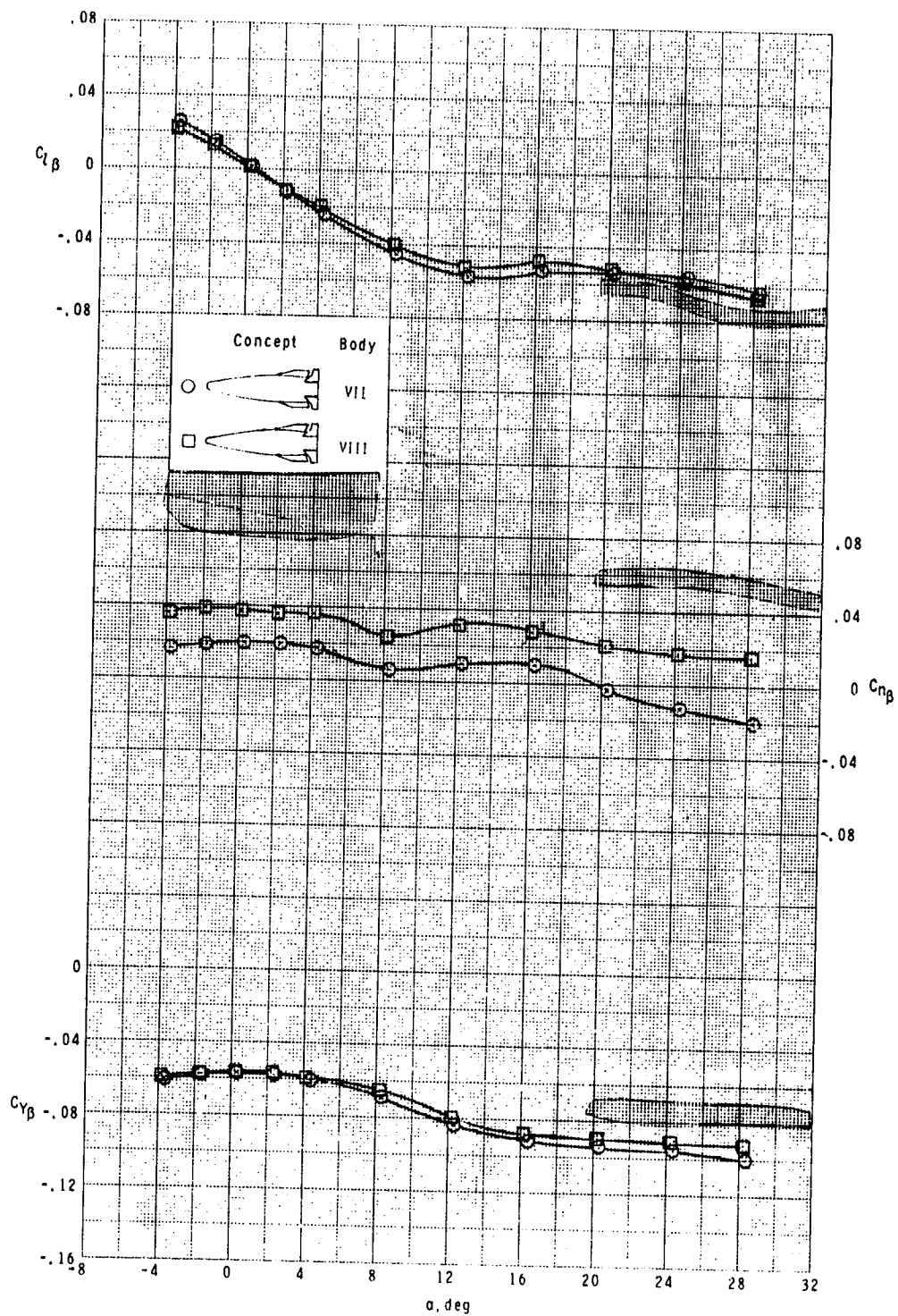
Figure 21.- Effect of some nose-forebody shapes on lateral-directional stability parameters of missile concept having variable cross-sectional eccentricity of afterbody with circular base.
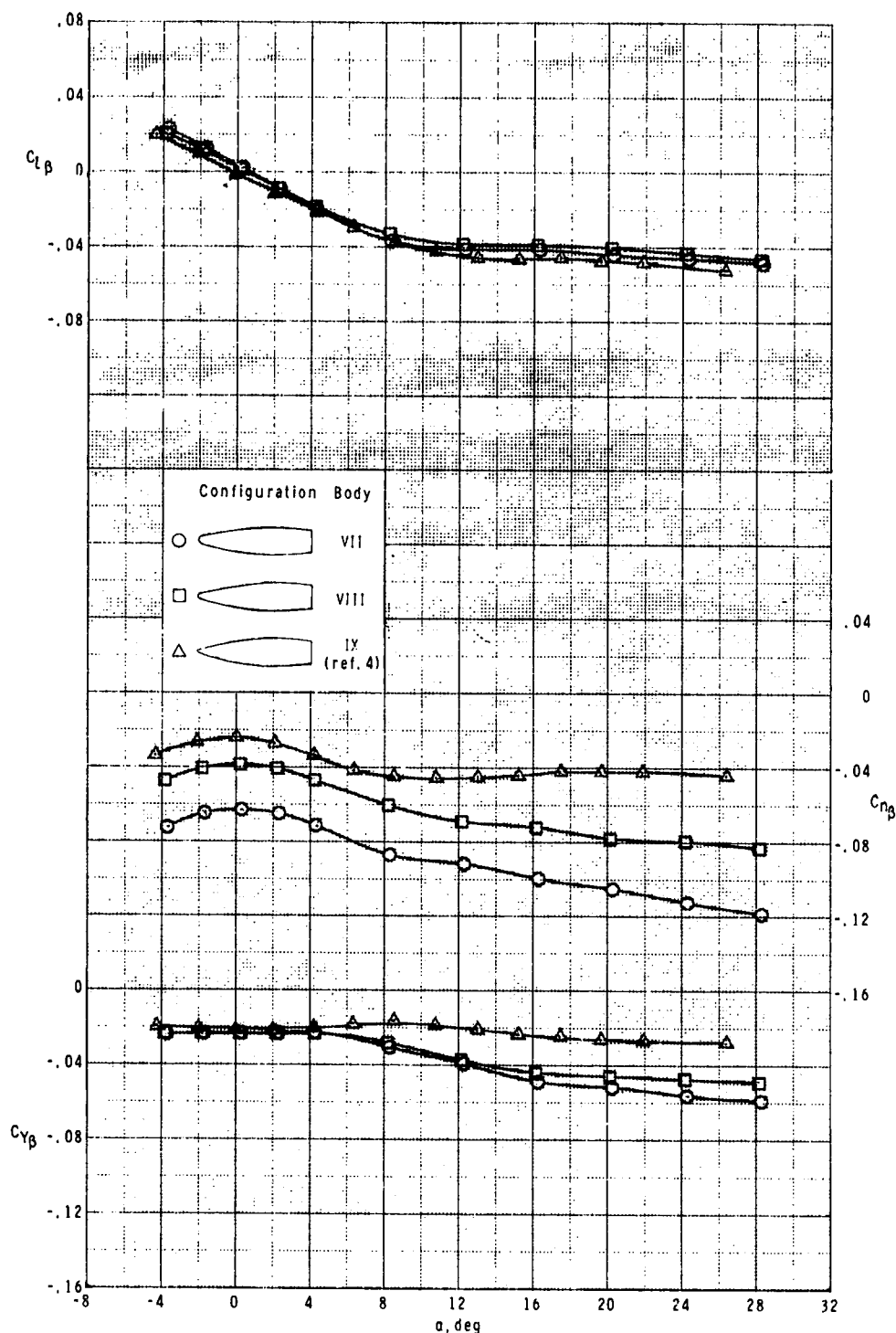
57
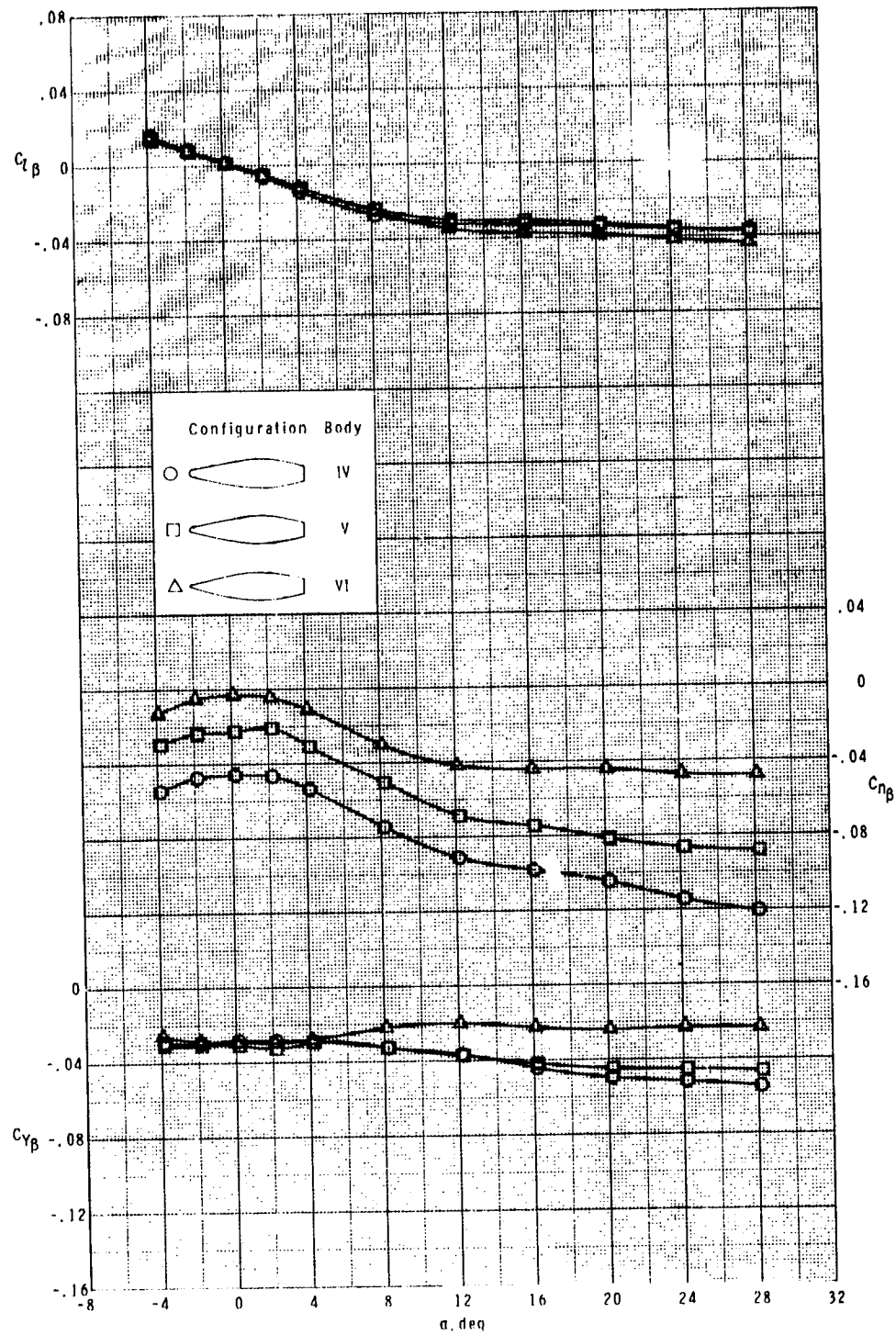
Figure 22.- Effect of some nose-forebody shapes on lateral-directional stability
parameters of body having variable cross-sectional eccentricity of afterbody
with circular base.

Figure 23.- Effect of wing and tail components on longitudinal aerodynamic char-
acteristics of missile concept having variable cross-sectional eccentricity
of forebody and constant cross-sectional eccentricity of afterbody with
elliptical base and large hemispherical nose.

59

Figure 23.- Concluded.
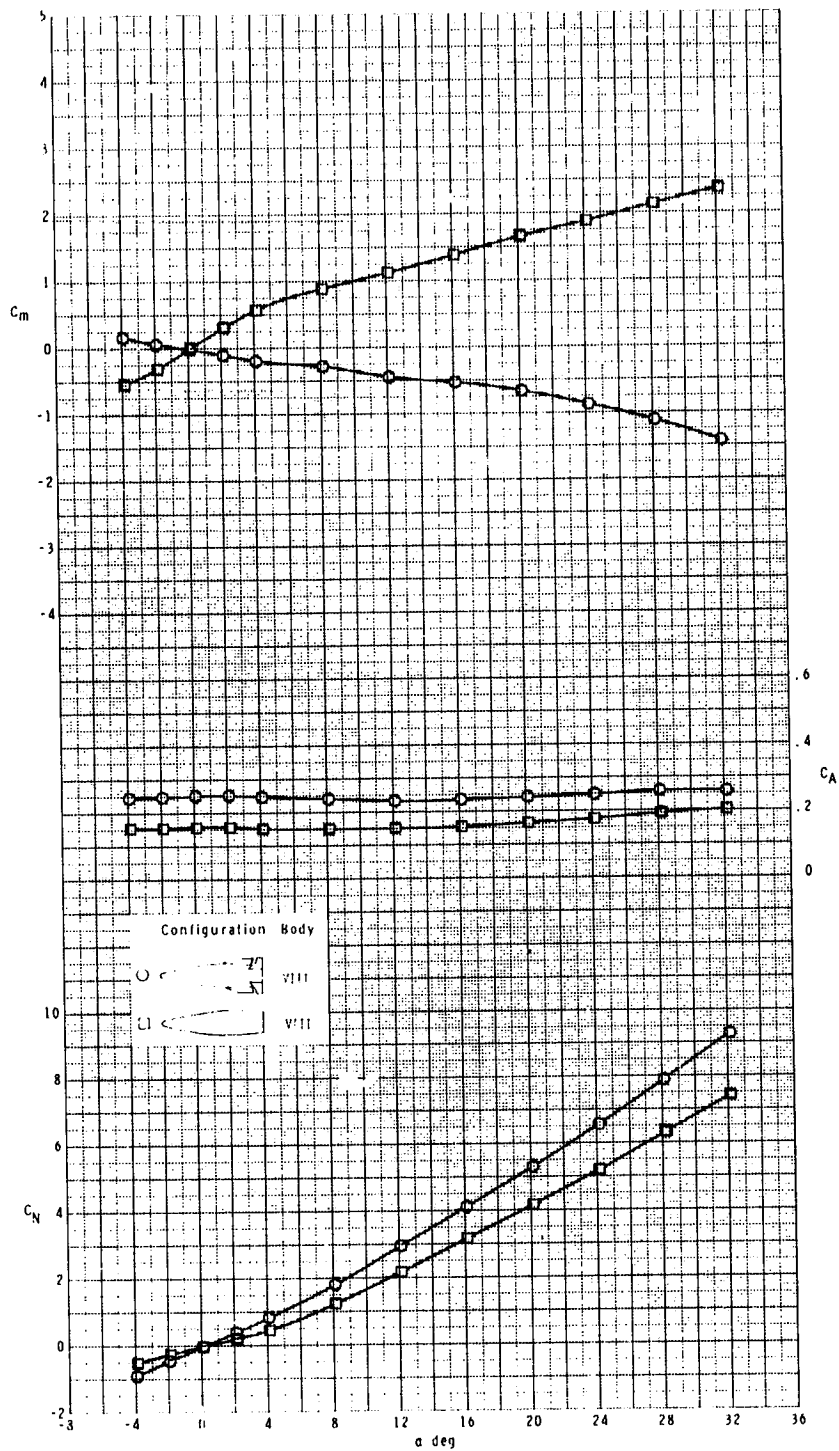
Figure 24.- Effect of wing and tail components on longitudinal aerodynamic characteristics of missile concept having variable cross-sectional eccentricity of forebody and constant cross-sectional eccentricity of afterbody with elliptical base and small hemispherical nose.

Figure 24.- Concluded.

62

Figure 25.- Effect of wing and tail components on longitudinal aerodynamic characteristics of missile concept having constant eccentricity of forebody and afterbody with elliptical base and pointed nose.
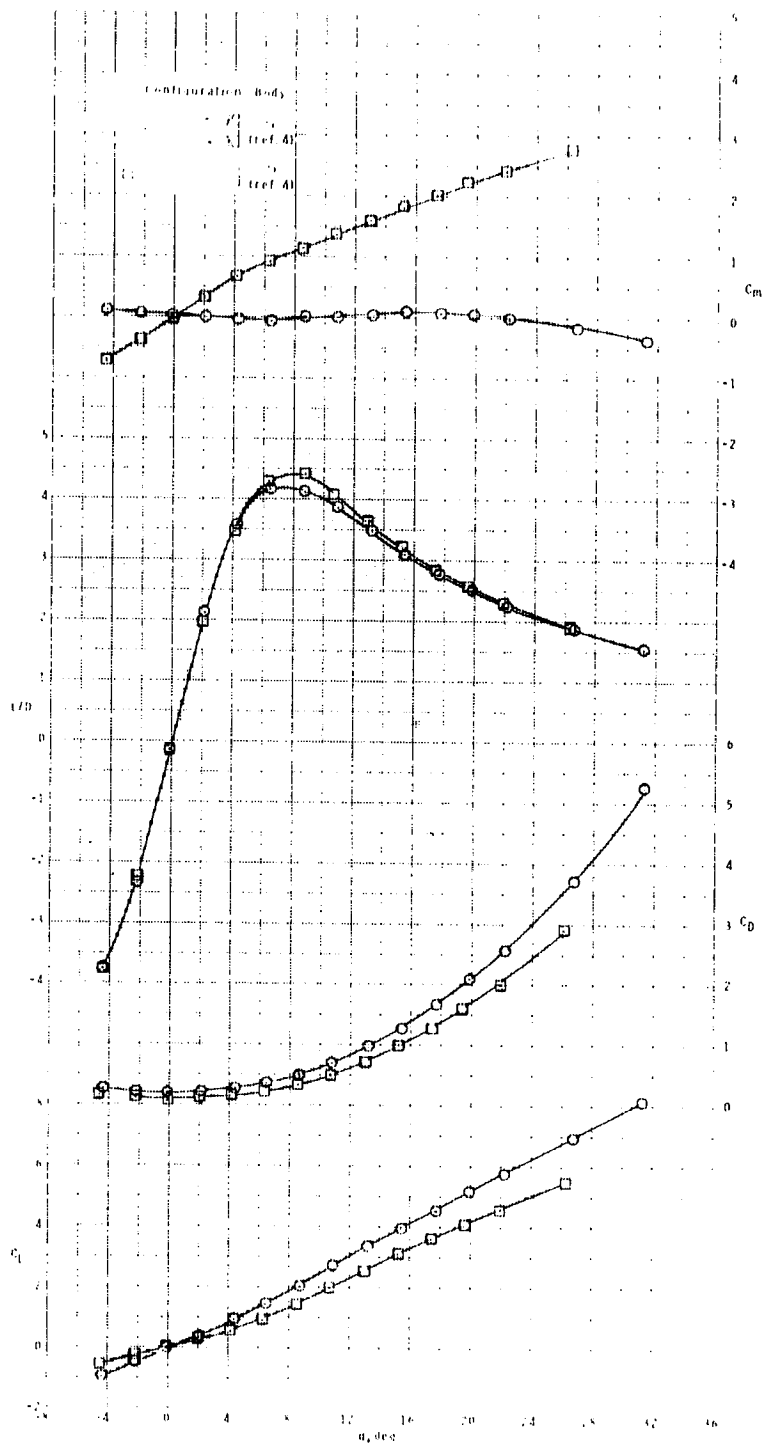
Figure 25.- Concluded.
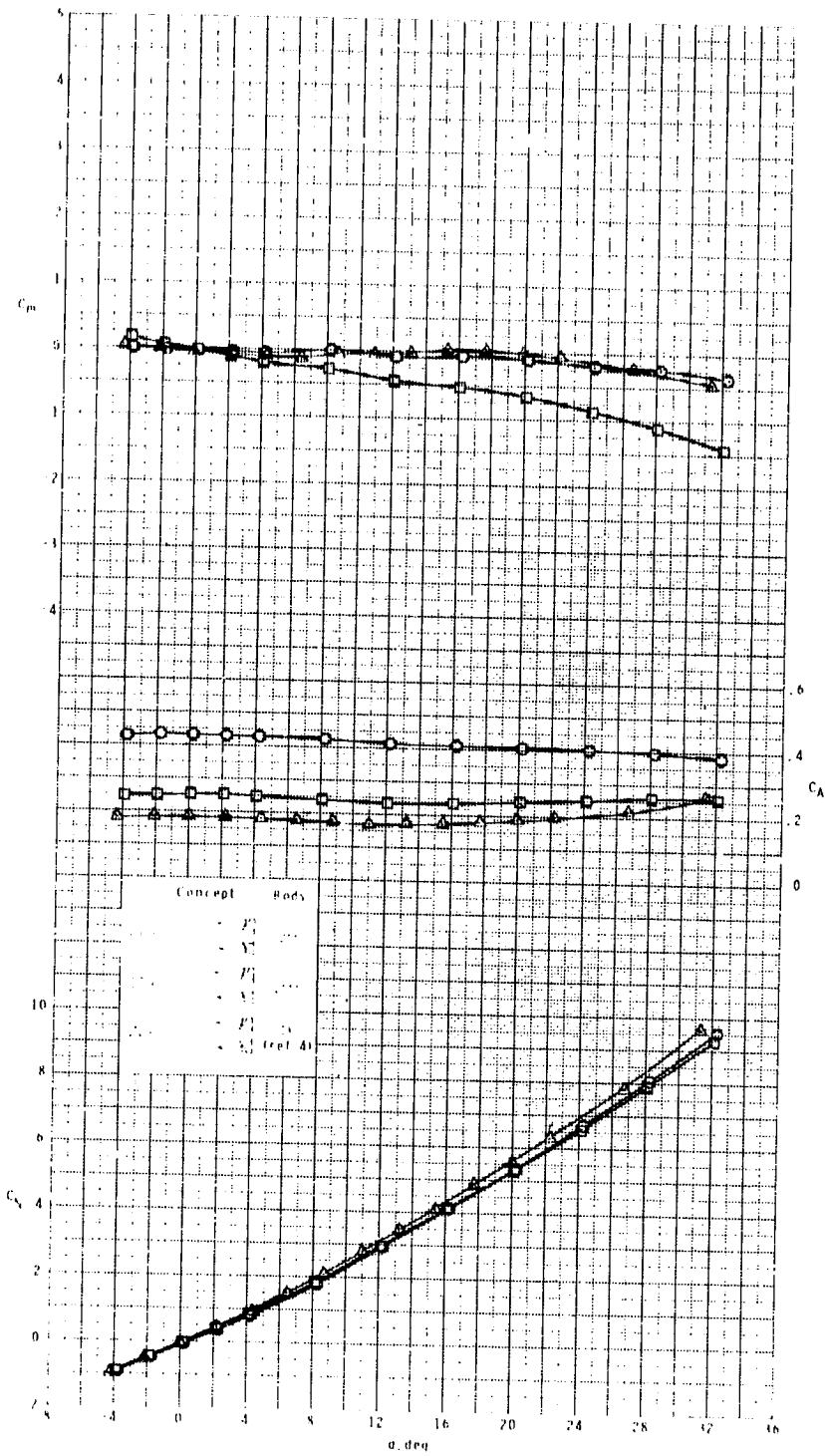
Figure 26.- Effect of nose size on longitudinal aerodynamic characteristics of missile concept having variable eccentricity of forebody and constant eccentricity of afterbody with elliptical base.

Figure 26.- Concluded.

Figure 27.- Effect of some nose-forebody shapes on longitudinal aerodynamic characteristics of body having variable cross-sectional eccentricity of forebody and constant eccentricity of afterbody with elliptical base.

Figure 27.- Concluded.

Figure 28.- Effect of wing and tail components on lateral-directional stability parameters of missile concept having variable cross-sectional eccentricity of forebody and constant cross-sectional eccentricity of afterbody with elliptical base and large hemispherical nose.

Figure 29.- Effect of wing and tail components on lateral-directional stability
parameters of missile concept having variable cross-sectional eccentricity
of forebody and constant eccentricity of afterbody with elliptical base and
small hemispherical nose.

70

Figure 30.- Lateral-directional stability parameters of configuration (body alone) having constant cross-sectional eccentricity of forebody and afterbody with elliptical base and pointed nose.

71

Figure 31.- Effect of some nose-forebody shapes on lateral-directional stability parameters of missile concept having constant cross-sectional eccentricity of afterbody with elliptical base.

Figure 32.- Effect of some nose-forebody shapes on lateral-directional stability parameters of body having constant cross-sectional eccentricity of afterbody with elliptical base.

73
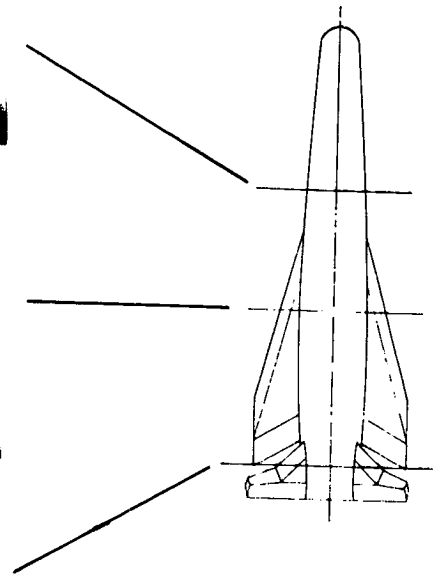
(a) Circular body concept; large hemispherical nose; body I; $\alpha = 15^{\circ}$.

Figure 33.- Flow visualization photographs.

74
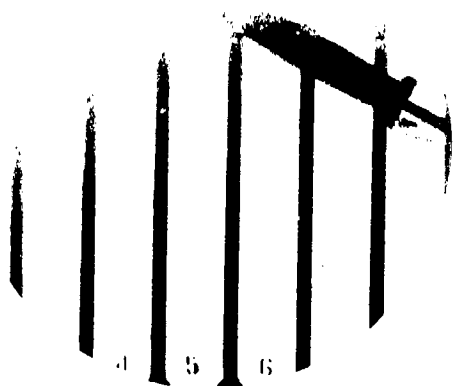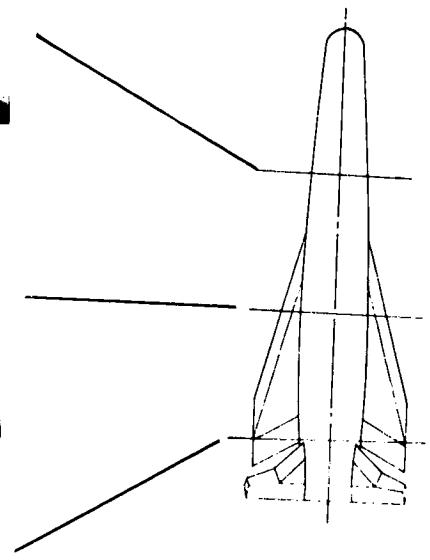
(b) Circular body concept; large hemispherical nose; body I; $\alpha = 30°$.

L-79-145

Figure 33.- Continued.
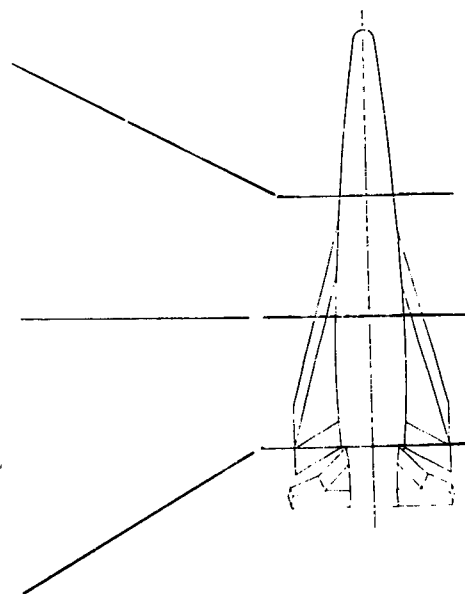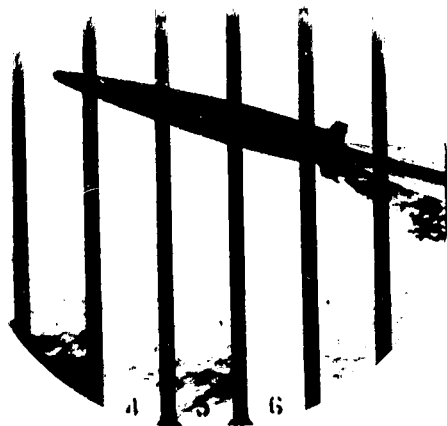
L-79-146

(c) Circular body concept; small hemispherical nose; body II; $\alpha = 15^{\circ}$.

Figure 33.- Continued.
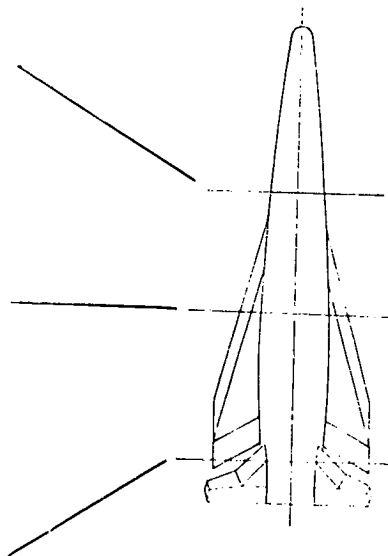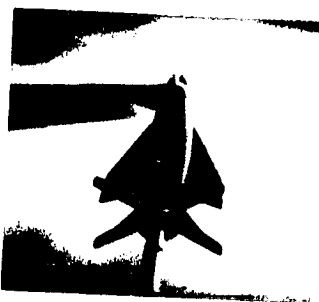
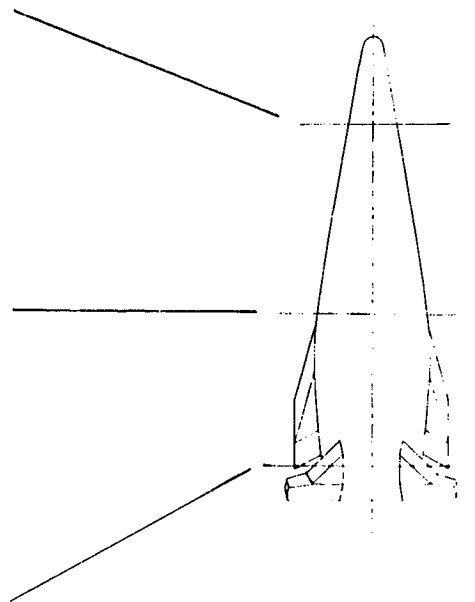(d) Circular body concept; small hemispherical nose; body II; $\alpha = 30^{\circ}$.

L-79-147

Figure 33.- Continued.
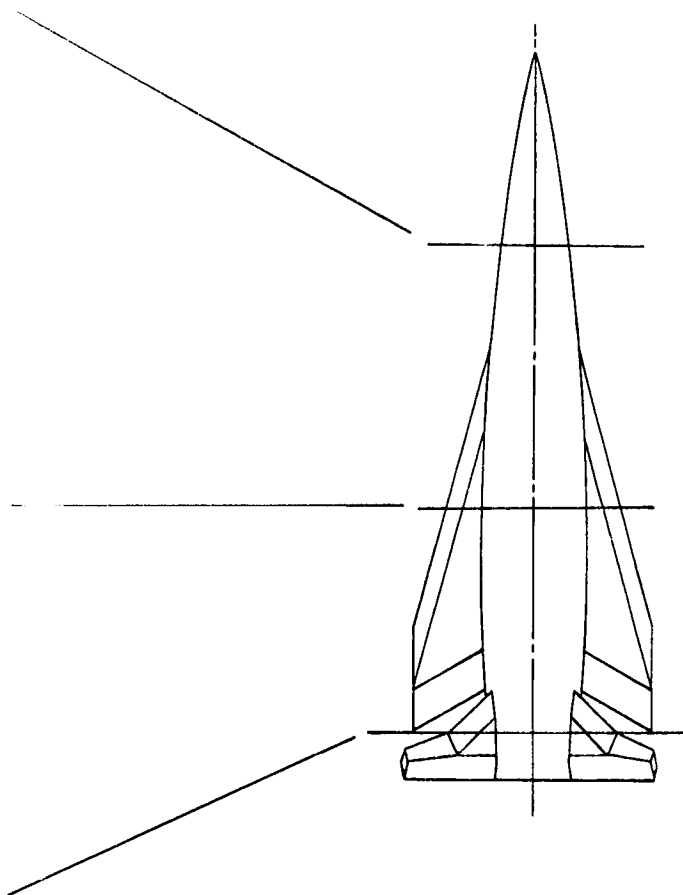
(e) Circular body concept; pointed nose; body III; $\alpha = 15^{\circ}$.

Figure 33.- Continued.
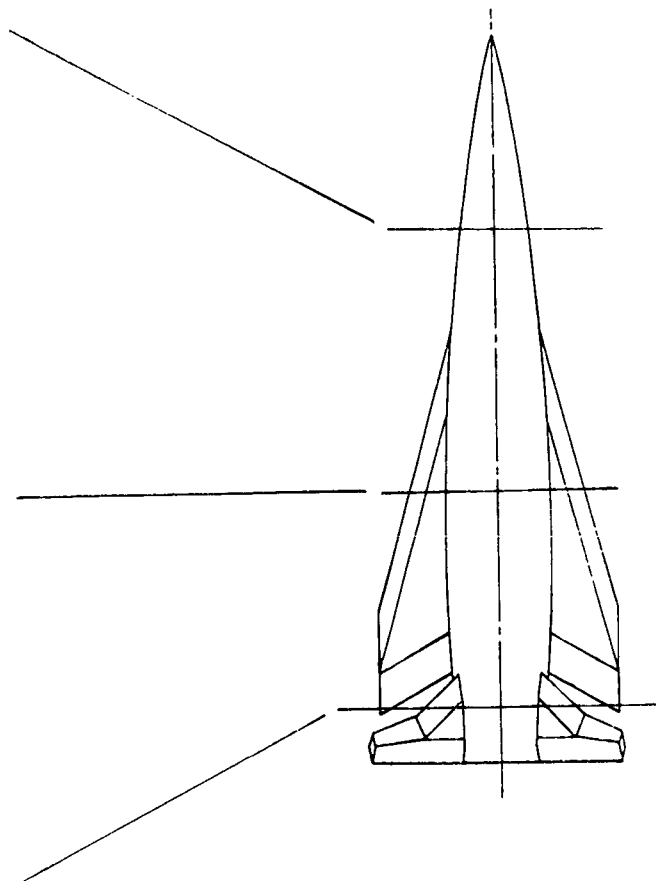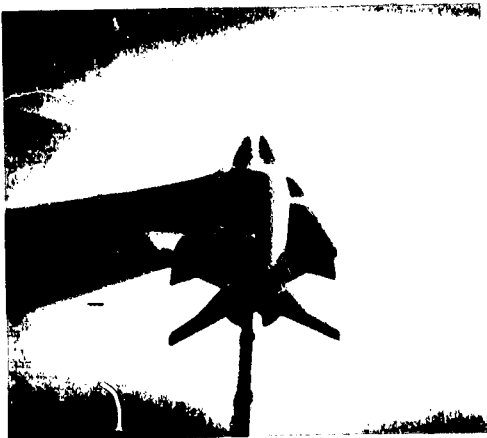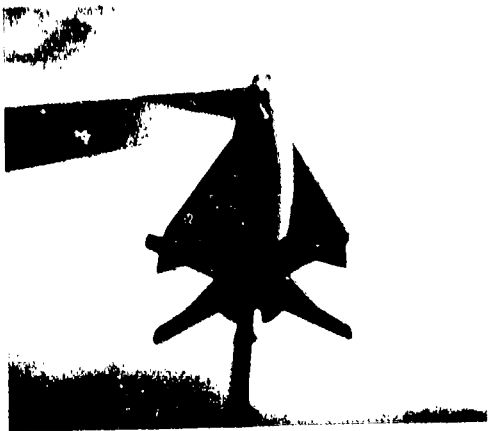
L-79-149

(f) Circular body concept; pointed nose; body III; $\alpha = 30^{\circ}$.

Figure 33.- Continued.
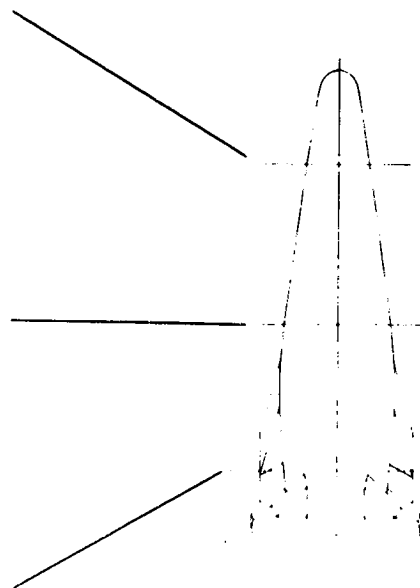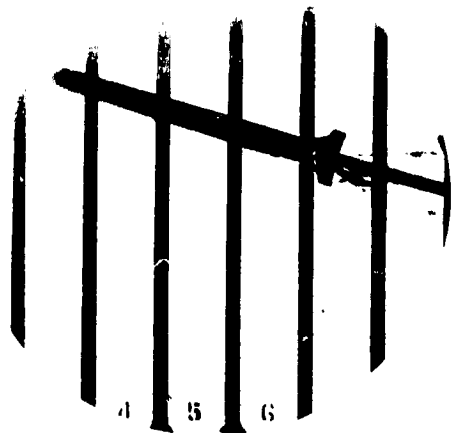
79

(g) Elliptical body concept; large hemispherical nose; body VII; $\alpha = 15^{o}$.
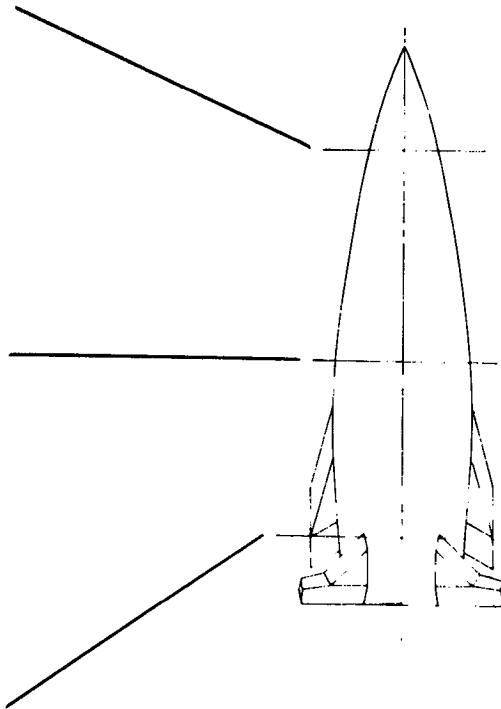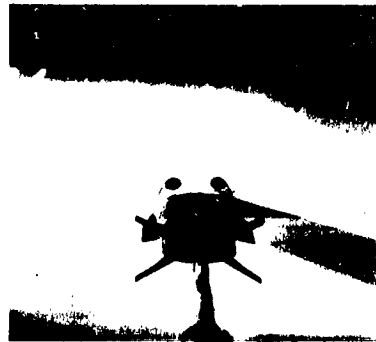
Figure 33.- Continued.
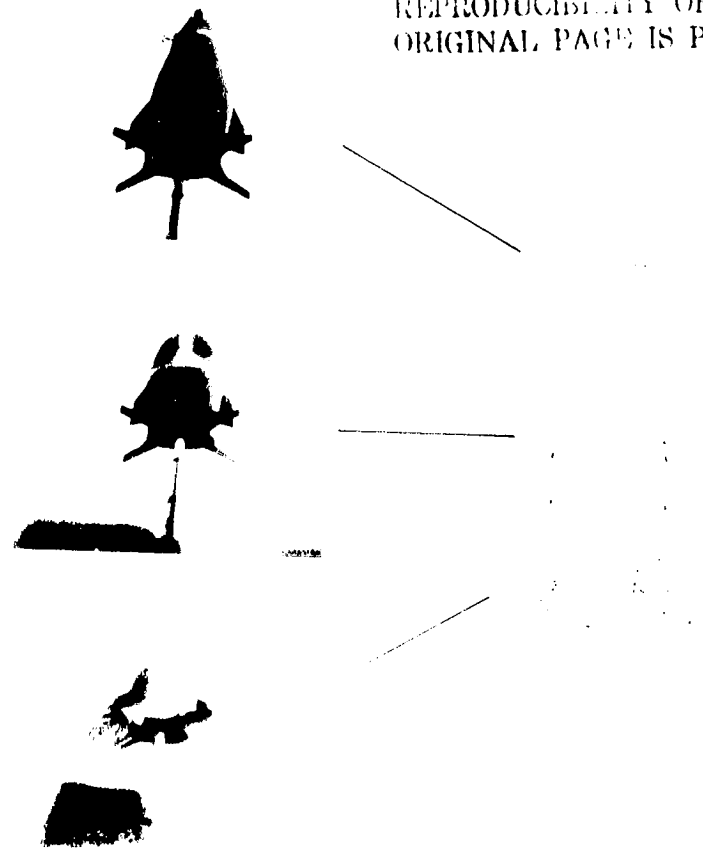
(h) Elliptical body concept; large hemispherical nose; body VII; $\alpha = 30^\circ$.

L-79-151

Figure 33.- Continued.

81
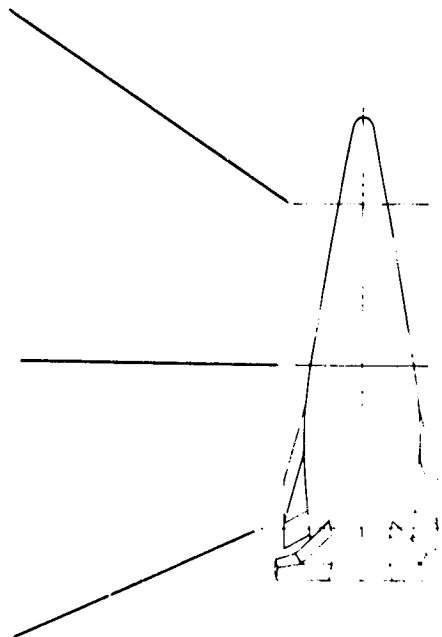
L-79-152

(i) Elliptical body concept; small hemispherical nose; body VIII; $\alpha = 15^{\circ}$.
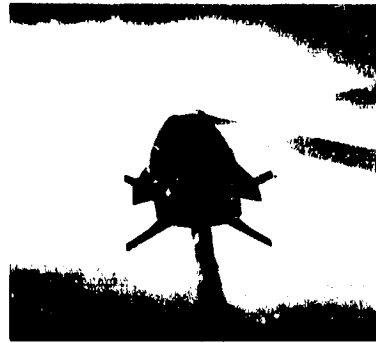
Figure 33.- Continued.

82

L-79-153

(j) Elliptical body concept; small hemispherical nose; body VIII; $\alpha = 30^\circ$.

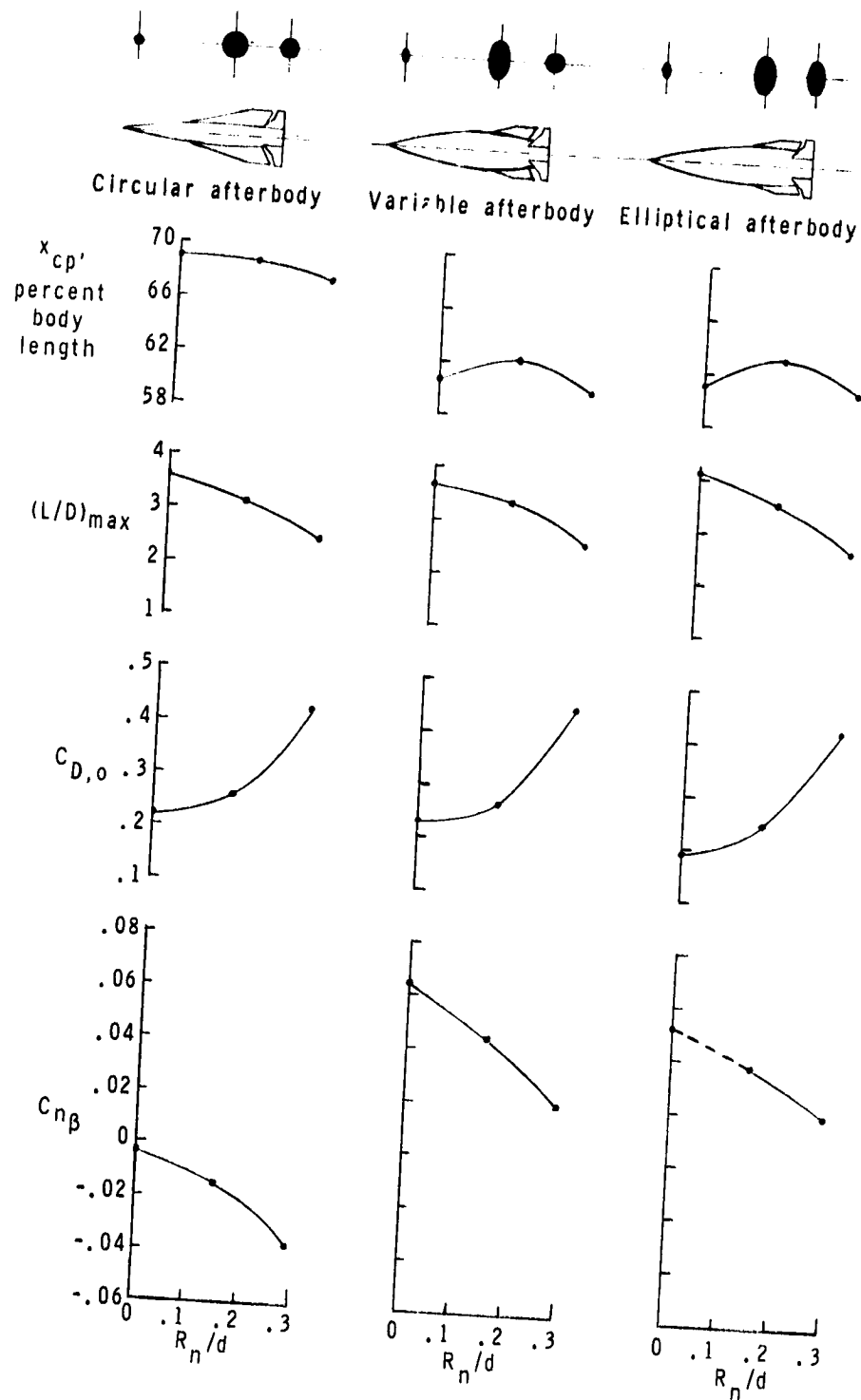Figure 33.- Continued.

83

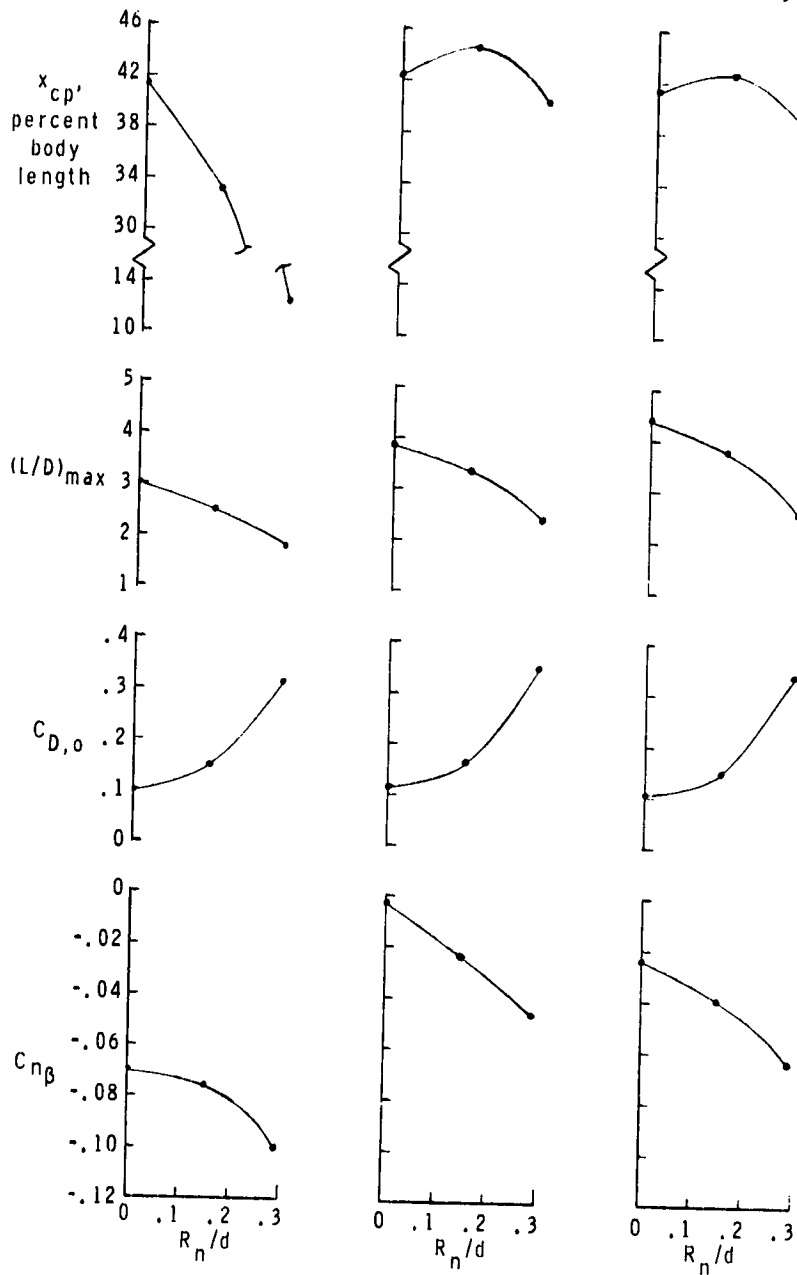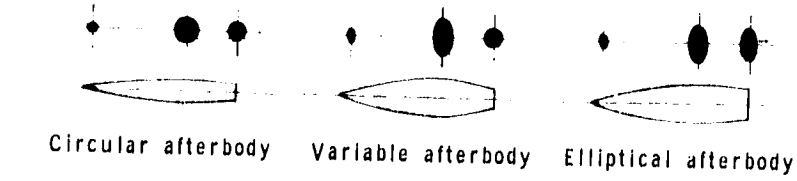(k) Elliptical body concept; pointed nose; body IX; $\alpha = 15^\circ$.

Figure 33.- Concluded.

Circular afterbody   Variable afterbody   Elliptical afterbody

(a) Concepts.

Figure 34.- Parameter summary data.

(b) Bodies.

Figure 34.- Concluded.